UNIVERSITY OF CALIFORNIA, SAN DIEGO

Dynamic Signaling and Adaptation in *Saccharomyces cerevisiae* Stress Response Pathways

A dissertation submitted in partial satisfaction of the
requirements for the degree Doctor of Philosophy

in

Biology

by

Zohreh AkhavanAghdam

Committee in charge:

Professor Nan Hao, Chair
Professor Jeff Hasty
Professor Lorraine Pillus
Professor Scott Rifkin
Professor Peter Yingxiao Wang

2017

The Dissertation of Zohreh AkhavanAghdam is approved, and it is acceptable in quality and form for publication on microfilm and electronically:

_____

_____

_____

_____

_____

Chair

University of California, San Diego
2017

Dedication

I'd like to dedicate this thesis to my mom, Nahid Amiri, for being my best friend and for sacrificing so much for my education and well-being. She is my hero in life and the most amazing person I have ever known. Thank you mom for all that you have done for me and those around you.

TABLE OF CONTENTS

LIST OF FIGURES

LIST OF TABLES

ACKNOWLEDGMENTS

My PI, Nan Hao- for being a wonderful and patient mentor and for teaching me how to be a better scientist, public speaker, and science communicator. I am so grateful for his guidance and support.

My Committee- Lorraine Pillus, Jeff Hasty, Scott Rifkin, and Yingxiao (Peter) Wang for their support and insight throughout the years.

The Hao lab and the Hasty lab (past and present members)- Thanks for taking the time to work with me, teaching me techniques, and helping me along with my projects. Graduate school has taught me that there are so many amazing and intelligent people who are also generous in sharing their knowledge with others. I have learned so much from all of you and hope I can one day reciprocate. Thank you for your scientific insight, technical assistance, and invaluable friendship.

My "honeybadger" graduate school classmates for helping me push through graduate school and for being the most wonderful friends.

Family and friends- I am lucky to have each and every one of you in my life. Thanks for sticking with me.

Chapter 1, in full, has been published in *Journal of Biological Chemistry*: Yanfei Jiang, Zohreh AkhavanAghdam, Lev S. Tsimring, and Nan Hao. "Coupled feedback loops control the stimulus-dependent dynamics of the yeast transcription factor Msn2." J Biol Chem (2017). The author of this

dissertation was the second investigator and author of this paper and performed the experiments while Yanfei Jiang performed the modeling.

Chapter 2, in full, has been published in *eLife*: Zohreh AkhavanAghdam*, Joydeb Sinha*, Omar. P. Tabbaa* and Nan Hao. "Dynamic control of gene regulatory logic by seemingly redundant transcription factors." eLife (2016). *Denotes co-first authorship. The author of this dissertation was the co-first author of this paper.

Chapter 3 will be prepared for submission for the publication of the material by December 2017: Zohreh AkhavanAghdam, Yanfei Jiang, Nan Hao. “Dynamics of Cellular Memory in Adaptation to Stress”. The dissertation author is the co-first author and investigator of the paper.

This work was supported, in part, by the National Institutes of Health Cell and Molecular Genetics training grant.

VITA

2006 – 2010 Bachelor of Science, University of California, Los Angeles

2011 – 2017 Doctor of Philosophy, University of California, San Diego

PUBLICATIONS:

Zohreh AkhavanAghdam*, Joydeb Sinha*, Omar. P. Tabbaa* and Nan Hao "Dynamic control of gene regulatory logic by seemingly redundant transcription factors", *eLife*, 5, 2016.

Yanfei Jiang, Zohreh AkhavanAghdam, Lev S. Tsimring, and Nan Hao. "Coupled feedback loops control the stimulus-dependent dynamics of the yeast transcription factor Msn2.", *J Biol Chem*, 2017

ABSTRACT OF THE DISSERTATION

Dynamic Signaling and Adaptation in *Saccharomyces cerevisiae* Stress Response Pathways

by

Zohreh AkhavanAghdam

Doctor of Philosophy in Biology

University of California, San Diego, 2017

Professor Nan Hao, Chair

Living cells respond to environmental cues through complex signaling and gene regulatory networks. A common theme throughout this thesis will be exploring design principles in biological networks and how they operate dynamically to process information and make decisions.

In Chapter 1, we tackle how different types of stresses induce distinct nuclear translocation dynamics of Msn2, an outstanding question in the field. In the absence of stress, PKA phosphorylates Msn2, causing it to be exported out of the nucleus. In response to stress, PKA activity is inhibited, Msn2 is dephosphorylated and translocated into the nucleus. In response to glucose limitation, Msn2 exhibits an initial homogenous pulse of nuclear translocation followed by sporadic nuclear pulses with dose-dependent frequency, but in response to osmotic stress Msn2 undergoes a single translocation pulse with dose-dependent duration. We hypothesized that the difference between glucose limitation and osmotic stress-induced Msn2 dynamics might be a result of glucose limitation-dependent Snf1 activation, since previous studies suggest that Snf1 and PKA mutually inhibit each other. We use modeling and experiments to demonstrate that these different upstream network structures could, in fact, be responsible for the differences we see in Msn2 translocation dynamics.

In Chapter 2, we study a recurring scheme in gene regulatory networks, which is combinatorial gene regulation by seemingly redundant transcription factors (TFs), using time-lapse microscopy and microfluidics. We use the seemingly redundant yeast homologous stress responsive TFs Msn2 and Msn4 as a model to quantitatively study the functional relevance of closely related TFs in the same single cells and find that Msn2 and Msn4 have non-redundant and distinct functions in combinatorial gene regulation. In response

to a transient input, either Msn2 or Msn4 alone is sufficient to induce the expression of target genes with fast kinetics promoters. Target genes with slow kinetics promoters, however, require activation of both Msn2 and Msn4 in these conditions. Importantly, slow kinetic promoter activation is dependent on duration of the upstream signal because in response to a prolonged input, slow kinetic promoter activation no longer requires both Msn2 and Msn4. Thus, in Chapter 2, we determine that coordinated gene regulation by seemingly redundant TFs is not fixed, but rather dependent on the dynamics of upstream signals.

In Chapter 3, we demonstrate that cells retain a memory of many of upstream signaling events that occur in response to stress, which primes the cells to respond to future severe stress events. We use microfluidics and time-lapse microscopy to modulate the amplitude and duration of priming stimulus and also increase the break time in between the priming stimulus and severe stress. Using this system, we have determined that cells acquire an amplitude-dependent short-term memory of priming stimulus, which is induced and lost rapidly, and a duration-dependent long-term memory which is stable for a long period of time before finally declining after 100 minutes. We use this information about the dynamical specificity of different types of cellular memory and their stability to determine the cellular pathways responsible for the observed memory.

Introduction

A large number of genomic and proteomic studies have revealed many of the interactions and biological network structures cells use to transmit information about the environment. It has becoming increasing clear, however, that these structures are not fixed and can be rewired by different upstream signaling inputs. This is because cells often encode information about the different environmental signals by controlling the temporal dynamics of signaling molecules (Purvis and Lahav 2013). For example, epidermal growth factor (EGF) induces transient activation of the mitogen activated protein kinase ERK which subsequently leads to cell proliferation, whereas nerve growth factor (NGF) induces sustained ERK activation, the result of which is cell differentiation (Marshall 1995). Thus, the cells encode different upstream growth factor identities with different ERK activation dynamics, which subsequently results in different phenotypic outcomes (Figure I.1A).

Transcription factors (TFs) also have been shown to encode information about upstream signals in their activation/localization dynamics. As shown in Figure I.1B, mammalian TF NF-κB exhibits oscillatory nuclear accumulation in response to tumor necrosis factor-α (TNF-α), which then results in the induction of adaptive immune response genes. However, in response to bacterial lipopolysaccharide (LPS), NF-κB exhibits slow prolonged nuclear accumulation, which leads to induction of adaptive immune response genes (Nelson, Ihekwaba et al. 2004, Werner, Barken et al. 2005). In another example in mammalian cells,

the highly studied transcription factor p53 responds to γ-irradiation with homogenous oscillatory pulses, resulting in cell cycle arrest, but responds to UV-radiation with a sustained pulse, resulting in apoptosis (Purvis, Karhohs et al. 2012) (Figure I.1C). In these examples, the identity of the stimulus is encoded in the dynamics of downstream signaling molecules. Recent studies have shown that cells can also encode the strength of external stimuli in the dynamics of the downstream signal with increasing dose of stimuli resulting in change in the amplitude, duration, or frequency of the signaling molecule.

Yeast TF Msn2 encodes the identity and strength of external stimuli in its dynamic pattern of nuclear translocation. In response to glucose limitation, Msn2 exhibits transient sporadic pulses of nuclear localization with dose dependent frequency, but in response to osmotic stress Msn2 undergoes a single transient translocation pulse with dose-dependent duration. Oxidative stress, meanwhile, induces sustained Msn2 nuclear translocation with dose-dependent amplitude (Hao and O'Shea, 2012 (Hao and O'Shea 2012). This localization appears to be regulated by Protein Kinase A (PKA) signaling. When PKA is active, Msn2 is phosphorylated and kept out of the nucleus, however, when PKA is inhibited through upstream stress signaling, Msn2 is unphosphorylated and translocates into the nucleus (Gorner, Durchschlag et al. 1998). It still remains elusive how different PKA signaling or other upstream signaling interactions can elicit different Msn2 translocation dynamics in response to different stress. In Chapter 1, we demonstrate that the sporadic pulses of Msn2 translocation seen in glucose

limitation but not seen in osmotic stress could be due to the fact that Snf1, another protein kinase, is activated in glucose limitation. Snf1 has been shown to inhibit PKA (Nicastro, Tripodi et al. 2015), but is also itself negatively regulated by PKA (Barrett, Orlova et al. 2012), resulting in upstream signaling interactions between the two pathways that could drive Msn2 oscillations. Thus, we show one way in which rewiring of upstream signaling interactions in response to different stresses results in different Msn2 dynamics. The upstream signaling interactions resulting in amplitude-dependent sustained Msn2 translocation in response to ethanol and oxidative stress remains unknown.

In order to determine how genes "decode" these different Msn2 dynamics, previous studies used a chemical genetics approach to directly control Msn2 dynamics and determine the effect on individual gene expression. Analog sensitive mutations (PKA^{as}) were introduced into the three catalytic isoforms of PKA (Tpk1, Tpk2, and Tpk3), making them sensitive to the small molecule 1-NM-PP1 (Hao and O'Shea 2012, Hao, Budnik et al. 2013). In this system, 1-NM-PP1 is added to cells to reversibly inhibit PKA therefore allowing Msn2 to be dephosphorylated and translocated into the nucleus. Since this inhibition is reversable, PKA inhibition is released when 1-NM-PP1 is removed from the cells, thereby allowing PKA to phosphorylate Msn2 causing it to be exported out of the nucleus. Using this system to control Msn2 dynamics, Msn2 specific target promoters (those not induced in an *msn2/4*Δ strain) were then characterized based on their promoter affinity and activation time (Hao and O'Shea 2012,

Hansen and O'Shea 2013). Target genes with fast kinetics promoters are fully induced in response to transient Msn2 inputs while slow kinetics promoters take longer to activate relative to these fast kinetic promoters and thus filter out these transient inputs.

More studies need to be done to determine what causes a promoter to be a fast kinetic or slow kinetic activation target promoter. Msn2 is a C2H2 zing finger that binds to these target promoters on specific sites termed STRE sites (5'-CCCCT-3') (Martinez-Pastor, Marchler et al. 1996). The activation time of these target promoters appears to be dependent on the number of these STRE sites, the position of the nucleosome, and the distance of these STRE sites from the TATA box (Hansen and O'Shea 2015). In Hansen and O'Shea, 2015, a slow activation kinetics promoter (P_{SIP18}) was converted to a fast activation kinetics promoter ($P_{SIP18\text{-}A4}$) by adding two more STRE sites and moving these sites closer to the TATA box. It would be interesting to determine if this can be reproduced with other Msn2 target promoters.

Thus far, all of these previously described studies were performed in cells in which Msn4, a homolog of Msn2, was deleted to simplify the relationship between TF input and gene expression output. Msn2 and Msn4 are regulated by the same upstream signals and bind to the same STRE sites. Thus, we realized we could use our system to study an outstanding question in biology: what is the functional relevance of homolog signal-dependent TFs co-existing in the same cells and how do these TFs coordinate regulation of common target genes. To

perform these experiments, we monitored and compared the dynamic responses and gene regulatory functions of Msn2 and Msn4 in single cells using time-lapse microscopy and microfluidics. We used single cell measurements in this study because population level measurements often hide the true dynamics seen in single cells. For example, p53 was originally thought to respond to DNA damage with damped oscillations, but single cell measurements determined that these were oscillations of fixed height and width and the appearance of the damped oscillations at the population level was simply because of loss of synchrony between cells (Lev Bar-Or, Maya et al. 2000, Lahav, Rosenfeld et al. 2004). In another example, population measurements gave the appearance that cleavage of caspase substrates occurs gradually, but in reality, the cleavage is switch-like but highly variable between cells (Tyas, Brophy et al. 2000). Both the p53 and caspase example are illustrated in Figure I.2, which is an adaptation from Purvis and Lahav, 2013.

Thus, by tracking subcellular localization of Msn2 and Msn4 and expression of their target genes in the same single cells, we found that the two factors play distinct and cooperative roles in gene regulation. For fast kinetic activation genes, either Msn2 or Msn4 is sufficient for gene activation in response to a transient input and both factors contribute similarly to the level of gene induction. In contrast, for slow kinetic activation genes both Msn2 and Msn4 are required to control gene induction in response to a transient input, in which Msn2 functions as a “switch” governing the ON and OFF state of genes, while

Msn4 serves as a “rheostat” to tune the level of gene products being made. In response to a prolonged input, however, the slow kinetic promoter no longer requires both Msn2 and Msn4 to be fully induced and both factors contribute similarly, indicating that this combinatorial gene regulation is not fixed and depends on the dynamics of upstream signals. The coupling of the two factors is analogous to a commonly found design in electrical circuits and may be beneficial for cell survival under rapidly changing environments.

Lastly, we sought to link Msn2/4 gene regulation to phenotypic outcome or function in the cells. However, previous studies have determined that nascent protein synthesis is not necessary for basal stress response, but rather for stress response to a subsequent stress (termed acquired stress response), which indicates that gene expression triggered by a stress (including Msn2/4 controlled gene expression) is not required to survive that immediate stress but serves more of a preparative role (Berry and Gasch 2008). Additionally, cells lacking *MSN2* and *MSN4* show a defect in this acquired stress response. Therefore, cells use signaling events to encode a “memory” of previous stress in order to prepare and re-wire cellular processes appropriately in preparation for future severe stresses. This memory or priming effect appears to occur in many other organisms and biological systems, including human cells and plant cells (Raffaghello, Lee et al. 2008, Savvides, Ali et al. 2016). The mechanism underlying this cellular memory remains unknown. Using microfluidics and time-lapse microscopy (to monitor an Hog1 as an adaptation osmotic stress reporter),

we modulated the amplitude and duration of mild stress pre-treatment as well as time in between the initial stress and the severe stress. Using this system, we determined that cells acquire an amplitude-dependent short-term memory of previous stress, which is induced and lost rapidly, and a duration-dependent long-term memory which undergoes a plateau phase of stability before finally declining after very long break in between the initial mild stress and severe stress. Finally, we used this information about the different time-scales and dynamical specificity of different types of cellular memory to determine the cellular pathways responsible for the observed memory.

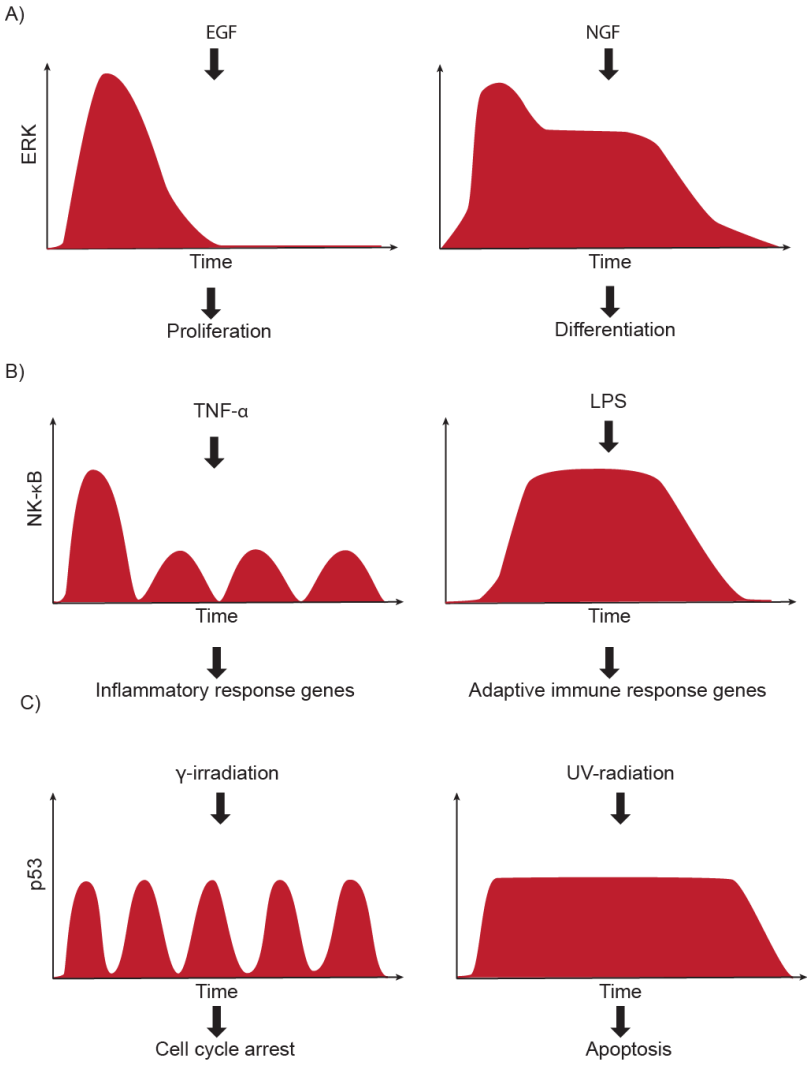

Figure I.1 Cells encode the identity of upstream signals in the dynamics of downstream signaling molecules, resulting in different phenotypic outcomes

A) In response to EGF, ERK undergoes a single transient pulse of activation, resulting in cell proliferation whereas NGF induces sustained ERK activation, resulting in cell differentiation. (B) In response to TNF-α, NF-κB exhibits oscillatory nuclear accumulation resulting in the induction of inflammatory response genes, but in response to LPS, NF-κB exhibits sustained nuclear accumulation, resulting in adaptive immune response gene induction. (C) p53, to γ-irradiation with homogenous oscillatory pulses, resulting in cell cycle arrest, but responds to UV-radiation with sustained dynamics, resulting in apoptosis.

Note: Adapted from Purvis and Lahav, 2013

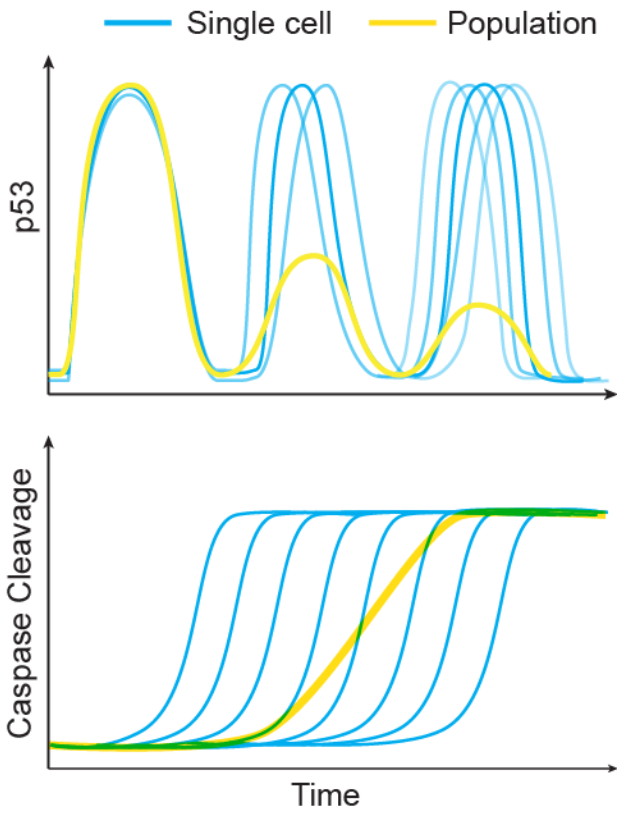

Figure I.2 Single cells measurements are important for revealing molecule dynamics

(A) Population level measurements (yellow) of p53 dynamics in response to DNA make it seem as if p53 undergoes damped oscillation, however, single cell measurements (blue) reveal that p53 actual exhibits homogenous oscillations of fixed width and height. The difference in these measurements is shown to be due to cells falling out of synchrony in their oscillation.

(B) Caspase cleavage of substrates appears to occur gradually in population level measurements (blue), but singe cell measurements (yellow), reveal the cleavage to be highly switch like but heterogeneous, accounting for the discrepancy in the two different measurements.

Note: Adapted from Purvis and Lahav, 2013

Chapter 1: Coupled Feedback Loops Control the Stimulus-Dependent Dynamics of the Yeast Transcription Factor Msn2

Abstract

Information about environmental stimuli often can be encoded by the dynamics of signaling molecules or transcription factors. In the yeast *Saccharomyces cerevisiae*, different types of stresses induce distinct nuclear translocation dynamics of the general stress-responsive transcription factor Msn2, but the underlying mechanisms remain unclear. Using deterministic and stochastic modeling, we reproduced *in silico* the different dynamic responses of Msn2 to glucose limitation and osmotic stress observed *in vivo* and found that a positive feedback loop on protein kinase A mediated by the AMP-activated protein kinase Snf1 is coupled with a negative feedback loop to generate the characteristic pulsatile dynamics of Msn2. The model predicted that the stimulus-specific positive feedback loop could be responsible for the difference between Msn2 dynamics induced by glucose limitation and osmotic stress. This prediction was further verified experimentally by time-lapse microscopic examinations of the *snf1Δ* strain. In this mutant lacking the Snf1-mediated positive feedback loop, Msn2 responds similarly to glucose limitation and osmotic stress and its pulsatile translocation is largely abrogated. Our combined computational and experimental analysis reveals a regulatory mechanism by which cells can encode information

about environmental cues into distinct signaling dynamics through stimulus-specific network architectures.

Introduction

An increasing number of studies have revealed that cells transmit environmental information by controlling the temporal dynamics of signaling molecules (Behar and Hoffmann 2010, Purvis and Lahav 2013). For example, NFκ-B exhibits oscillatory nuclear accumulation in response to tumor necrosis factor--α, but prolonged nuclear accumulation in response to bacterial lipopolysaccharide (Nelson, Ihekwaba et al. 2004, Werner, Barken et al. 2005). Similarly, the tumor suppressor p53 shows oscillatory nuclear accumulation in response to irradiation, but prolonged nuclear accumulation upon UV radiation (Batchelor, Loewer et al. 2011, Purvis, Karhohs et al. 2012). In some cases, the strength of stimulus can also be encoded into the dynamics of signaling molecules. For instance, the yeast calcium responsive transcription factor (TF) Crz1 exhibits rapid stochastic bursts of nuclear localization, the frequency of which increases with extracellular calcium concentration (Cai, Dalal et al. 2008). We have recently discovered that the yeast general stress responsive TF Msn2 encodes both the identity and strength of external stimuli into dynamic patterns of nuclear translocation (Hao and O'Shea 2012, Hao, Budnik et al. 2013). In response to glucose limitation, Msn2 exhibits an initial uniform peak of nuclear localization followed by sporadic nuclear pulses with dose-dependent frequency,

whereas in response to osmotic stress Msn2 undergoes a single translocation peak with dose-dependent duration. These different dynamic patterns of Msn2 have been shown to be crucial for inducing specific gene expression programs (Hao and O'Shea 2012, Hansen and O'Shea 2013, Hansen and O'Shea 2015, AkhavanAghdam, Sinha et al. 2016, Hansen and O'Shea 2016), however the mechanisms that give rise to distinct Msn2 dynamics remain elusive. In this study, we combined computational modeling with quantitative single-cell imaging experiments to investigate the upstream signaling networks that govern Msn2 dynamics under different stress conditions.

Results

A Model of Signaling Circuits that Drive Msn2 Translocation

We have previously revealed that different stimuli induced qualitatively distinct dynamics of Msn2 nuclear translocation in single cells (Hao and O'Shea 2012, Hao, Budnik et al. 2013). The response to glucose limitation features two phases. During the first phase, cells exhibit an adaptive translocation peak, the duration of which increases with the intensity of glucose limitation. Following the first peak, cells show persistent pulsatile nuclear localization with dose-dependent frequency (Figure 1.1A, left). In contrast, osmotic stress elicits a similar single adaptive translocation peak with dose-dependent duration, but not the subsequent pulses of nuclear localization (Figure 1.1A, right). To investigate the mechanisms underlying the differences in Msn2 dynamics, we considered the

upstream signaling pathways responsible for Msn2 nuclear translocation in response to different stimuli. Under non-stress conditions, Msn2 is phosphorylated by protein kinase A (PKA) and localized in the cytoplasm (Gorner, Durchschlag et al. 1998). Upon glucose limitation, PKA activity is reduced and, as a result, Msn2 is dephosphorylated and rapidly translocates into the nucleus (Gorner, Durchschlag et al. 2002). In addition to repression of the PKA pathway, glucose limitation activates the yeast AMP-activated protein kinase (AMPK) Snf1 (Jiang and Carlson 1996), which also participates in regulation of Msn2 by phosphorylation (De Wever, Reiter et al. 2005). Intriguingly, recent biochemical studies uncovered that Snf1 directly phosphorylates adenylate cyclase and inhibits PKA activity (Nicastro, Tripodi et al. 2015), whereas at the same time PKA also negatively regulates Snf1 activity (Barrett, Orlova et al. 2012). These findings suggest the existence of a mutual inhibitory network that acts on the upstream of Msn2 in response to glucose limitation. In contrast, osmotic stress does not induce Snf1 activation (Hong and Carlson 2007) and triggers Msn2 nuclear localization primarily through repressing PKA activity (Petrenko, Chereji et al. 2013). Based on these previous studies, we hypothesized that the difference between glucose limitation and osmotic stress-induced Msn2 dynamics might be attributed to specific upstream network structures, in particular, the glucose limitation-dependent Snf1 activation (Figure 1.1B).

To test this hypothesis *in silico*, we developed a computational model of signaling circuits that process environmental stimuli and drive Msn2 translocation. The model is centered on the regulation of PKA signaling and includes a negative feedback loop mediated by the small G-protein Ras and its GTPase-activating proteins (GAPs)(Nikawa, Cameron et al. 1987) and a positive feedback loop through Snf1. The inputs of the model are the levels of extracellular glucose and osmotic stress, which are measured by dimensionless parameters (Gluc, OsmStr). The output is the nuclear localized Msn2 ($Msn2_n$). Previous models of the yeast Ras-cAMP-PKA network proposed that the negative feedback loop mediated by Ras plays a crucial role in shaping Msn2 dynamics (Garmendia-Torres, Goldbeter et al. 2007, Gonze, Jacquet et al. 2008). To further simplify the system while keeping this core network structure, we assume that the PKA activity is always proportional to and at equilibrium with the cAMP level and combined cAMP and PKA into a single variable denoted as "cAMP/PKA". Similarly, we combined Ras and adenylate cyclase into a single variable "Ras/CYCL". Importantly, we also incorporated into the model the AMPK Snf1, the activity of which is dependent on the glucose level but not the osmotic stress level. Based on previous experimental results, a positive feedback loop on PKA activity takes the form of PKA inhibition of Snf1, which represses PKA activation. Finally, both PKA and Snf1 promote the exit of Msn2 from the nucleus. The schematic of the model is illustrated in Figure 1.1C and the details are included in Materials and Methods– *Computational modeling*.

Model Simulations of Msn2 Dynamics upon Different Stimuli

To examine whether this model can describe the observed Msn2 dynamics under different conditions, we focused on reproducing three primary dynamic features of Msn2 responses: (1) the initial adaptive peak upon glucose limitation or osmotic stress; (2) the persistent pulsatile pattern upon glucose limitation but not osmotic stress; (3) the dependence of translocation duration or frequency on stress intensity (Hao and O'Shea 2012).

The simulated time traces from the deterministic version of the model are shown in Figure 1.2A. Glucose limitation first triggers a strong increase in Snf1 activity (green curve) and a strong drop in PKA activity (black curve). Because of the effect of negative feedback loop via GAP, PKA activity recovers and rises up after a short period of time. Meanwhile, due to the cross-inhibition between PKA and Snf1, the increase in PKA activity causes a decrease in Snf1 activity, which further pushes the rise of PKA activity across the baseline. When PKA reaches its peak value, the negative feedback loop takes effect to bring down PKA activity. Snf1 then rises again to push the drop of PKA activity across the baseline. In this way, the coupled negative and positive feedback loops force PKA to overshoot and undershoot the steady state repeatedly, resulting in sustained oscillations of PKA activity accompanied with the anti-phase oscillation of Snf1 activity. These temporal patterns of PKA and Snf1 lead to an initial adaptive peak with subsequent pulsatile dynamics of Msn2 translocation (red

curve) (Figure 1.2A, left). In contrast, osmotic stress does not regulate Snf1 activity directly. Instead, the stress induces a strong decrease in PKA activity, which causes a slight increase of Snf1 that is insufficient to enable dramatic overshooting of PKA from the steady state. As a result, both PKA and Snf1 undergo rapidly damped oscillations that reach steady states quickly and Msn2 exhibits a single translocation peak without following pulsatile nuclear localization (Figure 1.2A, right). These distinct dynamic behaviors can also be demonstrated by the corresponding phase plane trajectories of PKA and GAP: the system approaches a stable limit cycle under glucose limitation (solid trajectory), but spirals into a steady state upon osmotic stress (dashed trajectory) (Figure 1.2B). To illustrate how stress intensity influences the oscillatory behaviors, we used a bifurcation graph to show the transition from a stable steady state to the oscillatory regime as a function of the stress level. As shown in Figure 1.2C, upon glucose limitation beyond a critical level, PKA oscillations occur spontaneously (solid curves; oscillation between maximal and minimal values); by contrast, in response to osmotic stress, the system always returns to the baseline as a stable steady state independent of stress intensity (dashed line). Note that the level of the steady state is independent of the osmotic stress level, which is a manifestation of the perfect adaptation that many signaling cascades exhibit (Ma, Trusina et al. 2009) (see more details in Materials and Methods–"Achieving perfect adaptation"). The robustness of the modeling behaviors, and particularly, the dependence of oscillations on the strength of negative and

positive feedback loops have been evaluated and discussed in details in Materials and Methods – “Robustness of the modeling behaviors”.

To account for the irregular nature of Msn2 dynamics observed in single cells, we further performed stochastic simulations of the model using the adaptive tau-leaping algorithm (Cao, Gillespie et al. 2007). As shown in Figure 1.3A, the time traces of Msn2 nuclear translocation from stochastic simulations nicely resembled single-cell time traces of Msn2 translocation in response to glucose limitation and osmotic stress from experimental results (Figure 1.1A)(Hao and O'Shea 2012, Hao, Budnik et al. 2013). In addition, to evaluate the effects of stress intensity on Msn2 dynamics, we quantified the durations of the initial peak and the frequencies of subsequent pulses from simulations under various stress conditions. As shown in Figure 1.3B, top panels (“Model simulations”), the durations of the initial peak increase with stress intensity upon glucose limitation (leftmost) and osmotic stress (rightmost). Furthermore, at low intensities of glucose limitation below the critical point for PKA oscillation (the transition point between the stable steady state and the oscillatory regime in Figure 1.2C), Msn2 pulses after the initial peak are primarily driven by noise (but not PKA oscillations) and hence are with low frequencies; in contrast, the pulsatile Msn2 dynamics at high intensity of glucose limitation above the critical point are driven by PKA oscillations and thereby exhibit higher frequencies. As a result, increasing intensity of glucose limitation results in a nonlinear increase in the frequency of translocation pulses with a substantial increase over the

threshold intensity that corresponds to the critical point (Figure 1.3B, “Model simulations” - middle). These dynamic modulations of Msn2 responses by stress intensity are consistent with our previous experimental results (Hao and O'Shea 2012) (Figure 1.3B, bottom panels - “Experimental results”).

Taken together, our model nicely reproduced the major dynamic patterns and dose dependence of Msn2 responses to different stresses and suggested that a glucose limitation-specific positive feedback loop mediated by Snf1 might give rise to the differences in Msn2 dynamics to stresses.

Model Predictions and Experimental Validation

To examine the effects of the Snf1-mediated positive feedback loop on Msn2 dynamics, we removed Snf1 from our model and simulated the time traces of Msn2 nuclear localization under different stress conditions. The removal of Snf1-mediated positive feedback loop slows down the effect of the GAP-mediated negative feedback and results in a prolonged drop in PKA activity (Figure 1.4A, top panels; compare with Figure 1.2A, top panels). This leads to an extended duration of the initial nuclear peak of Msn2 (Figure 1.4A, bottom panels *vs* Figure 1.3A; an increase of 26.9% in the simulated initial peak duration), consistent with our experimental observations (an increase of 27.7% in the measured average duration of the initial peak) and previously published literature (De Wever, Reiter et al. 2005, Petrenko, Chereji et al. 2013). More importantly, the model predicted that the deletion of *SNF1* abrogates PKA oscillations and, as

a result, Msn2 responds similarly to glucose limitation and osmotic stress, both with a single translocation peak but no following pulses (Figure 1.4A, bottom panels). We further showed that the absence of oscillations is independent of the intensity of glucose limitation (Figure 1.4B). To test the model predictions, we performed experiments using time-lapse microscopy to monitor Msn2 nuclear localization in single yeast cells lacking the *SNF1* gene (Figure. 1.4C). We observed that the majority of *snf1Δ* cells no longer exhibited persistent pulsatile Msn2 translocation following the initial peak in response to glucose limitation (Figure 1.4C, left), strikingly different from WT cells (Figure 1.4D). In contrast, upon osmotic stress, the absence of *SNF1* did not alter the dynamic response of Msn2 following the initial peak (Figure 1.4C, right). As a result, in the *snf1* mutant, glucose limitation and osmotic stress induced similar dynamic patterns of Msn2 translocation, both showing a major adaptive peak. These experimental results validated the model predictions and confirmed the important role of Snf1 in generating persistent pulsatile Msn2 dynamics.

In summary, our combined computational and experimental analysis uncovered a mechanism that accounts for differential Msn2 dynamics to distinct types of stresses. Glucose limitation directly modulates both PKA and AMPK Snf1 to activate a positive feedback loop that is coupled with the PKA-driven negative feedback to enable persistent oscillations and pulsatile dynamics. Osmotic stress, however, can only modulate PKA activity and hence fails to

activate the Snf1-dependent positive feedback, resulting in rapidly damped oscillations and adaptive Msn2 dynamics.

Discussion

Substantial modeling efforts have been devoted to simulating the yeast cAMP/PKA pathway and the pulsatile dynamics of Msn2 (Garmendia-Torres, Goldbeter et al. 2007, Gonze, Jacquet et al. 2008, Besozzi, Cazzaniga et al. 2012, Pescini, Cazzaniga et al. 2012, Petrenko, Chereji et al. 2013). Most of these models are derived from an earlier work by Goldbeter, Jacquet and co-workers (Garmendia-Torres, Goldbeter et al. 2007), in which a negative feedback loop enables sustained PKA oscillations and pulsatile Msn2 translocation. Building upon these previous efforts, we took a step further to consider the signaling network structures that give rise to the distinct Msn2 responses to different stresses. Importantly, we incorporated in our model the stimulus-specific activation of the AMPK Snf1, which interconnects with and constitutes a positive feedback on cAMP/PKA signaling (Figure 1.1C). Using modeling and experiments, we showed that this newly added positive feedback loop, coupled with the previously characterized negative feedback on PKA, plays a crucial role in generating persistent pulsatile Msn2 translocation and producing specific dynamic responses to various stresses. Network topologies with these coupled feedback loops have been proposed as a general design principle for robust oscillators in various systems (Novak and Tyson 2008, Stricker, Cookson et al.

2008). In addition, because of our aim at identifying the core network structures, we significantly reduced the complexity of previous models and constructed our model in a very concise manner with a minimum number of variables and parameters. Remarkably, while previous models focused primarily on describing the persistent pulsatile patterns of Msn2 translocation, our model, although very simple, was capable of reproducing both these oscillations and other major dynamic behaviors of Msn2 observed experimentally, such as the initial adaptive peak and the dose-dependent durations and frequencies (Figure 1.2 and Figure 1.3). Finally, we want to note that about half of the cells exhibit a second translocation peak of Msn2 following the initial peak in response to the sorbitol treatment (see Figure 1.4C, right column, “Cell 3” as an example). This second peak has been shown to depend on stress-dependent downstream transcriptional responses (Petrenko, Chereji et al. 2013) and hence was not taken into consideration in our model. We also noticed that some *snf1Δ* cells did not fully recover to the baseline after adaptation or showed small fluctuations around the steady state (with the amplitude way below the threshold for pulse identification defined in Supplemental Information and previous studies (Hao and O'Shea 2012); see Figure 1.4C, left column, “Cell 4” as an example), which are distinct from translocation pulses. These observations might suggest a role of Snf1in adaptation and noise regulation that is not included in the current model.

Biologically, our work revealed a novel mechanism for encoding stimulus-specific dynamics, in which the stimulus-dependent integration of the AMPK Snf1

pathway with the PKA pathway gives rise to distinct Msn2 dynamics upon glucose limitation and osmotic stress. PKA and AMPK are both highly conserved kinases and mediate parallel signaling pathways that play important roles in regulating metabolism, cell growth and stress resistance in response to nutrients and stresses (Hardie 2007, Zaman, Lippman et al. 2008, Conrad, Schothorst et al. 2014). How these two pathways interact and coordinate is of significant interest to the field (Shashkova, Welkenhuysen et al. 2015). Previous studies have been primarily focused on identifying the genetic and biochemical connections between the pathways. The functional relevance of pathway interconnectivity, however, remains largely unclear. Our work demonstrated that the interconnections of the PKA and AMPK pathways generate persistent pulsatile dynamics of a common downstream TF Msn2 and contribute to response specificity to different stimuli. More generally, our findings represent a striking example in which the integration of different signaling pathways leads to specific dynamic patterns of downstream TFs that encode environmental information.

Our work focused specifically on glucose limitation and osmotic stress. How cells encode other stresses remains unaddressed. For example, oxidative or ethanol stress induces sustained Msn2 accumulation in the nucleus, the amplitude of which increases with stress intensity (Hao and O'Shea 2012). It would be interesting to investigate the signaling pathways and regulatory mechanisms that underlie this amplitude modulation of TF dynamics. The other

remaining question is how cells respond to combinations of stresses. As described in Materials and Methods - “Stress inputs”, our current model was designed to simulate the dynamic responses to glucose limitation or osmotic stress, but not combined stress treatments. A careful quantitative examination of the interaction between glucose and osmotic stress at the level of Ras activation will enable us to incorporate a more accurate mathematical description of this interaction and to further improve the predictive power of our model towards complex environmental cues. Finally, another important question in the temporal coding of signals is how cells interpret the dynamic patterns of TF activation to achieve specificity in cellular responses (Bardwell, Zou et al. 2007). Our previous work has focused on the simple scenario in which individual downstream genes directly decode dynamic TF input into differential expression output depending on their promoter affinity and activation kinetics (Hao and O'Shea 2012). Given that many TFs, such as Msn2, regulate a large set of downstream genes that interact into a complex network, further analysis is needed to understand how transcriptional networks process TF dynamics to control cellular functions. In particular, previous studies have identified a few recurring characteristic circuit patterns, termed “network motifs” (Milo, Shen-Orr et al. 2002, Milo, Itzkovitz et al. 2004, Alon 2007), which are considered the basic building blocks of transcriptional networks of diverse organisms, from bacteria to humans (Alon 2007). How these network motifs function to decode TF dynamics would be an interesting topic for future studies.

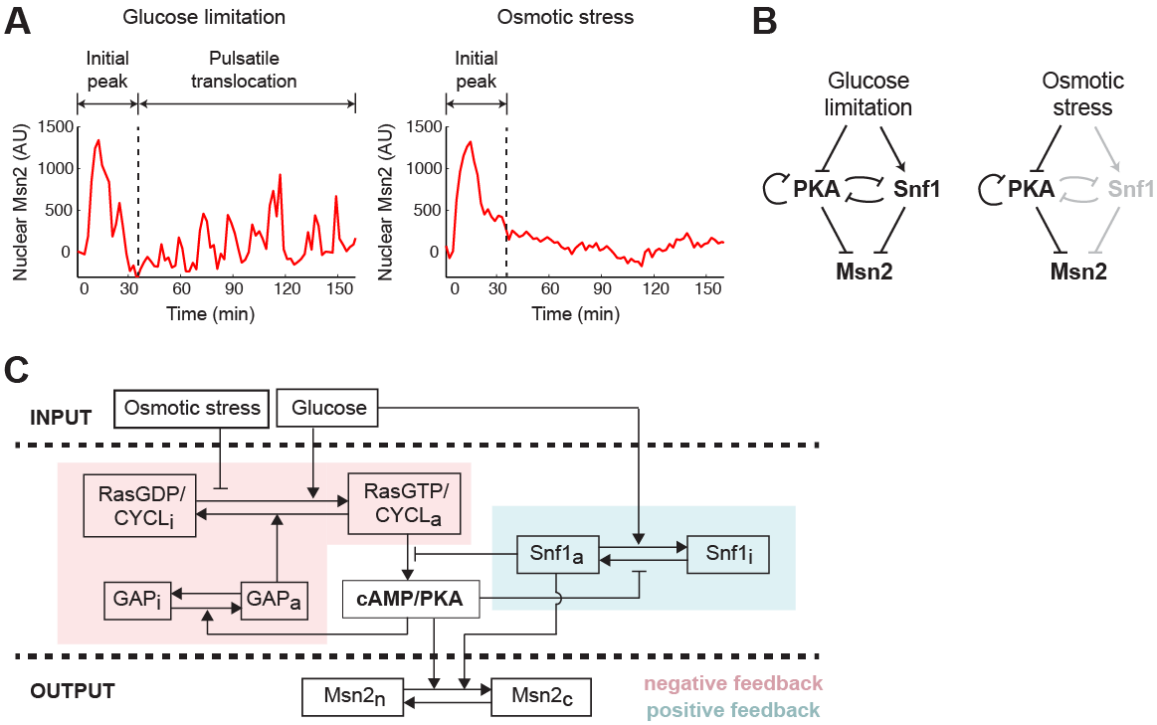

Figure 1.1. A computational model for stimulus-dependent Msn2 dynamics. (A) Illustration of distinct Msn2 dynamics in response to glucose limitation and osmotic stress. Representative single-cell time traces of Msn2 nuclear localization in response to 0.2% glucose (left: glucose limitation) or 1 M sorbitol (right: osmotic stress) are shown. (B) Diagram of major signaling pathways that govern Msn2 responses. Glucose limitation is mediated by both PKA and Snf1 to drive Msn2 dynamics (left). Osmotic stress is primarily mediated through PKA, so Snf1 is grayed out to illustrate that it is not activated by osmotic stress (right). (C) Scheme of the computational model. The variables of the model include: RasGDP/CYCL$_i$ and RasGDP/CYCL$_a$ – the inactive and active fractions of Ras/adenylate cyclase, GAP$_i$ and GAP$_a$ – the inactive and active fractions of GAP proteins (Ira1/2), cAMP/PKA – the level of cAMP/active PKA, Snf1$_i$ and Snf1$_a$ – the inactive and active fractions of Snf1, and Msn2$_c$ and Msn2$_n$ – the cytoplasmic and nuclear fractions of Msn2. The glucose level influences the activation of Ras/cyclase and the inactivation of Snf1, while the level of osmotic stress represses only the activation of Ras/cyclase. A negative feedback loop through GAP and Ras/cyclase on PKA is highlighted in pink and a positive feedback loop via Snf1 on PKA is highlighted in blue

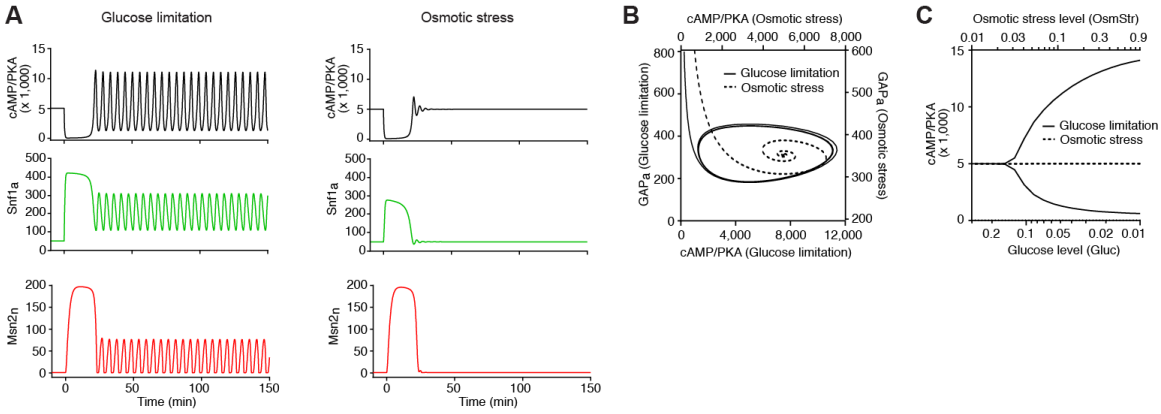

Figure 1.2 Model simulations of PKA, Snf1, and Msn2 dynamics in response to different stresses. (A) Simulated time traces of active PKA (cAMP/PKA – black), active Snf1 ($Snf1_a$ – green), and nuclear Msn2 ($Msn2_n$ – red) in response to glucose limitation (left) and osmotic stress (right) from the deterministic model. The unit for y-axis is molecules/cell. For glucose limitation and osmotic stress, we used the dimensionless parameters Gluc and OsmStr to measure the intensity of stresses. Gluc = 1, OsmStr = 0 are used for the non-stress condition; Gluc = 0.05, OsmStr = 0 are used to generate the simulated time traces for glucose limitation (left); Gluc = 1, OsmStr = 0.95 are used to generate the simulated time traces for osmotic stress (right). As described in details in Supplemental Information, the rate of Ras activation is assumed to depend linearly on both glucose and osmotic stress levels in the form of $rate \propto Gluc.(1 - OsmStr)$. The above values of Gluc and OsmStr are selected so that glucose limitation and osmotic stress would have the same effect on Ras activation and hence any difference in the output can only be attributed to the Snf1-mediated positive feedback. (B) Phase plane trajectories of cAMP/PKA and GAP_a corresponding to the simulated system dynamics in (A). The trajectory under glucose limitation is represented by solid curve (use y-axis on the right and x-axis on the bottom); the trajectory under osmotic stress is represented by dashed curve (use y-axis on the left and x-axis on the top). (C) Bifurcation diagram showing the maximum and minimum values of cAMP/PKA in the asymptotic regime ($t \to \infty$) as a function of the intensity of glucose limitation (solid curves; use x-axis on the bottom) or osmotic stress (dashed line; use x-axis on the top).

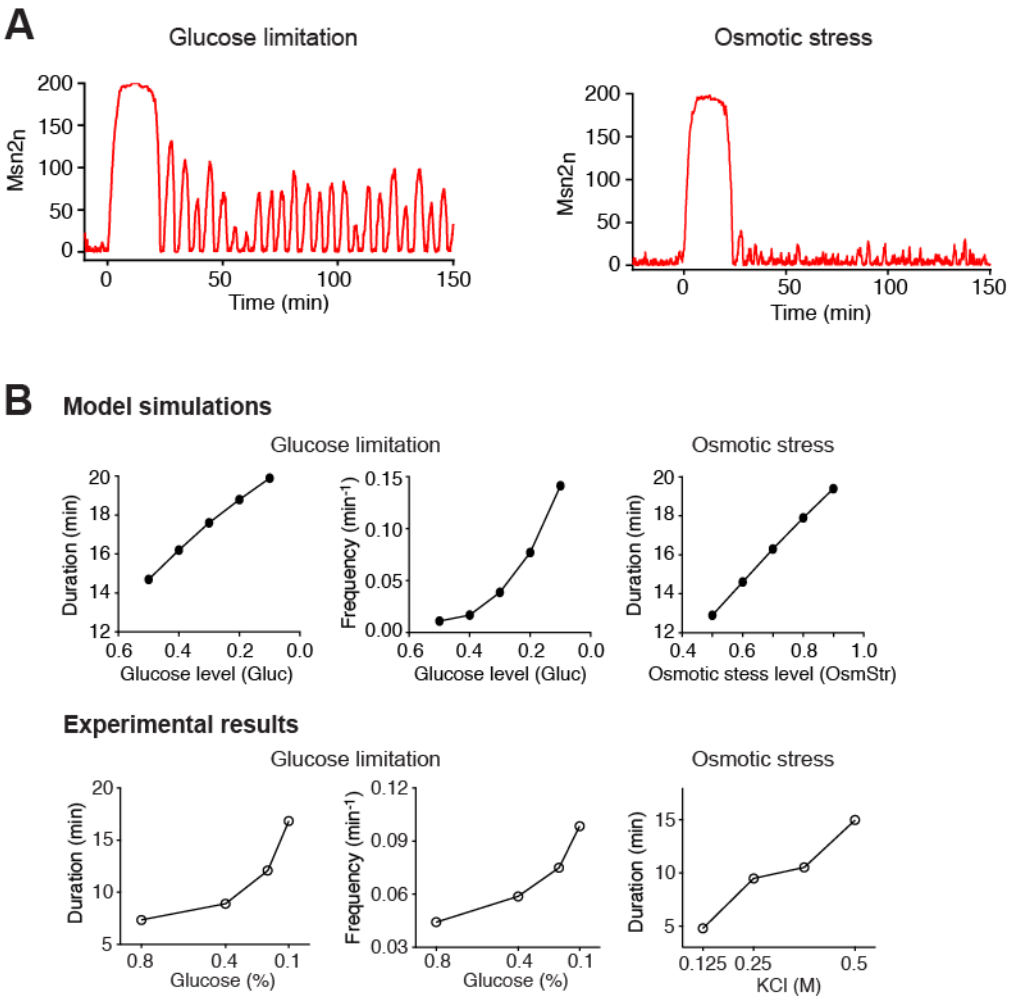

Figure 1.3 Model simulations of Msn2 dynamics in response to different stresses. (A) Simulated time traces of nuclear Msn2 from the stochastic model in Figure 1.2. The values of Gluc and OsmStr are identical to those used in (Figure 1.2A) to simulate glucose limitation and osmotic stress. (B) Dependence of Msn2 dynamics on stress intensity. Top panels are model simulations. The durations of the initial peaks for both glucose limitation (leftmost) and osmotic stress (rightmost) were quantified from deterministic simulations and the pulse frequencies under glucose limitation (middle) were calculated from stochastic simulations by setting a threshold for pulse identification (see Materials and Methods for details). Bottom panels are experimental results. The plots were generated using single-cell data from (Hao and O'Shea 2012).

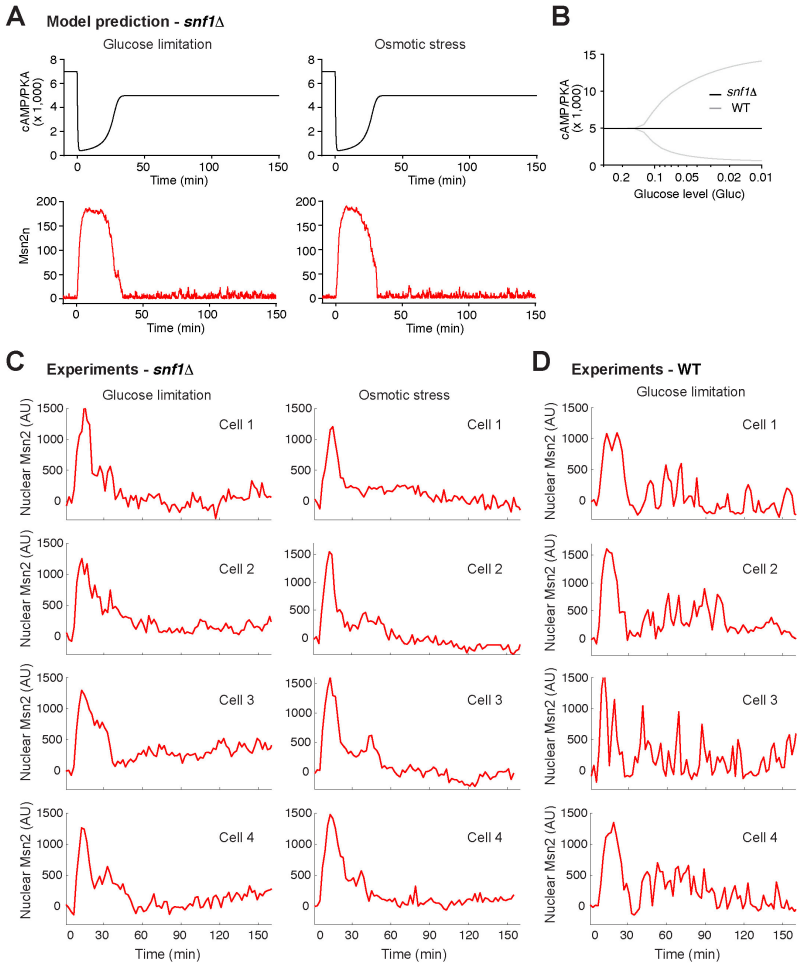

Figure 1.4 Model prediction and experimental validation of Msn2 dynamics in the absence of Snf1. (A) Simulated time traces of active PKA (cAMP/PKA – black) and nuclear Msn2 ($Msn2_n$ – red) in the absence of Snf1 in response to glucose limitation (left) and osmotic stress (right) from the stochastic model. The values of Gluc and OsmStr are identical to those used in Figure 1.2A to simulate glucose limitation and osmotic stress. (B) Bifurcation diagram showing the maximum and minimum values of cAMP/PKA during oscillations as a function of the intensity of glucose limitation, in the presence (gray) or absence (black) of Snf1. (C) Experimental results of Msn2 dynamics in the absence of Snf1. Representative single-cell time traces of Msn2 nuclear localization in the *snf1Δ* mutant are shown for the responses to 0.2% glucose (left: glucose limitation; the total number of cells imaged: n=186) or 1 M sorbitol (right: osmotic stress; the total number of cells imaged: n=176). (D) Experimental results of Msn2 dynamics in WT cells. Representative single-cell time traces of Msn2 nuclear localization in WT are shown for the responses to 0.2% glucose (glucose limitation; the total number of cells imaged: n=212).

Materials and Methods:

Strain construction

Standard methods for the growth, maintenance and transformation of yeast and bacteria and for manipulation of DNA were used throughout. All *Saccharomyces cerevisiae* strains used in this study are all derived from W303 ADE+ *MAT*a trp1 leu2 ura3 his3 can1 GAL+ psi+. A standard lithium acetate based transformation method was used to generate our synthetic yeast strains. DNA fragments for genomic insertion were amplified using Phusion High Fidelity DNA Polymerase and purified using Invitrogen PureLink PCR purification kit. A list of yeast strains generated and used in this study is provided in Table 1.1. Msn2 was C-terminally tagged with a linker- yeast codon-optimized mCherry from a pKT vector. The *snf1Δ* strain was generated by replacing the endogenous *SNF1* ORF with *URA3*. Nhp6a has been C-terminally tagged with iRFP to serve as a nuclear marker for imaging analysis

Table 1.1 Yeast strains used in Chapter 1 study

Strain Name	Description
NH0267	W303 *MAT*a, *NHP6a-iRFP-kanMX, MSN2-mCherry-TRP*
NH0582	W303 *MAT*a, *snf1::URA3, NHP6a-iRFP-kanMX, MSN2-mCherry-TRP*

Medium and solutions

The low fluorescence Synthetic Complete (SC) medium + 2% glucose used to culture cells for microfluidics was made up of 1.71g YNB-Folic Acid-Riboflavin Powder, 0.74 g Complete Supplemental Mixture (CSM), 2% glucose, and 5g Ammonium Sulfate per 1L of medium. Concanavalin A (Con A) (Type IV, Sigma-Aldrich) solution containing 5 mM $CaCl_2$, 5 mM $MnCl_2$, and 2 mg/mL Con A was stored at -20°C and thawed at room temperature just before each experiment. For the glucose limitation treatment, the medium (low fluorescence SC medium + 0.2% glucose) was made up of 1.71g YNB-Folic Acid-Riboflavin Powder, 0.74 g Complete Supplemental Mixture (CSM), 0.2% glucose, and 5g Ammonium Sulfate per 1L of medium. For the osmotic stress condition, the medium (low fluorescence SC medium + 0.2% glucose + 1M sorbitol) was made up of 182.17 g sorbitol powder, 1.71g YNB-Folic Acid-Riboflavin Powder, 0.74 g Complete Supplemental Mixture (CSM), 2% glucose, and 5g Ammonium Sulfate per 1L of medium.

Microfluidics

Fabricating microfluidics wafers and chips

The microfluidics device used in this study is modified from a previously reported device (Hersen, McClean et al. 2008), so that two independent experiments can be run in parallel on a single chip. The mask was designed to allow for bonding of two antiparallel Y-shaped devices on one microfluidics chip.

The SU8 wafer was fabricated using standard photolithography with channel width 400μm and channel height 111μm. It is important to note that the inhibitor is absorbed by PDMS and therefore one must design the channel such that its volume is much greater than surface area (e.g. minimize surface interactions between the PDMS and inhibitor). Microfluidic chips were made by pouring PDMS (polydimethylsiloxane) onto the wafer, degassing, and curing in 80°C oven for one hour. The PDMS was then removed from the wafer and individual chips were cut and hole punched using a Harris Uni-Core 1.00 puncher. The chips were cleaned using first 70% ethanol and then water to remove debris. Coverslips (Thermo Scientific Gold Seal Cover Glasses; Rectangles; 24 x 50mm; Thickness 1.5) were subsequently cleaned with heptane, methanol, and water. The coverslips and microfluidics chips (with features facing up) were then exposed to ozone in a UVO bonder for three minutes after which the chips were immediately placed on top of coverslips and left in an 80°C oven overnight to secure the bonding.

Yeast growth conditions for microfluidics

Yeast were inoculated in in low fluorescence Synthetic Complete (SC) media + 2% glucose overnight at 30°C. Next, 2µL (for WT) or 10µl (for the *snf1Δ* *s*train) of the overnight culture was then transferred to independent flasks containing 20 mL of low fluorescence SC + 2% glucose and grown to an A_{600nm} of

0.5 (exponential growth phase) the following day for loading into microfluidics chip.

Setting up microfluidics experiments

For each experiment, two media inlet tubes with 20 mL of media and one waste outlet tube with 10 mL SC were set up next to the microscope. The tubes were set up to allow for a 10 cm height difference between the inlets and the outlet. Soft polyethylene tubing (Intramedic, inner diameter, 0.86 mm; outer diameter, 1.27 mm) was then placed into the media and a 1 mL syringe was used to prime the lines. A binder clip was then used to stop the flow and a 20 gauge connector was inserted into the end of the tubing for later attachment of the line to the microfluidics chip.

The microfluidics chip was placed in a vacuum chamber for 20 minutes before starting the experiment to evacuate any air from the channels. Once removed from the vacuum, water drops were then immediately added to each port to prevent re-introduction of any air. A solution of 2 mg/mL concanavalin A (ConA) was then injected into the channels of the chip using a 1 mL syringe inserted into an ~1.5in segment of polyethylene tubing with a 20 gauge connector. The chip was then left to incubate for roughly 15 minutes. Using a similar method, SC from a fresh syringe was then flowed into our channel used to wash off excess ConA after incubation. Yeast cells were then spun down at 3000 rpm for one minute (Eppendorf 5804/5804R centrifuge) and re-suspended in 3-5

mL of SC depending on OD. The resuspended cells were then loaded into the microfluidics channel and incubated inside the chip for 10 minutes to allow for sufficient adhesion to the glass. A small air bubble followed by a small volume of SC was then intentionally introduced into each channel using our syringe to remove any vertically stacked yeast and obtain a monolayer of yeast cells for imaging. The chip was then mounted onto our microscope using a specially designed holder and taped securely to the stage to prevent unwanted movement. The chip was then connected to the two media inlets first. The flow from the inlet with low glucose media was always immediately cut off using a binder clip allowing flow only from SC to avoid pre-stressing cells. The waste port was then connected, completing the flow circuit in our device. Tubing was subsequently taped to the stage to minimize any stresses or vibrations on the chip that can cause spurious stage movement during experiments

Time-lapse microscopy

All time-lapse microscopy experiments were performed on a Nikon Ti-E inverted fluorescence microscope with Perfect Focus, coupled with an EMCCD camera (Andor iXon X3 DU897). The light source is a Spectra X LED system. Images were taken using a CFI Plan Apochromat Lambda DM 60X Oil Immersion Objective (NA 1.40 WD 0.13MM). During experiments, the microfluidic device was taped to a customized device holder and inserted onto the motorized stage (with encoders) of the microscope. Six positions were chosen for each

channel and the microscope was programmed to acquire Phase, mCherry, and iRFP images every two minutes for 3 hours. The exposure and intensity settings for each channel were set as follows: mCherry 300 ms at 10% lamp intensity, and iRFP 200 ms at 15% lamp intensity. The camera was set to an EM Gain of 300 (within the linear range). When the image acquisition started, cells were first maintained in low fluorescence SC media + 2% glucose for the first five minutes to obtain a fluorescence baseline prior to the introduction of any stressor. To introduce glucose limitation or osmotic stress, the flow from the inlet with low fluorescence SC media + 2% glucose was manually switched to the flow from the inlet with the stressor media using binder clips. Fluorescence microscopy image stacks were pre-processed using ImageJ for background subtraction. Images were then processed using a custom MATLAB code for single-cell tracking and fluorescence quantification as described previously (Hao and O'Shea 2012, Hao, Budnik et al. 2013).

Computational modeling

The computational model and all our simulations were done with the biochemical simulation software “COPASI” (Hoops, Sahle et al. 2006). The adaptive SSA/tau leaping algorithm was used for all the stochastic simulations (Cao, Gillespie et al. 2007). All simulations were done with time interval of 0.1 minute. Simulated data were analyzed using MATLAB.

Model structure and species

Compared to previous models of the yeast cAMP/PKA pathway (Garmendia-Torres, Goldbeter et al. 2007, Gonze, Jacquet et al. 2008, Besozzi, Cazzaniga et al. 2012, Pescini, Cazzaniga et al. 2012, Petrenko, Chereji et al. 2013), our model combined some species to reduce the numbers of variables and parameters and to simplify the simulations. Specifically, we assume that the PKA activity is always proportional and at equilibrium with the cAMP level so that cAMP and PKA were considered as one single species, denoted as "cAMP/PKA" in our diagram. Similarly, Ras and CYCL were combined as one single species, too. Its active form is "RasGTP/$CYCL_a$" and its inactive form is "RasGDP/$CYCL_i$" in our diagram. In the model, glucose and osmotic stress are inputs measured by dimensionless parameters (Gluc, Str) that mainly change some rate constants while Msn2 is coupled to the core network and considered as the output. The core network is composed of both a negative feedback and a positive feedback. The negative feedback involves the GAP activation by PKA, which then decreases cAMP/PKA production/activation by promoting inactivation of Ras. The positive feedback is mediated through the Snf1 inhibition by PKA, resulting in an increase in the cAMP/PKA activity (because Snf1 represses PKA). This positive feedback is only present when glucose level is low, which is implemented in our model using a Hill function of glucose in our model ($k_{9)}$. The coupling of Msn2 to PKA pathway is relatively simple compared to previous models. There are only two Msn2 related species in our model - the nuclear

localized Msn2, $Msn2_n$ and the cytoplasmic localized Msn2, $Msn2_c$. Translocation of Msn2 from the nucleus to the cytoplasm is controlled by PKA and Snf1.

Units and initial conditions

In our model, the numbers of molecules per cell were used as the units for species levels (instead of concentrations) to enable easy implementations of both deterministic and stochastic simulations. The steady state of the WT strain in absence of any stresses was chosen to be the initial condition. The molecule numbers of all species at the initial condition are summarized below in Table 1.2.

Table 1.2. Initial conditions of all the species.

Species	Molecules/cell	Reference
cAMP/PKA	5007	(Ghaemmaghami, Huh et al. 2003)
RasGDP/$CYCL_i$	2697	Species not defined in this work
RasGTP/$CYCL_a$	303	Species not defined in this work
GAP_i	2	(Breker, Gymrek et al. (2013)
GAP_a	3998	(Breker, Gymrek et al. (2013)
$Snf1_a$	38	(Ghaemmaghami, Huh et al. 2003)
$Snf1_i$	462	(Ghaemmaghami, Huh et al. 2003)
$Msn2_n$	0	(Ghaemmaghami, Huh et al. 2003)
$Msn2_c$	200	(Ghaemmaghami, Huh et al. 2003)

Reactions and rate constants

In order to do stochastic simulations with COPASI, all reactions were chosen to be irreversible. Their rate constants and binding constants are listed below in Table 1.3.

Table 1.3. Reactions and rate constants in the model

Name	Reaction	Rate	Rate constants (min^{-1})	Binding constants (#)	Notes
GAP activation	$GAP_i \rightarrow GAP_a$	$\frac{k_1[cAMP/PKA][GAP_i]}{Km_1 + [GAP_i]}$	$k_1 = 0.032$	$Km_1 = 1$	Km_1 and Km_2 are chose to be very small in order to achieve cAMP/PKA adaptation
GAP inactivation	$GAP_a \rightarrow GAP_i$	$\frac{k_2[GAP_a]}{Km_2 + [GAP_a]}$	$k_2 = 160$	$Km_2 = 1$	
cAMP/PKA production/ activation	→ cAMP/PKA	$k_3[RasGTP/CYCL_a]$	$k_3 = \frac{5000}{50 + [Snf1_a]}$		
cAMP/PKA degradation/inactivation	cAMP/PKA →	$k_4[RasGTP/CYCL_a]$	$k_4 = 3$		
Ras/CYCL activation	$RasGDP/CYCL_i$ → $RasGTP/CYCL_a$	$\frac{k_5[RasGDP/CYCL_i]}{Km_5 + [RasGDP/CYCL_i]}$	$k_5 = 20000 \cdot Gluc \cdot (1 - Str) + 1200$	$Km_5 = 100$	The 1200 term in the k_5 is the basal level activation rate

Table 1.3 Reactions and rate constants in the model, continued

Name	Reaction	Rate	Rate constants (min^{-1})	Binding constants (#)	Notes
Ras/CYCL inactivation	$RasGTP/CYCL_a \rightarrow RasGDP/CYCL_i$	$\frac{k_7[GAP_a][RasGTP/CYCL_a]}{Km_7 + [RasGTP/CYCL_a]}$	$k_7 = 10$	$Km_7 = 200$	
Snf1 activation	$Snf1_i \rightarrow Snf1_a$	$k_8[Snf1_i]$	$k_8 = \frac{6000}{500 + [cAMP/PKA]}$		PKA negatively regulates Snf1 activation
Snf1 inactivation	$Snf1_a \rightarrow Snf1_i$	$\frac{k_9[Snf1a]}{Km_9 + [Snf1_a]} + k_{10}[Snf1_a]$	$k_9 = \frac{16000 \cdot Gluc^4}{1 + Gluc^4}$ $k_{10} = 2$	$Km_9 = 1000$	Hill function is intended for Snf1 sharp response to glucose level change. k_{10} is the basal level Snf1 inactivation
Msn2 phosphoralation/translocation from nucleus to cytoplasm	$Msn2_n \rightarrow Msn2_c$	$\frac{k_{11}[cAMP/PKA][Msn2_n]}{Km_{11} + [Msn2_n]} + \frac{k_{12}[Snf1_a][Msn2_n]}{Km_{12} + [Msn2_n]}$	$k_{11} = 0.02$ $k_{12} = 0.002$	$Km_{11} = 300$ $Km_{12} = 200$	
Msn2 dephos/translocation from cytoplasm to nucleus	$Msn2_c \rightarrow Msn2_n$	$\frac{k_{13}[Msn2_c]}{Km_{13} + [Msn2_c]}$	$k_{13} = 200$	$Km_{13} = 0.2$	

Stress inputs

Glucose limitation and osmotic stress are two different types of stresses. In order to compare their effects in the model, both glucose and osmotic stress levels are specified by dimensionless parameters (Gluc, OsmStr) chosen to be between 0 and 1. We set Gluc to be 1 under the normal condition and then decrease to the level between 0 and 1 to simulate glucose limitation conditions. For osmotic stress, we set OsmStr to be 0 under the normal condition and then increase the level to values between 0 and 1 to simulate osmotic stress conditions (Gluc = 1). We also assumed that the dependence of Ras activation on these parameters is represented in a bi-linear fashion in the form of: $\boldsymbol{rate} \propto \boldsymbol{Gluc}.\ (\mathbf{1} - \boldsymbol{OsmStr})$ (rate constant of Ras activation, k_5, see Table 2.3). By doing so, the effects of two different stresses can be fairly compared in our analysis. For example, in Figure 1.2A, Gluc = 1, OsmStr = 0 are used for the non-stress condition; Gluc = 0.05, OsmStr = 0 are used to generate the simulated time traces for glucose limitation; Gluc = 1, OsmStr = 0.95 are used to generate the simulated time traces for osmotic stress. These values of Gluc and OsmStr are selected so that glucose limitation and osmotic stress would result in the same values of $\boldsymbol{Gluc}.\ (\mathbf{1} - \boldsymbol{OsmStr})$ and hence the same effect on Ras activation. Any difference in the output can be attributed to the Snf1-mediated positive feedback.

We chose to use the multiplicative function to represent the effects of glucose and osmotic stress on Ras activation simply for the sake of convenience. An additive function can be also used to achieve qualitatively similar dynamic

behaviors. Meanwhile, we want to note that neither the multiplicative nor the additive form can be used to describe the conditions with combined stress treatments. A quantitative analysis of the interaction between glucose and osmotic stress at the level of Ras activation will be needed for an accurate mathematical of this interaction and for simulating the responses to combined stresses.

Predictions of the *snf1Δ* mutant

In our model, Snf1 reduces cAMP production and PKA activation, as indicated by the rate constant, $k_3 = \frac{5000}{50+[Snf1_a]}$. It should also be noted that the dependence of Snf1 deactivation on glucose level is set to be a Hill function. This enables a sharp response of Snf1 to the glucose limitation. To simulate the snf1Δ mutant, $[Snf1_a]$ and $[Snf1_i]$ are set to be 0, leaving k_3 constantly equal to 100.

Quantifying the dynamic dependence on the stress intensity

The bifurcation diagrams were calculated from 250-minute deterministic simulation results. With stresses starting at 25 minutes, the maximum and minimum values of [cAMP/PKA] between 100 minutes and 250 minutes of each trajectory was found and their dependences upon the stress levels are plotted. The durations of the adaptation peaks were also calculated from 250-minute deterministic simulation results. The peak widths at half-maximum were calculated and used in our graph. The frequencies of the Msn2 pulses were

calculated from 10000-minute stochastic simulation results. These long simulations were used to obtain the statistics similar to those obtained from a large number of single-cell traces. The stresses start at 25 minutes. The number of pulses after 100 minutes were calculated and then divided by 9900 minutes to obtain the frequencies. The threshold for pulse identification is defined as the mean + 4 x standard deviation of the time traces under non-stress conditions, similar to that used in previous studies (Hao and O'Shea (2012)).

Robustness of the modeling behaviors

The core structure of our model is composed of two feedback loops on PKA, a negative feedback through GAP and a positive feedback through Snf1, which are coupled to generate oscillations in PKA activity. To evaluate the robustness of the oscillatory behaviors and the dependence on feedback strengths, we varied the molecule numbers of either GAP or Snf1 to tune the strength of the negative or the positive feedback loop, respectively. We found that the system can achieve oscillations as long as the molecular number of GAP is larger than 300 (4000 in our original model, obtained from (Breker, Gymrek et al. (2013)) and the positive feedback remains intact. However, in the absence of the positive feedback loop (when Snf1 is removed), we did not observe any oscillations for all the molecular numbers of GAP we have tested, ranging from 0 – 4000000. Therefore, a certain level of negative feedback strength is necessary, but not sufficient, to produce oscillations; a positive feedback loop is also

needed. In fact, the oscillatory behaviors are more sensitive to the strength of the positive feedback loop. We found that the system oscillates only when the molecular number of Snf1 falls between 400 and 2000 (500 in our original model, obtained from (Ghaemmaghami, Huh et al. (2003).We have discussed in the main text (Figure 1.2) about how the positive feedback loop promotes oscillation, which explains the requirement of a minimum level of positive feedback strength. At the same time, however, because the positive feedback loop is constituted by two connected negative inhibitions, PKA on Snf1 and Snf1 on PKA, a level of Snf1 above 2000 will inhibit PKA activity to an extent that abolishes oscillations. Therefore, an intermediate level of positive feedback strength (within a certain range) is also required for the oscillatory behaviors in our model.

Achieving perfect adaptation

In the absence of the Snf1-dependent positive feedback, our model is actually a derivative of one of the two major core network structures that have ability to achieve adaptation identified by Ma et al, a negative feedback loop with a buffering node. In our case, GAP is the buffering node. To illustrate this, at equilibrium while GAP concentration does not change, $\frac{k_1[cAMP/PKA][GAP_i]}{Km_1+[GAP_i]} = \frac{k_2[GAP_a]}{Km_2+[GAP_a]}$. Given both Km_1 and Km_2 are very small, [cAMP/PKA] equals to $\frac{k_2}{k_1}$ and is independent of any inputs.

Acknowledgements

Chapter 1, in full, has been published in *Journal of Biological Chemistry*: Yanfei Jiang, Zohreh AkhavanAghdam, Lev S. Tsimring, and Nan Hao. "Coupled feedback loops control the stimulus-dependent dynamics of the yeast transcription factor Msn2." J Biol Chem (2017). The author of this dissertation was the second investigator and author of this paper. Yanfei Jiang developed the computational models. The author of this dissertation (Zohreh AkhavanAghdam) performed the experiments. Lev S. Tsimring and Nan Hao supervised the project. Yanfei Jiang, Zohreh AkhavanAghdam, Lev S. Tsimring, and Nan Hao wrote the paper.

Chapter 2: Dynamic Control of Gene Regulatory Logic by Seemingly Redundant Transcription Factors

Abstract

Many transcription factors co-express with their homologs to regulate a common set of target genes, however the functional advantages of such redundancies remain elusive. Using single-cell imaging and microfluidics, we study the yeast general stress response transcription factor Msn2 and its seemingly redundant homolog Msn4. Upon biologically relevant transient inputs, activation of either Msn2 or Msn4 is sufficient to induce target genes with fast promoter activation kinetics. In contrast, both factors are required for the induction of target genes with slow promoter kinetics. At the single-cell level, the expression of such genes depends specifically on Msn4 activity in a linear fashion. While target genes with fast promoters are expressed homogenously, target genes with slow promoters are fully induced in only a fraction of cells with high Msn4 activity. Therefore, Msn4 plays a distinct regulatory role from Msn2 and diversifies the gene expression responses to environmental stresses within a cell population.

Introduction

Homologous transcription factors (TFs) often co-exist in eukaryotic cells, resulting in seemingly redundant regulation of their target genes. Although a

large number of TF homologs have diversified over time to obtain distinct target genes from their partners, others have remained relatively conserved and share the same DNA binding motif, which limits their downstream interactions to identical target genes. Recent studies suggest that some closely related TF homologs or isoforms, which regulate a shared set of target genes, might have diverged expression patterns, dynamic responses or gene regulatory functions. For example, the yeast transcriptional regulator Dig1 inhibits the expression of mating response genes to pheromone stimulation, whereas its homolog Dig2 exhibits both negative and positive regulation depending on the conditions (Chou, Zhao et al. 2008, Houser, Ford et al. 2012). In mammalian cells, two TF isoforms NFAT1 and NFAT4 display distinct nuclear translocation dynamics in response to stimuli. It has been suggested that this dynamic diversity of isoforms might enhance temporal signal processing function of the cell (Yissachar, Sharar Fischler et al. 2013). In addition, a very recent study showed that the TF homologs STAT5A and STAT5B differentially contribute to the immune transcriptional response due to their different expression levels (Villarino, Laurence et al. 2016). Here we use the yeast homologous stress responsive TFs Msn2 and Msn4 as a model to quantitatively study the functional relevance of closely related TFs in the same single cells.

Msn2 and Msn4 are C_2H_2 zinc-finger TFs that regulate cellular responses to a wide range of environmental stresses (Schmitt and McEntee 1996). Upon stress stimulation, both TFs rapidly translocate from the cytoplasm to the nucleus

where they bind to the same DNA recognition sequence and induce the expression of a common set of stress responsive genes (Martinez-Pastor, Marchler et al. 1996). Their nucleocytoplasmic translocation is controlled by phosphorylation and is directly regulated by protein kinase A (PKA) and phosphatases (Gorner, Durchschlag et al. 1998) (Figure 2.1A, left). Therefore, it has been long believed that Msn2 and Msn4 are functionally redundant in regulating gene expression response. In fact, since Msn2 is assumed to play a more pronounced role in gene regulation, many previous studies focused only on Msn2, deleting the *MSN4* gene to simplify analysis (Hao and O'Shea 2012, Hansen and O'Shea 2013, Petrenko, Chereji et al. 2013, Hansen and O'Shea 2015, Lin, Sohn et al. 2015, Hansen and O'Shea 2016). A microarray analysis, however, suggested that Msn2 and Msn4 might have different contributions to gene induction at individual promoters (Berry and Gasch 2008), but the mechanism underlying these differences remains unknown.

Here we combine quantitative single-cell imaging and high-throughput microfluidics to monitor and compare the dynamic responses and gene regulatory functions of Msn2 and Msn4 in single cells. We find that Msn2 and Msn4 have non-redundant and distinct functions in combinatorial gene regulation. We have previously demonstrated that Msn2/4 target genes differ significantly in their promoter activation kinetics, which dramatically influences their responses to dynamic inputs (such as transient versus sustained inputs) (Hao and O'Shea 2012). In this work, we show that, in response to a transient

input, either Msn2 or Msn4 alone is sufficient to induce the expression of target genes with fast kinetics promoters, constituting what is essentially a biological “OR” logic gate. In contrast, the induction of target genes with slow kinetics promoters requires activation of both factors, forming an “AND” gate. At the single-cell level, even though Msn2 and Msn4 show similar nuclear translocation dynamics, they exhibit different levels of heterogeneity in nuclear localization and distinct gene regulatory functions. Msn2 is activated in a relatively homogeneous manner and functions as a low threshold “switch” essential for turning on slow kinetics promoters. In contrast, Msn4 activation is highly heterogeneous and it serves as a “rheostat” to effectively tune the induction level of target genes with slow kinetics promoters in individual cells. Therefore, while target genes with fast kinetics promoters are uniformly expressed in most cells, those with slow promoters are more likely to be fully induced in only a fraction of cells with high Msn4 activity. Our work reveals that the seemingly redundant TF Msn4 has a distinct gene regulatory role from its homolog Msn2 and enables diversified gene expression responses within a cell population, which might be beneficial for survival under rapidly changing environments.

Results

Msn4 is required for the induction of target genes with slow promoter kinetics

To investigate gene regulation by Msn2 and Msn4 in single cells, we fused Msn4 with a yellow fluorescent protein (YFP) and Msn2 with a red fluorescent protein (RFP) at their native loci. A cyan fluorescent protein (CFP) reporter under Msn2/4 specific target promoters was introduced into the same strain to monitor downstream gene expression. To understand gene responses to dynamic TF activation, we have previously developed a chemical genetics method for controlling Msn2/4 nuclear localization using a small molecule 1-NM-PP1 that specifically inhibits protein kinase A (PKA) activity (Hao and O'Shea 2012, Hao, Budnik et al. 2013). Here we combine this method with quantitative time-lapse microscopy and microfluidics (Hao and O'Shea 2012, Hao, Budnik et al. 2013, Hansen, Hao et al. 2015) to simultaneously track Msn2 and Msn4 localization and target gene expression in a large number of individual cells in response to dynamic inputs (Figure 2.1A). In each experiment, we measure single-cell responses over a 3-hour period, which is sufficient for the fluorescent gene expression reporter to reach the plateau in most cells (Figure 2.1A, right).

Our previous studies revealed that Msn2/4 target promoters can be characterized as having fast or slow activation kinetics relative to one another based on the time needed for their activation (Hao and O'Shea 2012, Hansen and O'Shea 2013). While target genes with fast kinetics promoters respond strongly to transient TF inputs, slow kinetics promoters, due to their long activation delay, filter out inputs with short durations. The activation kinetics of target promoters depends on their promoter architectures, in particular, the

organization of TF binding sites and nucleosomes (Hao and O'Shea 2012, Hansen and O'Shea 2015). To analyze dynamic gene regulation by Msn2 and Msn4, we focus here on two well-characterized promoters - P_{DCS2} and P_{SIP18}, which are Msn2/4 specific (not induced in a *msn2*Δ*msn4*Δ strain)(Hansen and O'Shea 2013), and have been routinely used to represent Msn2/4 target promoters with fast (P_{DCS2}) or slow (P_{SIP18}) activation kinetics, respectively (Hansen and O'Shea 2013, Hansen and O'Shea 2015, Hansen and O'Shea 2015, Hansen and O'Shea 2016). The *DCS2* promoter can be activated 5 times faster than the *SIP18* promoter for a given TF input (Hansen and O'Shea 2013).

To first determine the dependence of target gene expression on Msn2 and Msn4, we measure the induction of Msn2/4 target promoters in response to TF inputs with various durations in wild-type cells and cells lacking *MSN2* or *MSN4* and plotted the distributions of single-cell expression responses (Figure 2.1; The dynamic profiles of reporter gene expression are shown in Figure 2.3). We find that, in response to a transient inhibitor input (30 min), activation of either Msn2 or Msn4 is sufficient to fully induce the fast kinetics promoter P_{DCS2} (Figure 2.1B, left). In contrast, the induction of slow kinetics promoter P_{SIP18} requires activation of both Msn2 and Msn4: the absence of either factor abolishes the expression of reporter gene (Figure 2.1B, right). Interestingly, in response to a prolonged input pulse (60 min), while Msn2 is still needed for the induction of the slow gene promoter, Msn4 is no longer required (Figure 2.1C). These results suggest that

Msn4 functions to shift the activation time-scales of slow kinetics promoters and thereby enables the induction of such promoters by transient inputs.

To determine whether the requirement of Msn4 for gene induction is specific to slow promoter kinetics, we employed a mutant of the P_{SIP18} promoter (P_{SIP18}-A4), which has been converted to a fast kinetics promoter by moving the Msn2/4 binding sites more adjacent to the TATA box (Hansen and O'Shea 2015). In accordance with the fast kinetics promoter P_{DCS2}, Msn4 is not needed for the expression of reporter gene under the P_{SIP18} mutant promoter (Figure 2.2A). To further examine whether other target gene promoters have similar dependence to Msn4, we analyzed the responses of fast kinetics promoter P_{DDR2} and slow kinetics promoter P_{TKL2}. Similar to the fast kinetics promoter P_{DCS2}, the expression of the P_{DDR2} reporter gene does not require Msn4. In contrast, Msn4 is needed for the full induction of P_{TKL2} in response to a transient input (Figure 2.4). These results suggest that the dependence on Msn4 might be a general feature of slow kinetics promoters. Finally, to determine whether target promoters would respond similarly when cells are faced with natural stressors, we monitored the reporter expression of P_{DCS2} and P_{SIP18}, respectively, in response to osmotic stress, which leads to a transient pulse of TF activation (Hao and O'Shea 2012, Hao, Budnik et al. 2013). Consistent with the inhibitor experiments, while Msn4 is not critical for the expression of fast kinetics promoter P_{DCS2}, it is required for the full induction of slow kinetics promoter P_{SIP18} (Figure 2.2B).

Therefore, our work reveals that, contrary to what has been previously believed, Msn4 is not redundant to its homolog Msn2 in regulating gene expression. In particular, while activation of either Msn2 or Msn4 is sufficient to trigger the expression of target genes with fast promoter kinetics, target genes with slow promoter kinetics depend on both Msn2 and Msn4 for their full induction in response to biologically relevant transient inputs.

Msn4 displays heterogeneous nuclear translocation in single cells

Having established that Msn4 is not redundant to its homolog Msn2, we next investigate the dynamic and functional differences between the two factors at the single cell level that can account for their specific contributions to gene regulation. We first focus on the dynamics of Msn2 and Msn4 nuclear translocation. We observe that Msn2 and Msn4 show similar temporal dynamics of translocation in the same single cells in response to a transient inhibitor input (Figure 2.5A). However, we find that the level of Msn4 nuclear translocation is highly heterogeneous across single cells: some cells show high level of nuclear translocation, while other cells have very low localization levels. In contrast, the translocation levels of Msn2 are relatively homogeneous amongst individual cells. To illustrate the noise levels of Msn2 and Msn4 translocation, we plotted the standard deviation of their single-cell time traces scaled by the mean and reported the coefficient of variation (CV: standard deviation scaled by the mean) for the peak point of time traces. As shown in Figure 2.5A (ii), Msn4 nuclear

translocation exhibits a higher level of cell-cell variability than that of Msn2. To investigate the dynamics of Msn2 and Msn4 translocation in response to natural stresses, we subject yeast cells to osmotic stress and ethanol stress treatments. As shown in Figure 2.5B and C, osmotic stress elicits a transient pulse of Msn2 and Msn4 translocation, while ethanol stress induces sustained nuclear localization of Msn2 and Msn4. In response to either stress, Msn4 exhibits similar temporal dynamics of nuclear translocation to Msn2 in single cells, consistent with the inhibitor treatments. In addition, the level of Msn4 nuclear localization shows a higher degree of cell-cell heterogeneity than that of Msn2 under natural stress conditions, in accordance with the inhibitor treatments.

To determine the relative nuclear concentrations of Msn2-RFP and Msn4-YFP molecules at the single cell level, we performed a control experiment to obtain a scaling factor that normalizes the nuclear fluorescence intensities of YFP and RFP into “normalized a.u.” (Figure 2.6). We observe that the nuclear localization level of Msn4 is generally lower (~3-fold lower) than that of Msn2 in the same cells under inhibitor or natural stress conditions (Figure 2.6B, yellow curves versus red curves). In addition, although Msn4 has a higher coefficient of variation, the standard deviation of Msn4 nuclear localization in single cells (without being scaled by the mean) is lower than that of Msn2 (Figure 2.7). These results suggest that the high degree of cell-cell variability of Msn4 might be largely due to its relatively low nuclear levels compared to that of Msn2.

Thus, our single-cell imaging analysis shows that, in response to various stimuli, nuclear translocation of Msn4 temporally correlates with that of Msn2 in the same cells; however, the level of Msn4 nuclear localization in individual cells is more heterogeneous than that of its homolog.

Msn4 exhibits distinct gene regulatory functions from Msn2 in single cells

Given that Msn2 and Msn4 show different levels of cell-cell variability in nuclear translocation, we speculate that they may play different regulatory roles in controlling heterogeneous gene expression at the single cell level. Using the deletion strains, we have revealed that target genes with different promoter activation kinetics exhibit different dependence to Msn2 and Msn4 (Figure 2.1). To further determine the dependence of gene regulation specifically on Msn2 or Msn4 in single cells when both factors are present, we simultaneously monitored nuclear localization of Msn2 and Msn4 and reporter gene expression under the fast kinetics promoter P_{DCS2} or the slow kinetics promoter P_{SIP18} in the same wild-type cells. We then quantified and plotted the maximal level of reporter expression versus the peak nuclear localization level of Msn2 and/or Msn4 of each single cell to analyze the relationship between gene expression and the activity of Msn2 and Msn4, respectively. To cover a full range of TF translocation levels, we combined the single cell responses to 30-min inhibitor inputs with various doses.

We find that, for the fast kinetics promoter P_{DCS2}, gene expression can be induced in the majority of cells in which either Msn2 or Msn4 is adequately activated Figure 2.8A, i). The level of reporter expression shows a similar graded relationship with both Msn2 and Msn4, reaching the saturation when either factor is activated over a low threshold level (Figure 2.8A, ii; Single-cell distributions of gene expression versus Msn2 or Msn4 are shown in Figure 2.9). The probabilities of gene induction versus Msn2 or Msn4 are shown in Figure 2.10A). These results are consistent with our observation by deletion analysis that Msn2 and Msn4 play largely redundant roles in regulating target genes with fast kinetics promoters (Figure 2.1).

In contrast, for the slow kinetics promoter P_{SIP18}, gene expression is highly heterogeneous among single cells, consistent with previous results (Hansen and O'Shea 2013). Furthermore, the reporter gene is fully induced predominantly in the fraction of cells in which Msn4 is highly activated (Figure 2.8B, i, red solid circles). In individual cells with a fixed level of Msn2 activity, a higher level of Msn4 activation results in an increase in both the probability and the level of gene induction (Figure 2.8B, i, with a fixed y-axis value and an increasing x-axis value). However, in single cells with a fixed level of Msn4 activity, higher Msn2 activation does not necessarily lead to higher gene induction; in fact, too much Msn2 activation will suppress gene induction in the same cell, suggesting a competing role of Msn2 for binding to the promoter (Figure 2.8B, i, with a fixed x-axis value and an increasing y-axis value). To quantitatively demonstrate this

competing role of Msn2 against Msn4, we plotted the relationship between gene expression and the ratio of Msn2 versus Msn4 in single cells. As shown in Figure 2.11, gene expression decreases dramatically when the ratio of Msn2 versus Msn4 increases. We further analyzed the relationship between reporter gene expression with Msn2 or Msn4 activity, individually. Gene expression shows a switch-like relationship to Msn2 activation with a low threshold (~10 normalized a.u.: ~25% of maximal Msn2 localization): while a low level of Msn2 activity is required for turning the gene on, the induction level is independent of Msn2 activity (Figure 2.8B, ii, left, averaged response of single cells binned based on their TF levels). In contrast, gene expression exhibits a linear relationship with Msn4 activity in which both the probability and the level of gene induction increase with the level of Msn4 activity in single cells (Figure 2.8B, ii, right; Single-cell distributions of gene expression versus Msn2 or Msn4 are shown in Figure 2.9B); The probabilities of gene induction versus Msn2 or Msn4 are shown in Figure 2.10B). In accordance with the deletion analysis in Figure 2.1C, in response to prolonged (60-min) input pulses, the reporter expression of P_{SIP18} no longer specifically depends on Msn4 and the level of reporter expression shows graded relationships with both Msn2 and Msn4 (Figure 2.12).

These results demonstrate that Msn2 and Msn4 play distinct and cooperative regulatory roles in controlling target genes with slow promoter kinetics. In response to transient inputs, consistent with the required role of Msn2 for slow promoter induction shown in Figure 2.1, Msn2 in single cells serves as a

low threshold “switch” for gene induction: it is required to be activated above a certain threshold (~25% of its maximal level) to turn on transcription in the cell; once its activity is above that threshold, a further increase in Msn2 activity cannot positively contribute to the extent of gene induction. In contrast, despite of its low expression level, Msn4 is a highly potent activator of slow target promoters and thus is also required the full induction of slow promoters (Figure 2.1). Once Msn2 turns on gene transcription in a cell, Msn4 functions as a “rheostat” in the same cell to effectively fine-tune the probability and level of gene induction. Furthermore, high levels of Msn2 in the nucleus may compete with Msn4 for binding to the same target promoters and can thus suppress gene induction. This possible inhibitory role of Msn2 against Msn4 counteracts its modest positive contribution to gene expression. Therefore, the expression level of target genes with slow promoter kinetics depends specifically on the Msn4 activity in individual cells. Furthermore, the homolog-specific gene regulation depends on the transient dynamics of TF inputs. In response to sustained inputs, the slow kinetics promoters no longer exhibit the specific dependence on Msn4 and behave like fast kinetics promoters upon transient inputs.

Finally, to evaluate the influence of other dynamic characteristics (such as nuclear import rate or export rate) of Msn2 or Msn4 translocation, we also plotted the level of gene expression versus the area under the curve (AUC) of Msn2 or Msn4 nuclear localization (Figure 2.13).

Msn4 controls the induction level of slow kinetics promoters in single cells under natural stress conditions

To determine whether Msn4 functions differently from Msn2 under natural stress conditions, we treated yeast cells with osmotic stress (0.5M KCl) or ethanol stress (4% ethanol), respectively, and measured nuclear localization of Msn2 and Msn4 and reporter gene expression under the slow kinetics promoter P_{SIP18} in the same cells. In response to 0.5 M KCl treatment, we find that the reporter gene is fully induced specifically in the cells with high Msn4 activity (Figure 2.14A, i and ii), in accordance with the inhibitor experiments. In addition, the probability and the level of gene induction are independent of Msn2 activity, but increase linearly with Msn4 activity in single cells (Single-cell distributions of gene expression versus Msn2 or Msn4 are shown in Figure 2.15A; the relationship between gene expression and AUC are shown in 1.15A). Because the osmotic stress treatment elicits Msn2 nuclear translocation above the threshold required for gene induction (~10 normalized a.u.: ~25% of maximal Msn2 localization; determined from the inhibitor experiments in Figure 2.8) in almost all of the cells, we could not observe the basal “off” state of gene expression when we binned the cells with their Msn2 levels (Figure 2.14A, ii, left). This result indicates that, in response to the stress condition, Msn2 is “switched on” in all of the cells and the induction level of slow kinetics promoters in individual cells is primarily controlled by Msn4 activity.

Similarly, in response to 4% ethanol treatment, the reporter gene is also induced specifically in cells with high Msn4 activity. The treatment of ethanol stress is a relatively harsh stress condition that leads to a global translational arrest (Ding, Huang et al. 2009, Stanley, Bandara et al. 2010). As a result, the majority of cells are not able to express the reporter gene under the slow kinetics promoter; however, the cells that do express the reporter gene are those with high Msn4 activity (Figure 2.14B, i). Similar to the osmotic stress condition, Msn2 is activated above the threshold required for gene induction in most cells; therefore, the probability of gene expression does not show any dependence on Msn2 activity in single cells (Figure 2.14B, ii, left). In contrast, the probability of gene expression shows a linear relationship with Msn4 activity in single cells (Figure 2.14B, ii, right; Single-cell distributions of gene expression versus Msn2 or Msn4 are shown in Figure 2.15; the relationship between gene expression and AUC are shown in Figure 2.16), consistent with the inhibitor and osmotic stress experiments.

Taken together, these results show that, under natural stress conditions, Msn4 plays a distinct regulatory role from Msn2 in controlling target genes with slow kinetics promoters. Similar to inhibitor treatments, expression of these genes depends specifically on Msn4 activity in a linear fashion at the single-cell level. Given its heterogeneous activity in single cells and its critical role in gene regulation, Msn4, working in parallel with its homolog Msn2, can diversify the

expression of a specific group of target genes within a cell population in response to natural stresses.

Distinct gene regulatory functions of Msn2 and Msn4 might extend more generally to other target promoters

To determine whether Msn2 and Msn4 exhibit distinct regulatory functions on promoters other than P_{DCS2} and P_{SIP18}, we measured the nuclear localization of Msn2 and Msn4 and reporter gene expression under fast kinetics promoter P_{DDR2} and slow kinetics promoter P_{TKL2}. We find that, similar to the fast kinetics promoter P_{DCS2}, expression of the P_{DDR2} reporter gene can be induced in most cells in which either Msn2 or Msn4 is activated over a low threshold level and the level of reporter expression shows a similar graded relationship with both Msn2 and Msn4 (Figure 2.17). In contrast, the slow kinetics promoter P_{TKL2} shows a similar response to that of P_{SIP18}, in which reporter expression is specifically induced in the fraction of cells with high Msn4 activity. The level of reporter expression shows a switch-like relationship to Msn2 activity, but a linear relationship with Msn4 activity (Figure 2.17B). These results suggest that the distinct functions of Msn2 and Msn4 in combinatorial gene regulation might be applicable to other target genes.

To further examine the generality of distinct regulatory functions of Msn2 and Msn4, we analyzed the gene expression response under the mutated P_{SIP18} promoter (P_{SIP18}-A4), which, by incorporating a few mutations, has been

converted from a slow kinetics promoter to a fast kinetics promoter (Hansen and O'Shea 2015). As shown in Figure 2.17C, in accordance with other fast kinetics promoters, gene expression under this mutant promoter is induced in most cells and displays a similar graded relationship with both Msn2 and Msn4. Therefore, Msn2 and Msn4 no longer show distinct regulatory functions when the P_{SIP18} promoter, with the majority of the promoter sequence intact, is mutated to obtain fast activation kinetics. We next tested the opposite situation in which we slow down a fast kinetics promoter. To this end, we monitored the gene expression response under the P_{DCS2} promoter in cells lacking the SWI/SNF chromatin remodeling complex *(snf6Δ*. It has been shown previously that this mutant significantly slows down the activation kinetics of fast promoters (Hansen and O'Shea 2013). Consequently, we observe that gene expression under the P_{DCS2} promoter in this mutant exhibits switch-like versus linear relationships with Msn2 and Msn4, respectively (Figure 2.17D), consistent with the responses of other slow kinetics promoters. In summary, these results suggest that the distinct regulatory functions of Msn2 and Msn4 might depend more generally on the kinetics of promoter activation, but not on specific target promoters.

In this study, we have focused on a few representative promoters because our single-cell analysis requires live-cell time-lapse experiments, the throughput of which hinders the examination of gene regulation at a more global level. However, we anticipate that, in near future, the technological advances will allow us to track single-cell gene regulation at the whole genome level. Such

technologies will undoubtedly provide further insights into combinatorial gene regulation by Msn2 and Msn4. For example, we previously grouped target genes with fast versus slow promoter kinetics based on a population-level assay using cells with the *msn4Δ* background (Hao and O'Shea 2012). Given the newly identified role of Msn4 in shifting the promoter activation timescales in a subpopulation of cells, we suspect that its presence might alter the classification of some target genes with intermediate promoter kinetics. A genome-wide single-cell analysis will enable a more accurate classification of target genes and, more importantly, will lead to a comprehensive understanding about dynamic regulation of global transcriptional responses to environmental stimuli.

Discussion

Here we show that the homologous TFs Msn2 and Msn4, which have long been assumed to be functionally redundant, play distinct roles in coordinating differential expression of target genes depending on their promoter kinetics. For target genes with fast promoter kinetics, both factors can contribute to gene expression in a graded manner. In contrast, for target genes with slow promoter kinetics, Msn2 and Msn4 play distinct and cooperative roles, in which Msn2 functions as a low threshold “switch” governing the “ON” and “OFF” state of promoter activation, while Msn4 serves as a “rheostat” to effectively tune the induction level of gene expression (Figure 2.18). Further biochemical analysis is needed to elucidate the mechanistic details underlying these distinct regulatory

functions of Msn2 and Msn4 at slow target promoters. One possible mechanism could involve the recruitment of distinct chromatin remodeling factors by Msn2 and Msn4 to target gene promoters. For example, to function as a low threshold “switch”, Msn2 might first recruit some initiation factors critical for opening up the tightly packed nucleosomes, characteristic of slow kinetics promoters (Hao and O'Shea 2012, Hansen and O'Shea 2013, Hansen and O'Shea 2015). This could be followed by the subsequent promoter binding of Msn4, leading to the recruitment of Msn4-specific chromatin remodelers or modifiers to effectively promote and stabilize chromatin disassembly. In accordance with this mechanism, we observe that Msn4 always follows Msn2 in nuclear translocation with a short delay (~2-3 min) under the inhibitor or natural stress conditions.

Target genes with fast and slow promoter activation kinetics are regulated differently and hence might have distinct physiological functions. In support of this, we find a close correlation between gene functions and promoter kinetics for previously identified target gene groups with fast or slow kinetics promoters (Figure 2.19; target gene groups are from Hao and O’Shea, 2012). Target genes with fast kinetics promoters are primarily involved in metabolic and cellular adaptation to glucose starvation (carbohydrate metabolism and autophagy), whereas the majority of target genes with slow kinetics promoters are involved in cellular protection against chronic stresses. These results suggest that, in response to carbon source changes that might require immediate adaptive response, cells could quickly modulate their metabolism via activating those

genes with fast kinetics promoters. In contrast, the induction of genes with slow kinetics promoters is more tightly controlled. These genes are important for preparing cells to survive under chronic stress conditions, the response to which might be less time-sensitive and the occurrence of which might be less frequent in natural habitats. Cells would only activate these genes upon a sustained presence of stresses. This temporal separation of target genes with different functions could avoid initiating resource-intensive cell protection processes in response to minor environmental fluctuations and thereby optimize resource allocation under rapidly changing environments. Furthermore, cells may use Msn4 to control the level of heterogeneity at the population level (Figure 2.18B), as part of a bet hedging strategy against unpredictable environmental conditions. During the first onset of stresses, a subpopulation of cells with high Msn4 activity induce the expression of stress resistance genes with slow kinetics promoters, preparing for upcoming severe or chronic stresses; meanwhile, other cells with low Msn4 activity cannot induce these genes and therefore may consequently obtain a better fitness advantage if the subsequent stress is minor or short term. In this way, cells can be divided into two subpopulations, each of which is specialized at coping with one of the possible environmental scenarios. Cells lacking Msn4, however, are not able to induce the slow target genes within the whole population, and hence might be more likely to go extinct in the face of extreme stresses. Therefore, the Msn4-dependent gene regulation may

represent a strategy that enables a homolog-“controlled” form of heterogeneity within a cell population.

The coupling of the homologous factors Msn2 and Msn4 in combinatorial gene regulation is analogous to logic gate systems commonly found in digital circuits: fast kinetics promoters behave as an “OR” gate, becoming fully induced with adequate amount of either factor, while slow kinetics promoters behave as an “AND” gate, requiring the activation of both Msn2 and Msn4 (Figure 2.18). Interestingly, this logic gate scheme is not fixed, but rather dependent on the upstream dynamics of TF input – an “AND” gate upon a transient input can become an “OR” gate when the input duration is prolonged. As shown in Figure 2.1B and C, in response to a 30-min input pulse, the slow kinetics promoter P_{SIP18} is an “AND” gate, requiring both Msn2 and Msn4 for gene induction; But it becomes an “OR” gate in response to a 60-min input pulse, in which Msn4 is no longer required. Therefore, given enough amount of time in the nucleus, Msn2 can also function as a “rheostat” to compensate the absence of Msn4 and tune the induction level of slow target promoters, consistent with a previous study showing that increasing the steady-state expression level of Msn2 leads to a graded induction of its target genes (Stewart-Ornstein, Nelson et al. 2013). Our results suggest that the architectures of gene regulatory networks are not static and could be rewired by various upstream dynamics of TF inputs. In yeast, a recent proteomic analysis found that most proteins that exhibit transient pulsatile dynamics to environmental changes are members of paralogous or closely

related TFs (Dalal, Cai et al. 2014). For example, Msn2 and a related transcriptional repressor Mig1, both having pulsatile dynamics, regulate their common target genes by modulating their relative pulse timing (Lin, Sohn et al. 2015). Moreover, in mammalian systems, an increasing number of TFs, including some closely related TF pairs such as NFAT1 and NFAT4 (Yissachar, Sharar Fischler et al. 2013), have been identified to possess highly diverse activation dynamics that contribute to gene expression responses (Werner, Barken et al. 2005, Behar and Hoffmann 2010, Tay, Hughey et al. 2010, Purvis, Karhohs et al. 2012, Purvis and Lahav 2013). Given the prevalence of seemingly redundant TFs in eukaryotes, we anticipate that the time-dependent combinatorial gene regulation revealed here for Msn2 and Msn4 will be widely applicable to homologous or closely related TFs that are controlled dynamically in other organisms including mammals.

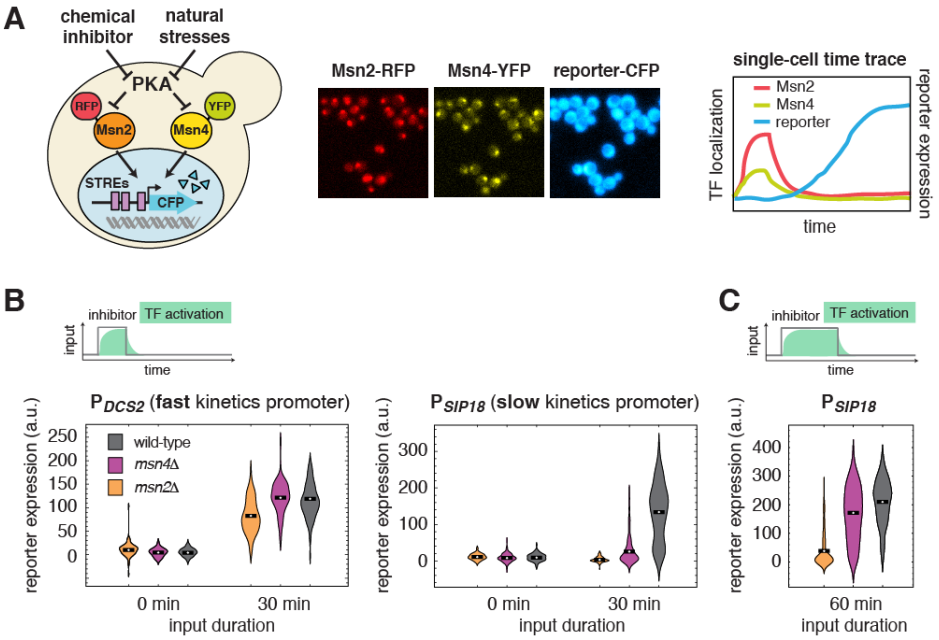

Figure 2.1 Msn4 is required for the induction of target genes with slow promoter kinetics.

(**A**) Homologous TFs Msn2 and Msn4 are regulated by the same upstream PKA signals in response to natural stresses or chemical inhibitors and control a common set of target genes with stress response elements (STREs) in their promoters. In the same strain, Msn2 and Msn4 are fused with RFP and YFP respectively, at their native loci; a CFP reporter under the Msn2/4 specific promoter is introduced to monitor gene expression responses. Middle: Translocation of Msn2-RFP and Msn4-YFP and reporter gene expression can be monitored in the same single cells over time. Right: In response to stimulation, time traces of Msn2 and Msn4 translocation and reporter gene expression can be quantified for each single cell. For each condition, single-cell data are collected from at least three independent experiments. (**B**) Violin plots showing the distributions of reporter expression under (left) the fast kinetics promoter P_{DCS2} or (right) the slow kinetics promoter P_{SIP18} in single cells in response to 3μM inhibitor inputs with 30-min pulse duration (illustrated by the top inset) in wild-type, *msn2Δ*, and *msn4Δ* strains, respectively (n: ~300 cells per condition per strain). The mean value of single cell responses was labeled using the black bar for each condition. The expression of reporter gene was tracked in single cells over a 3-hour period in which the reporter fluorescence in most cells has already reached the plateau. The last point of each single-cell time trace was used in the plots (a.u.: arbitrary units). (**C**) Violin plots showing the distributions of reporter expression under the slow kinetics promoter P_{SIP18} in response to a 60 min pulse of inhibitor input.

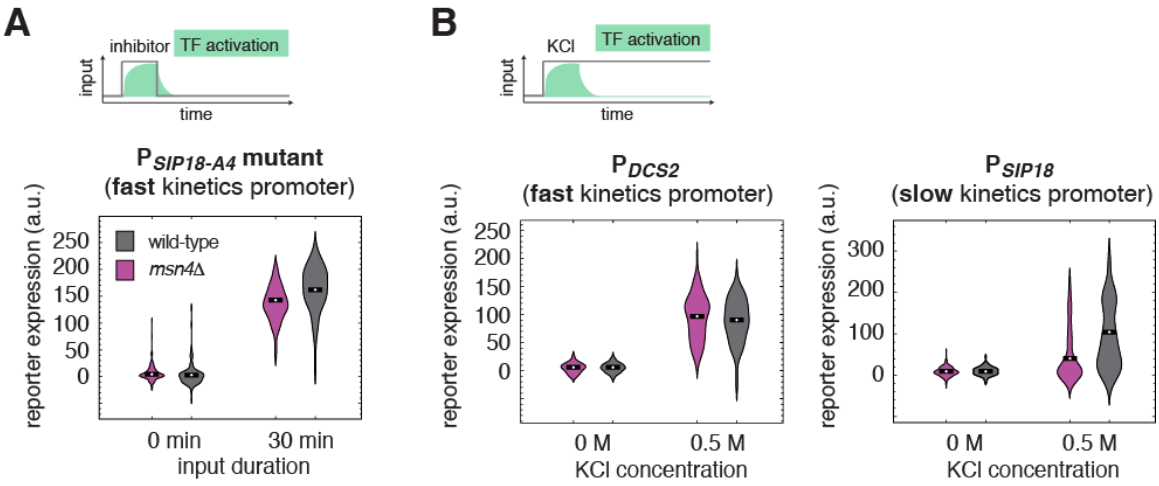

Figure 2.2 The role of Msn4 is gene expression is specific to slow kinetic promoters and occurs under natural stress conditions.
(**A**) Violin plots showing the distributions of reporter expression under the faster mutant promoter $P_{SIP18\text{-}A4}$ in wild-type and *msn4Δ* strains, respectively, in response to 30-min inhibitor input. **(B)** Violin plots showing the distributions of reporter expression under (left) the fast kinetics promoter P_{DCS2} or (right) the slow kinetics promoter P_{SIP18} in response to 0.5 M KCl in wild-type and *msn4Δ* strains, respectively. The sustained KCl stimulation leads to a transient pulse of TF activation, as illustrated in the top cartoon panel in Figure 2.1.

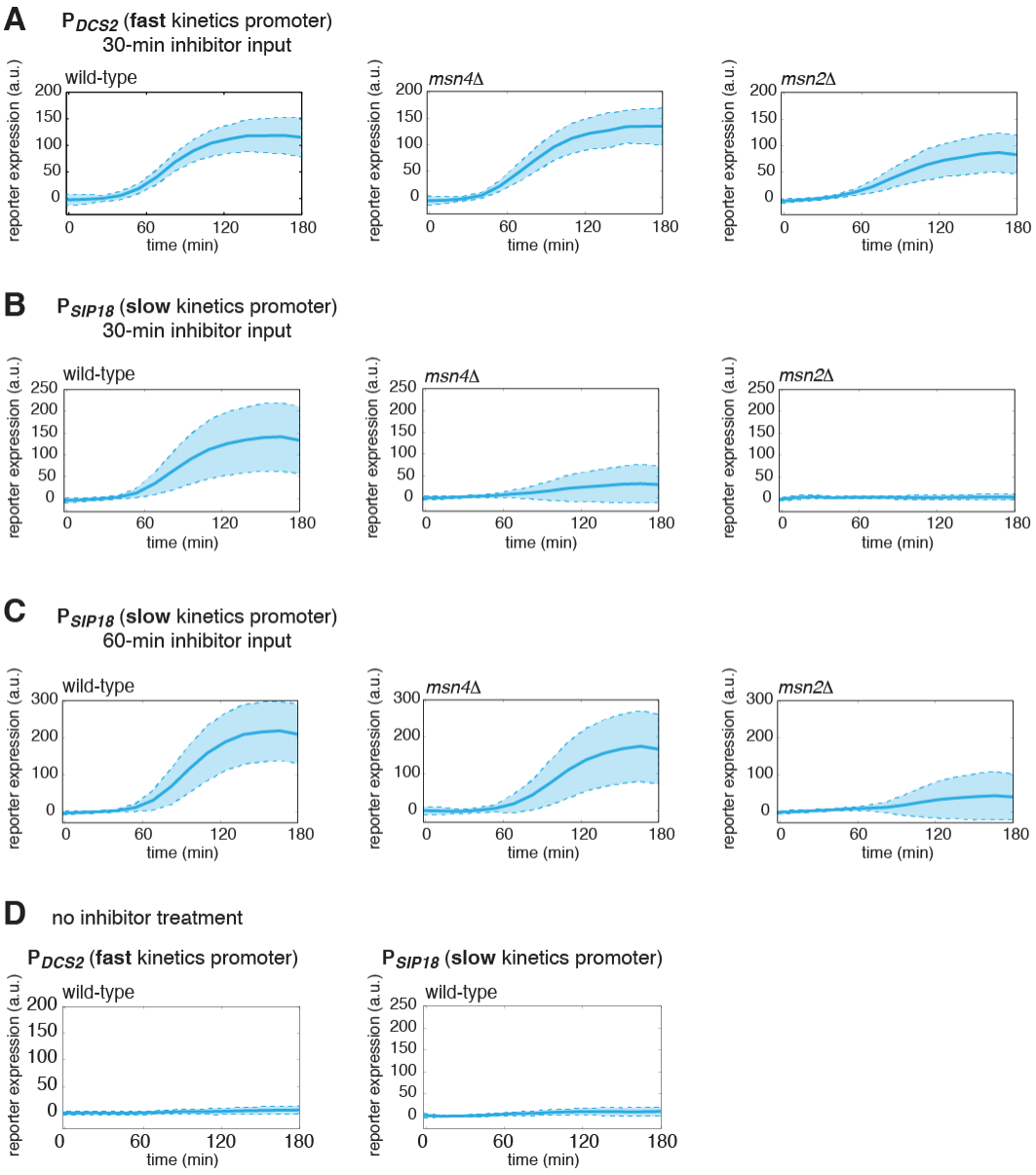

Figure 2.3 Dynamic profiles of reporter gene expression.
Averaged single-cell time traces of reporter gene expression under (A) the fast kinetics promoter P_{DCS2} and (B) the slow kinetics promoter P_{SIP18}, in response to 30-min inhibitor inputs, (C) the slow kinetics promoter P_{SIP18}, in response to 60-min inhibitor inputs, and (D) under no inhibitor condition. The single-cell data are the same data used to generate Figure 2.1, B and C. The solid curves represent the averaged single-cell time traces; the shaded regions represent the standard deviations of single cell responses. For each condition, single-cell responses have been measured over a 3-hour period, which is sufficient for the fluorescent gene expression reporter to reach the plateau in most cells.

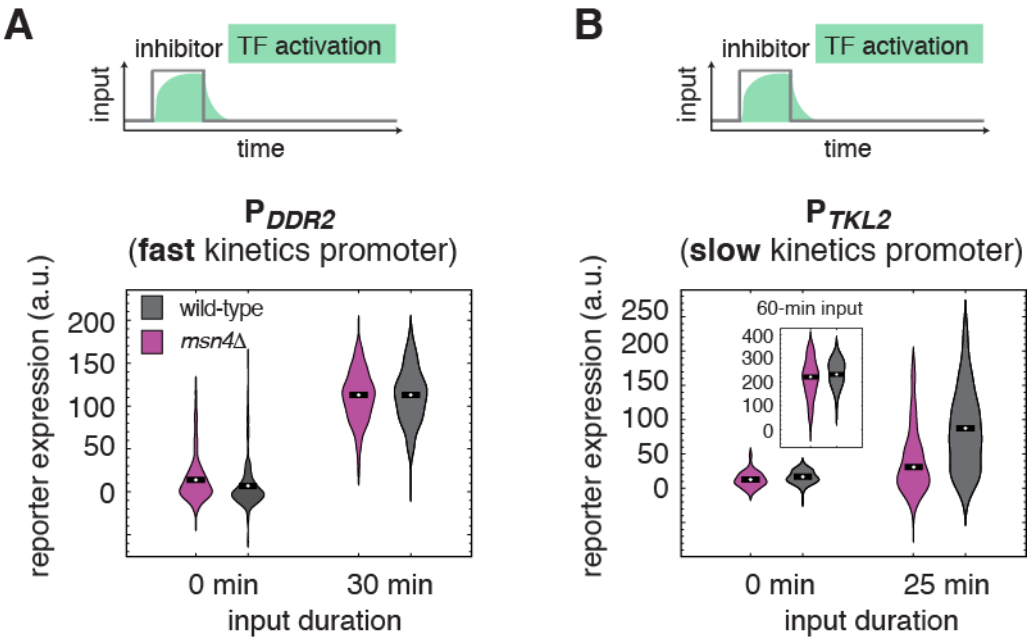

Figure 2.4 The dependence on Msn4 might expand generally to slow kinetics promoters.

Violin plots showing the distributions of reporter expression under (**A**) the fast kinetics promoter P_{DDR2} and (**B**) the slow kinetics promoter P_{TKL2}, respectively. In (B), the inset shows the distributions of P_{TKL2} reporter expression in response to 60 min pulse of inhibitor input.

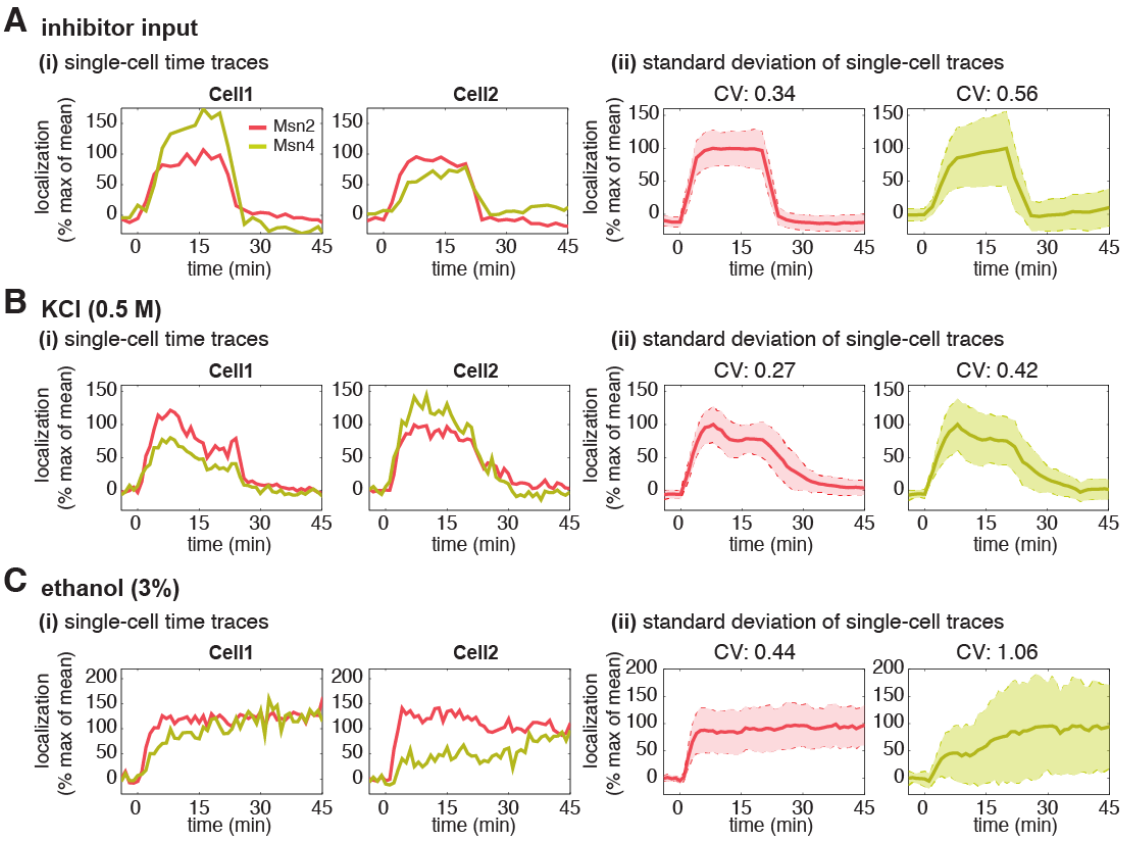

Figure 2.5 Msn2 and Msn4 show different levels of heterogeneity in single cells.

Time traces of Msn2 and Msn4 nuclear translocation in the same single cells in response to (**A**) 20-min 1 μM inhibitor pulse, (**B**) 0.5M KCl, or (**C**) 3% ethanol. In each panel, (i) representative single-cell time traces of Msn2 and Msn4 nuclear translocation in the same single cells; (ii) standard deviation of single-cell time traces. For each condition, the single-cell time traces and standard deviations of single cell responses are scaled by the peak value of the averaged time traces (% max of mean). In (ii), the solid curve represents the averaged time trace; the shaded region represents the scaled standard deviation of single cell responses. The coefficient of variation (CV; the standard deviation divided by the mean) is calculated for the peak time point of time traces for each condition and displayed above each time trace.

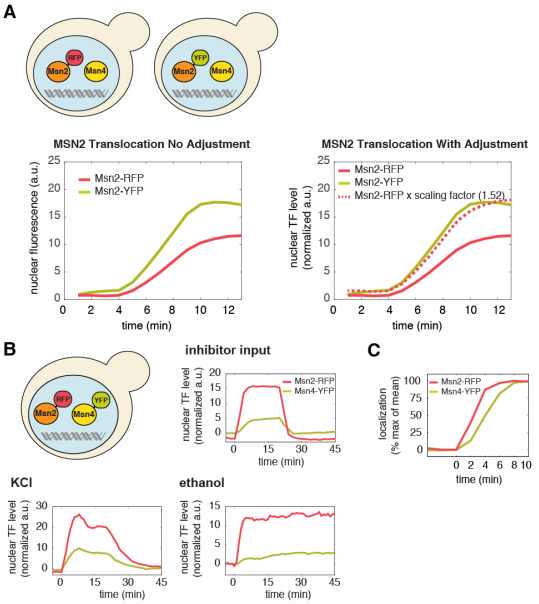

Figure 2.6 A direct comparison of the levels of Msn2 and Msn4 nuclear localization in the same cells.

(**A**) To directly compare the nuclear level of Msn2-RFP relative to that of Msn4-YFP in the same single cells (Figure 2.1A), a scaling factor between RFP and YFP is needed to account for unique microscope settings used in each channel as well as inherent emission differences between each fluorophore. This was determined by creating two yeast strains in which Msn2 was C-terminally tagged with either florescent protein RFP or YFP, respectively (illustrated in the top panel). Left: Sustained nuclear translocation of Msn2 was induced in both stains with an identical stimulus and the averaged single-cell time traces of Msn2 translocation were generated for both strains (n: ~100 cells per strain). Right: The scaling factor (1.52) was determined by taking the ratio between the maximal fluorescence intensity of each averaged trace. The time trace of Msn2-RFP, when times the scaling factor (dashed curve), overlaps with the time trace of Msn2-YFP. Therefore, this factor normalizes the fluorescence arbitrary unit of RFP with the fluorescence arbitrary unit of YFP and enables the direct comparison of the nuclear level of Msn2-RFP with that of Msn4-YFP in the same single cells (in the unit of “normalized a.u.”). (**B**) Averaged time traces of Msn2 and Msn4 nuclear translocation in the same single cells in response to 20-min 1 μM inhibitor pulse, 0.5M KCl, or 3% ethanol, as indicated. The top left panel illustrates that Msn2-YFP and Msn4-RFP are expressed in the same strain. The averaged traces were normalized by the scaling factor to allow a direct comparison of Msn2 and Msn4 in the same cells. (**C**) Averaged time traces of Msn2 and Msn4 nuclear translocation from the same cells were normalized as % of max. The traces were plotted together and zoomed in to the early time period of the response to demonstrate the small time delay of Msn4 translocation.

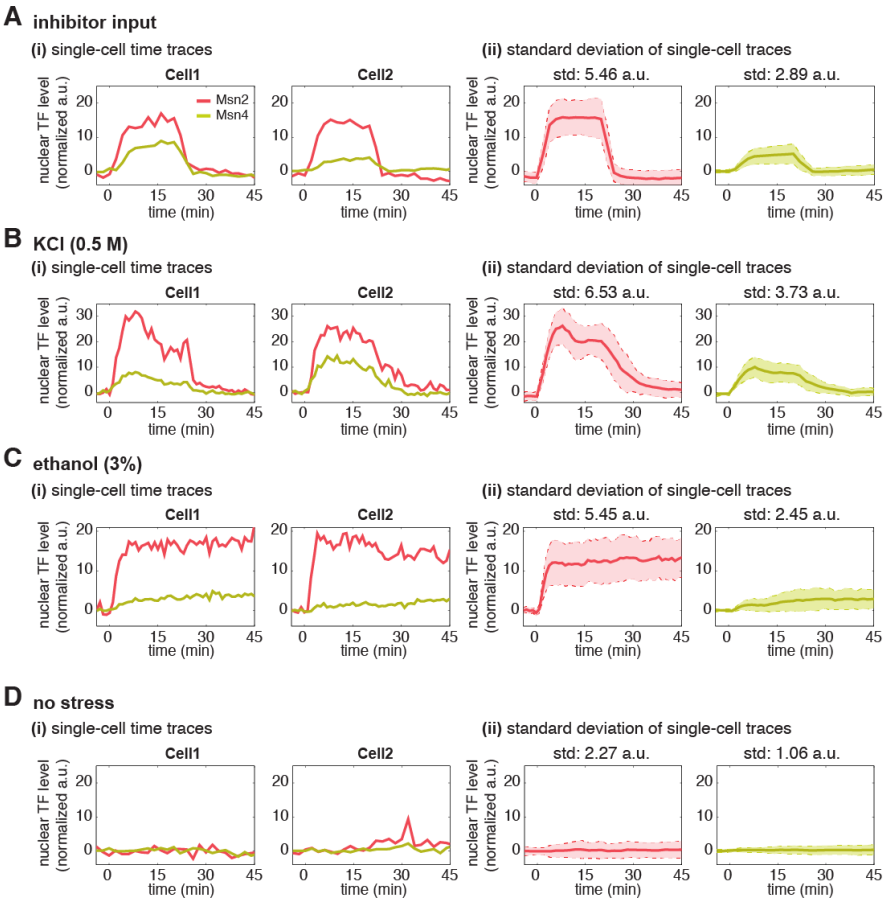

Figure 2.7 Single-cell time traces of Msn2 and Msn4 after normalization of YFP and RFP fluorescence.

After the YFP and RFP normalization as shown in Figure 2.6, time traces of Msn2 and Msn4 nuclear translocation are plotted in the same single cells in response to (**A**) 20-min 1μM inhibitor pulse, (**B**) 0.5M KCl, (**C**) 3% ethanol, or (**D**) no stress. Each panel shows (i) representative single-cell time traces of Msn2 and Msn4 nuclear translocation in the same single cells; (ii) standard deviation of single-cell time traces. For each condition, the single-cell time traces and standard deviations of single cell responses are normalized so that the levels of Msn2 and Msn4 can be compared directly. In (ii), the solid curve represents the averaged time trace; the shaded region represents the standard deviation of single cell responses. The standard deviation is calculated for the peak time point of time traces for each condition and displayed above each time trace. For the condition without stress, the standard deviation is calculated for the time point used in the inhibitor condition.

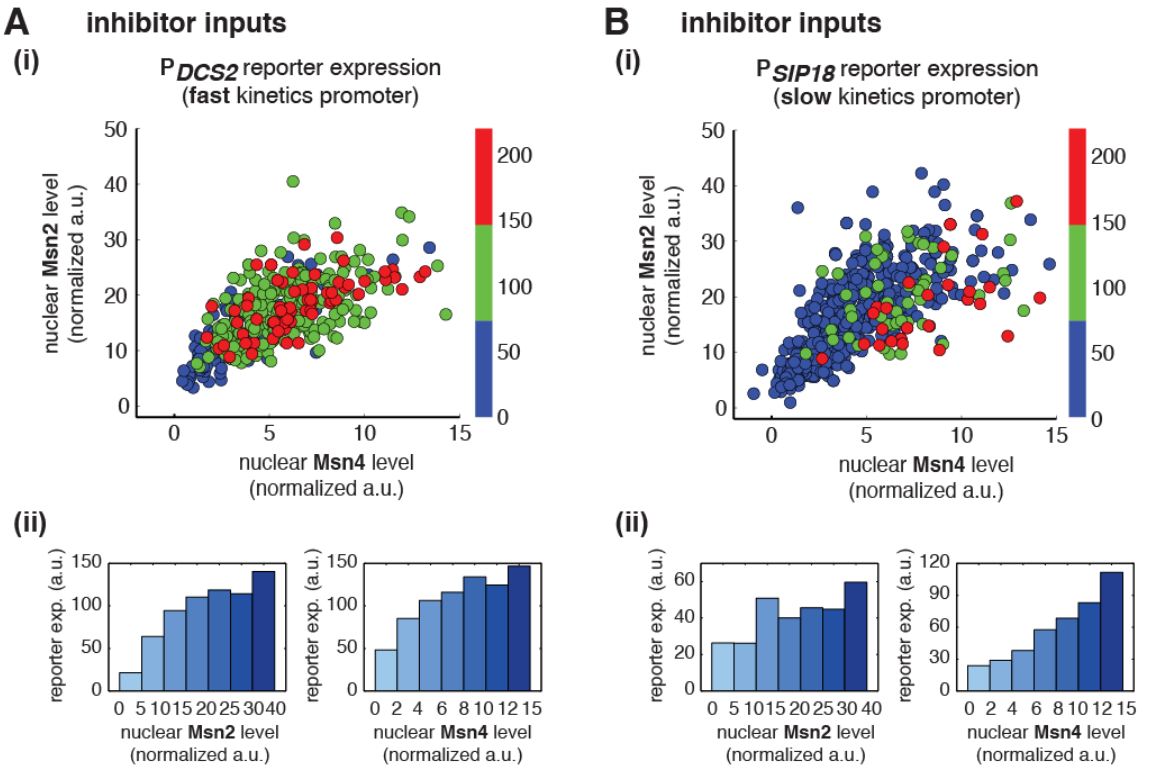

Figure 2.8 Msn2 and Msn4 exhibit distinct gene regulatory functions in single cells in response to 30-min inhibitor inputs.
(**A**) (i) A scatter plot showing the relationship of the fast kinetics promoter P_{DCS2} reporter expression with Msn2 and Msn4 activation at the single cell level. Each dot represents a single cell. Single-cell time traces were tracked over a 3-hour period in which the reporter fluorescence in most cells has already reached the plateau. The x and y axes represent the peak values of Msn4 and Msn2 nuclear translocation (the maximal values in the first 30 min of translocation time traces), respectively; and the dot color represents the maximal level of gene expression as indicated in the color bar. To cover the full dynamic range of TF translocation, the data from the experiments using 30 min inhibitor pulses with 0.1, 0.25, 0.5, 0.75 and 1μM doses have been combined (n: 444 cells). (ii) Plots show the relationships between P_{DCS2} reporter expression and (left) Msn2 or (right) Msn4, respectively. Single cells are binned based on their Msn2 or Msn4 nuclear level as indicated in the x-axis and the average of reporter expression is calculated for each binned groups of single cells and shown in the bar graphs. (**B**) Scatter plots and bar graphs showing the relationship of the slow kinetics promoter P_{SIP18} reporter expression with Msn2 and Msn4 activation at the single cell level. The data analysis and presentation schemes are consistent with those in (A) (n: 595 cells).

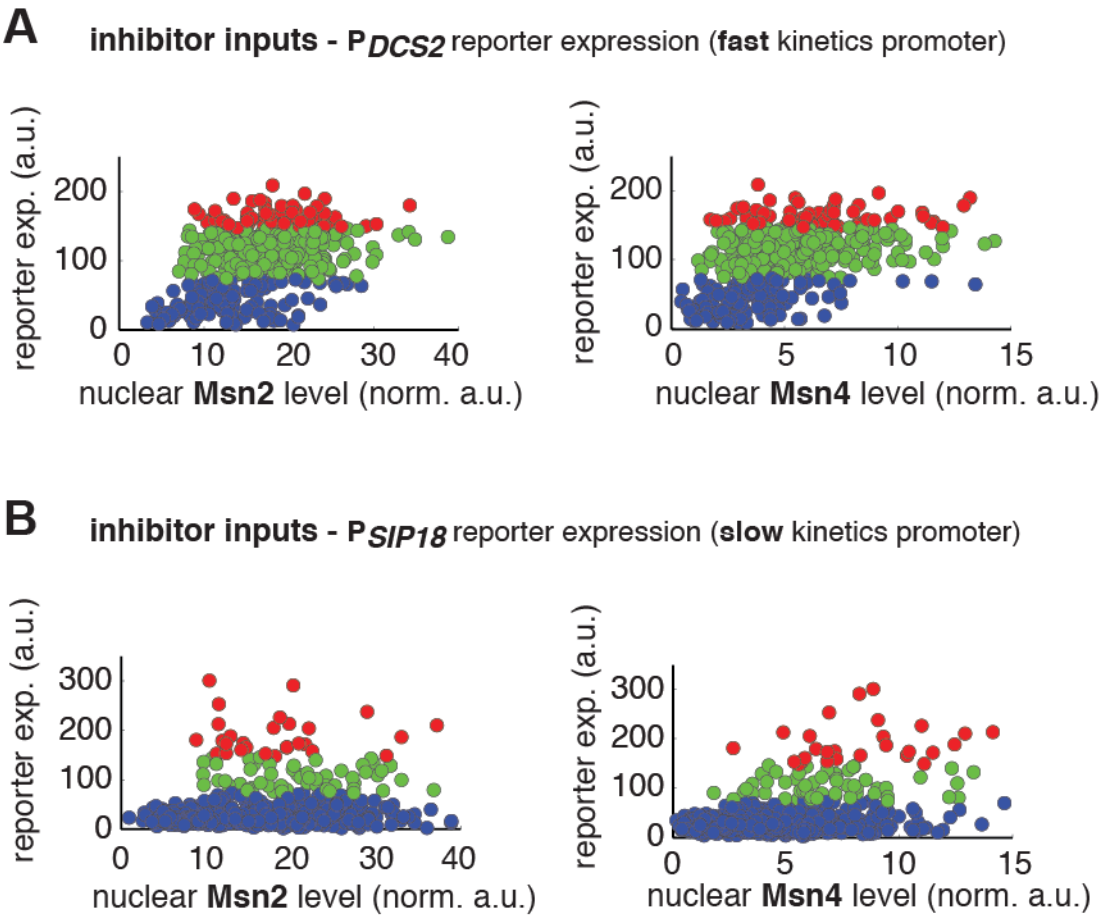

Figure 2.9 Single-cell distributions of reporter gene expression versus nuclear TF levels in response to 30-min inhibitor inputs.
(**A**) Single-cell scatter plots showing the relationships between P_{DCS2} reporter expression with (left) Msn2 or (right) Msn4 nuclear level, respectively. Single-cell data are from Figure 2.8A. (**B**) Single-cell scatter plots showing the relationships between P_{SIP18} reporter expression with (left) Msn2 or (right) Msn4 nuclear level, respectively. Single-cell data are from Figure 2.8B.

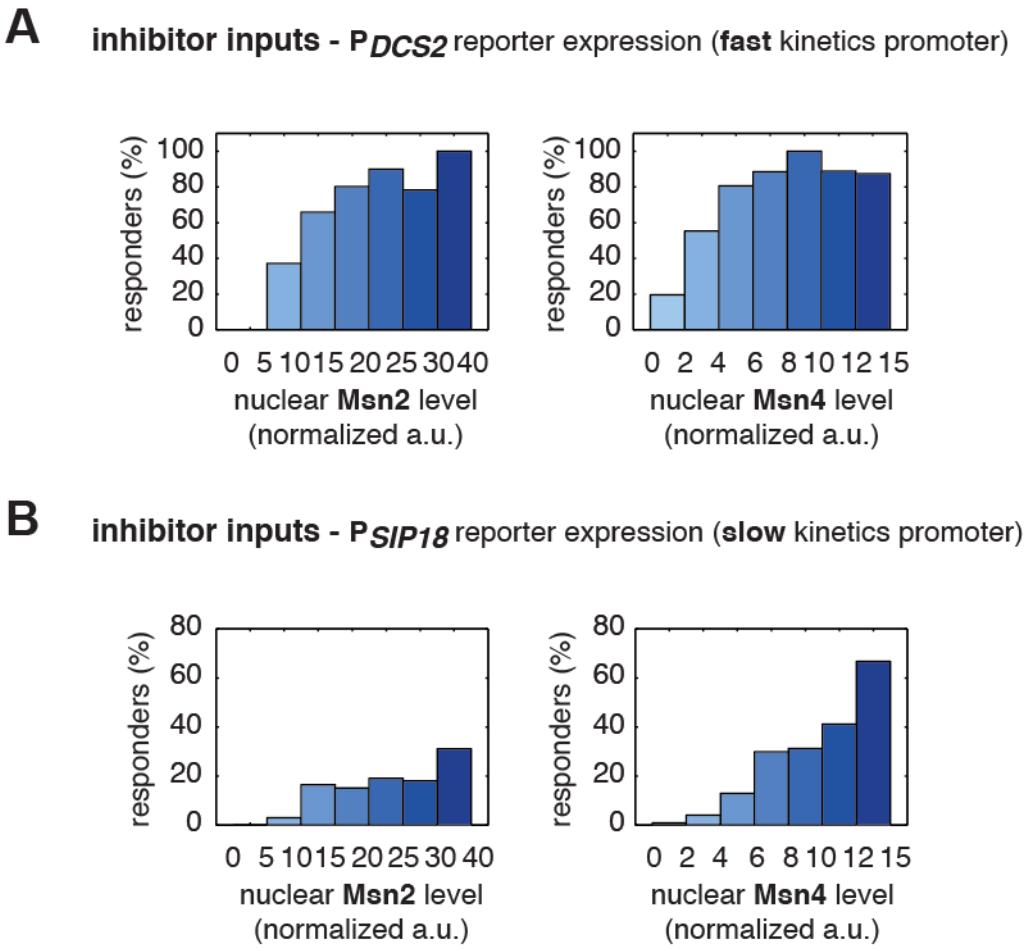

Figure 2.10 The relationship between the probability of reporter gene expression and nuclear TF levels in response to 30-min inhibitor inputs.
(**A**) Bar graphs showing the relationships between the probability of P_{DCS2} reporter expression with (left) Msn2 or (right) Msn4 nuclear level, respectively. Single-cell data are from Figure 2.8A. Single cells are binned based on their Msn2 or Msn4 nuclear level as indicated in the x-axis and the proportion of "responder" cells (green and red cells in Figure 2.8), instead of the average of reporter expression, is calculated for each binned groups of single cells and shown in the bar graphs. (**B**) Bar graphs showing the relationships between the probability of P_{SIP18} reporter expression with (left) Msn2 or (right) Msn4 nuclear level, respectively. Single-cell data are from Figure 2.8B.

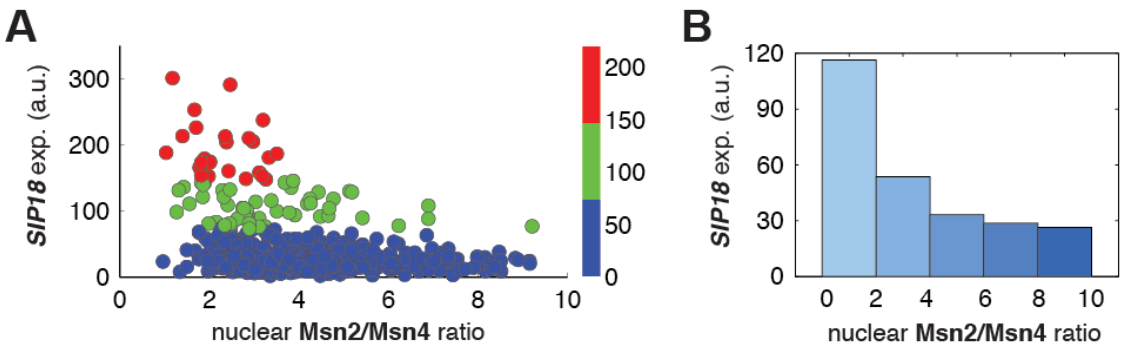

Figure 2.11 Relationship between P_{SIP18} reporter gene expression and the ratio of nuclear Msn2 versus Msn4 in response to 30-min inhibitor inputs. (**A**) Scatter plot showing the single-cell distribution of P_{SIP18} reporter expression with the ratio of nuclear Msn2 versus Msn4. Single-cell data are from Figure 2.8B. (**B**) Bar graph shows the relationship between P_{SIP18} reporter expression and the ratio of nuclear Msn2 versus Msn4. Single cells are binned based on their ratio of nuclear Msn2 versus Msn4 as indicated in the x-axis and the average of reporter expression is calculated for each binned groups of single cells and shown in the bar graphs.

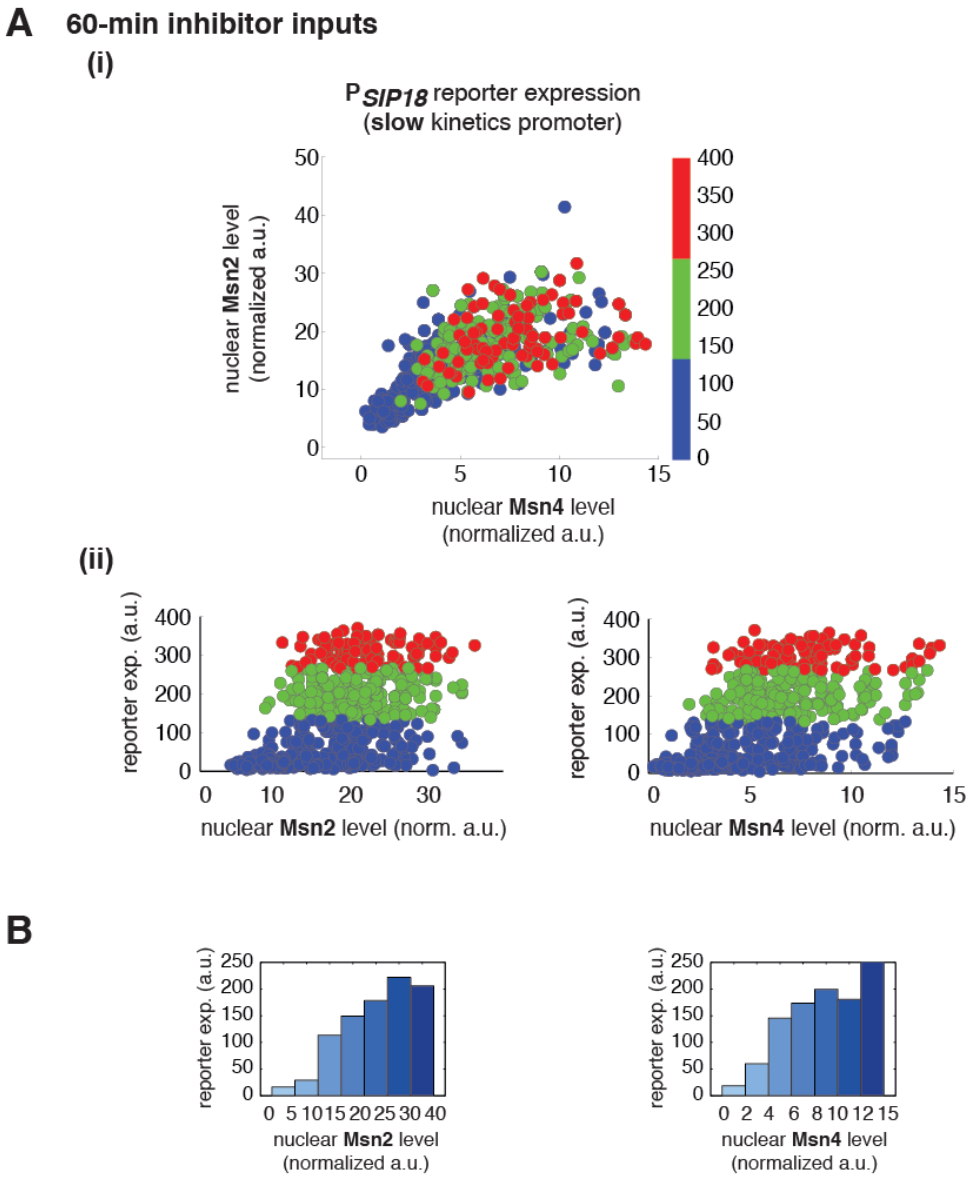

Figure 2.12 Msn2 and Msn4 exhibit similar gene regulatory functions in single cells in response to 60-min inhibitor inputs.

(**A**) (i) A scatter plot showing the relationship of the slow kinetics promoter P_{SIP18} reporter expression with Msn2 and Msn4 activation at the single cell level. To cover the full dynamic range of TF translocation, the data from the experiments using 60 min inhibitor pulses with 0.1, 0.25, 0.5, 0.75 and 1 μM doses have been combined (n: 702 cells). (ii) Single-cell scatter plots showing the relationships between P_{SIP18} reporter expression with (left) Msn2 or (right) Msn4 nuclear level, respectively. Single-cell data are from (i). (**B**) Plots show the relationships between P_{SIP18} reporter expression and (left) Msn2 or (right) Msn4, respectively. Single cells are binned based on their Msn2 or Msn4 nuclear level as indicated in the x-axis and the average of reporter expression is calculated for each binned groups of single cells and shown in the bar graphs.

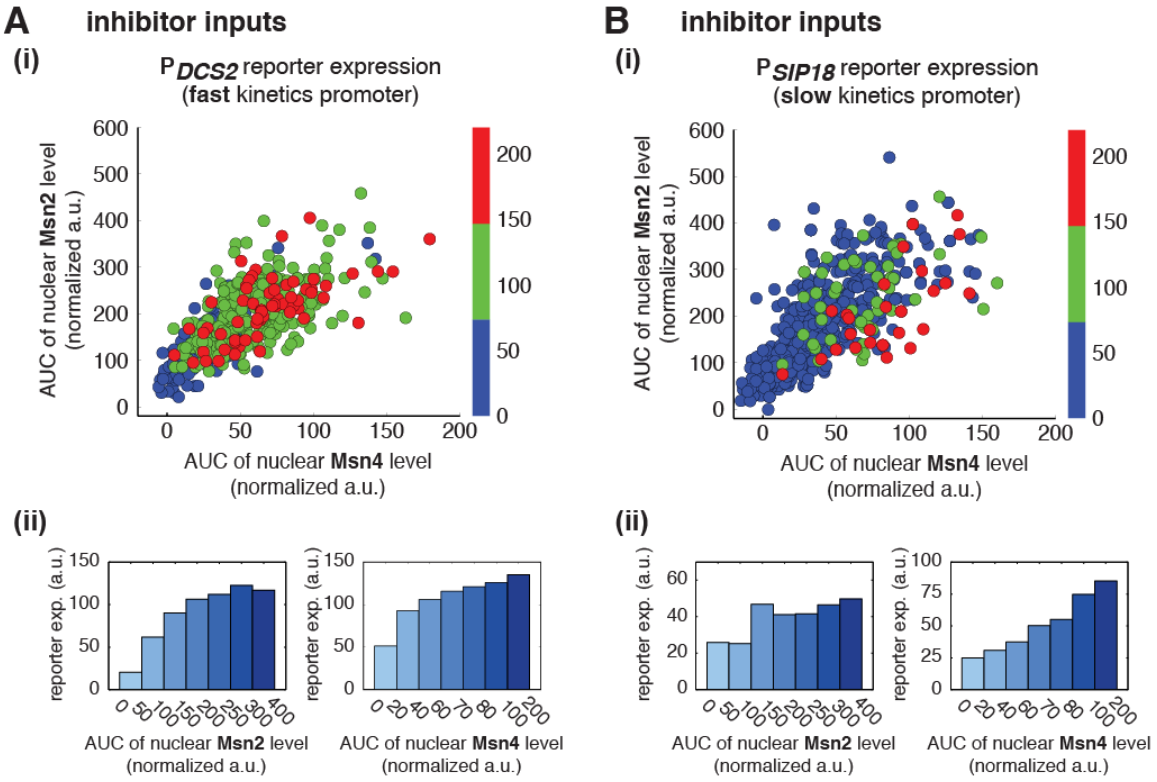

Figure 2.13 Relationship between reporter gene expression and the area-under-the-curve (AUC) of nuclear TF levels in response to 30-min inhibitor inputs.

Single-cell data from Figure 2.8 were analyzed to show the relationship of (**A**) the fast kinetics promoter P_{DCS2} or (**B**) the slow kinetics promoter P_{SIP18} reporter expression with the AUC of Msn2 and Msn4 nuclear translocation. The AUC is calculated as the sum of TF nuclear levels for each single-cell time trace (data points taken every two minutes). (i) Scatter plots showing single-cell distributions; (ii) Bar graphs showing average level of gene expression in single cells binned based on their TF AUCs.

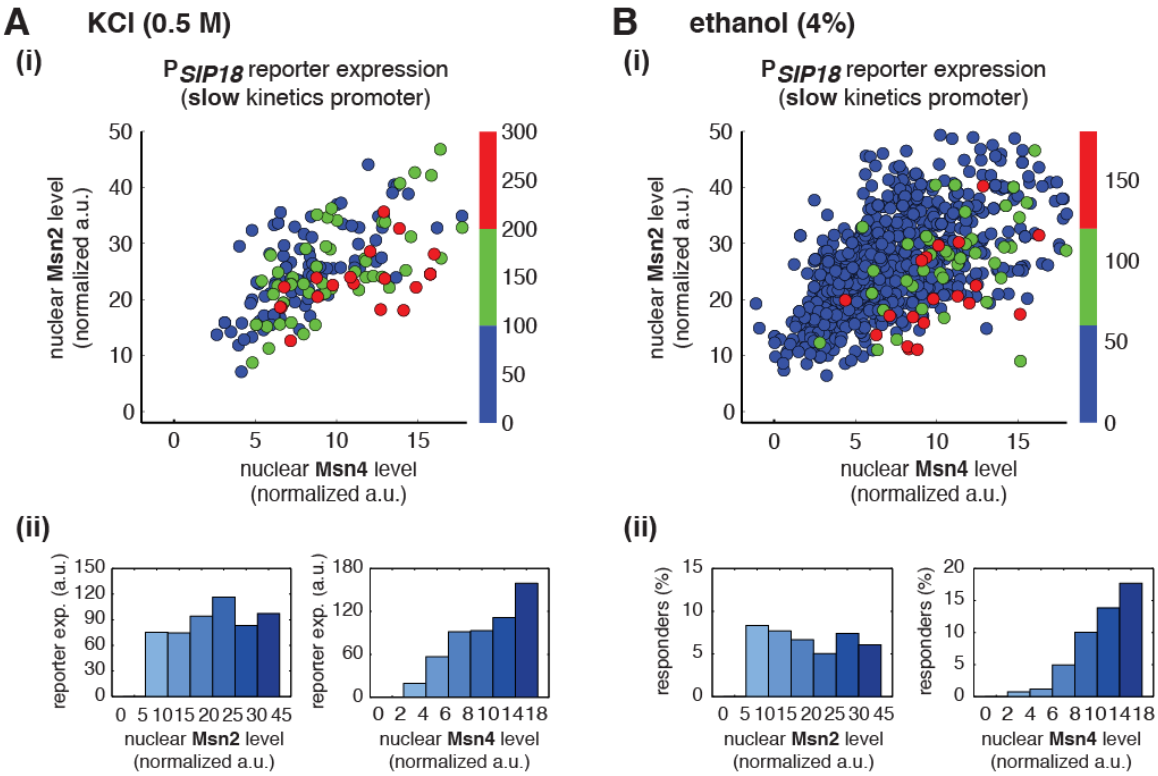

Figure 2.14 Msn2 and Msn4 exhibit distinct gene regulatory functions in single cells in response to natural stresses.

(**A**) (i) A scatter plot showing the relationship of the slow kinetics promoter P_{SIP18} reporter expression with Msn2 and Msn4 activation at the single cell level in response to 0.5M KCl. Each dot represents a single cell. The x and y axes represent the peak values of Msn4 and Msn2 nuclear translocation (the maximal values in the first 30 min of translocation time traces), respectively; and the dot color represents the peak level of gene expression as indicated in the color bar (n: 182 cells). (ii) Plots show the relationships between P_{SIP18} reporter expression and (left) Msn2 or (right) Msn4, respectively. Single cells are binned based on their Msn2 or Msn4 nuclear level as indicated in the x-axis and the average of reporter expression is calculated for each binned groups of single cells and shown in the bar graphs. (**B**) Scatter plots and bar graphs showing the relationship of the slow kinetics promoter P_{SIP18} reporter expression with Msn2 and Msn4 activation at the single cell level in response to 4% ethanol. The data analysis and presentation schemes are consistent with those in (A). Because the majority of cells are not able to express the reporter gene, the proportion of "responder" cells (green and red cells) is quantified and shown in the bar graphs, instead of the average of reporter expression. Data from a large number of single cells are collected to obtain enough responders (n: 924 cells). Single-cell data used in these plots are provided in the source data files.

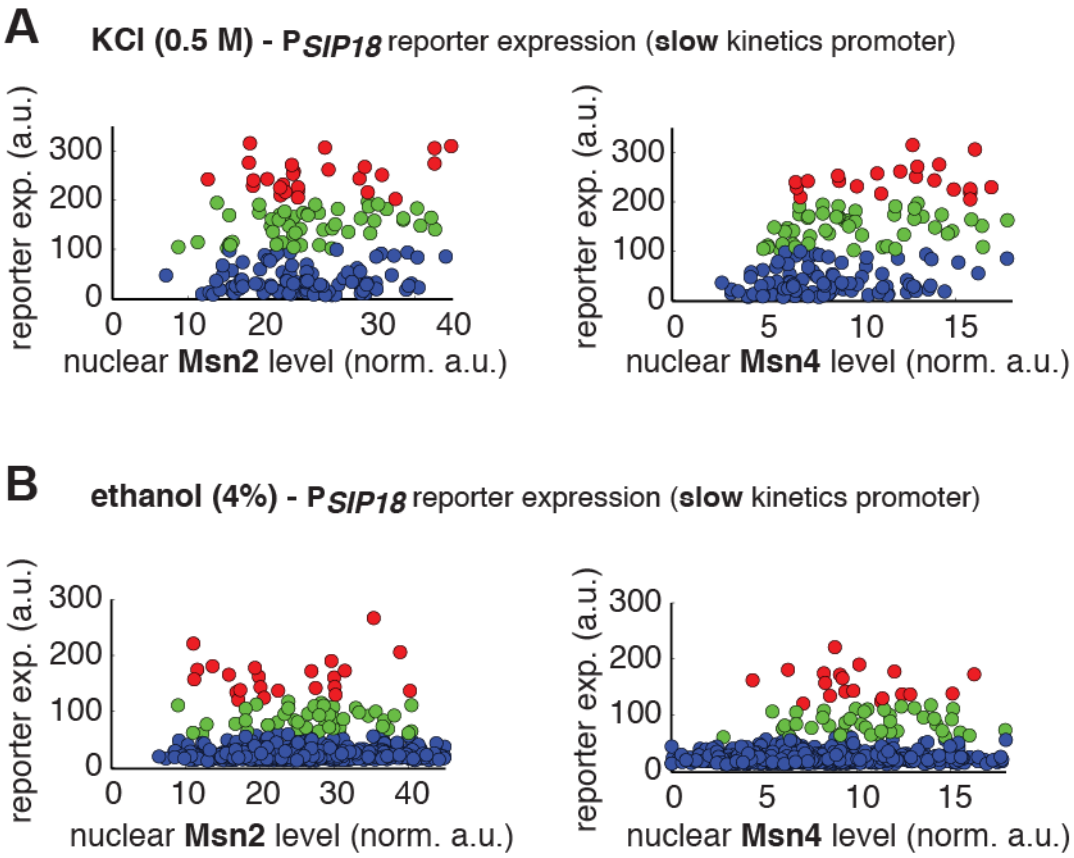

Figure 2.15 Single-cell distributions of reporter gene expression versus nuclear TF levels in response to natural stresses.
(**A**) Single-cell scatter plots showing the relationships between P_{SIP18} reporter expression and (left) Msn2 or (right) Msn4 nuclear level, respectively, in response to 0.5 M KCl. Single-cell data are from Figure 2.14A. (**B**) Single-cell scatter plots showing the relationships between P_{SIP18} reporter expression and (left) Msn2 or (right) Msn4 nuclear level, respectively, in response to 4% ethanol. Single-cell data are from Figure 2.14B. Because the majority of cells are not able to express the reporter gene, scatter plots, instead of box plots, are used here to show the distributions of responder cells (green and red) and non-responder cells (blue) with different TF levels.

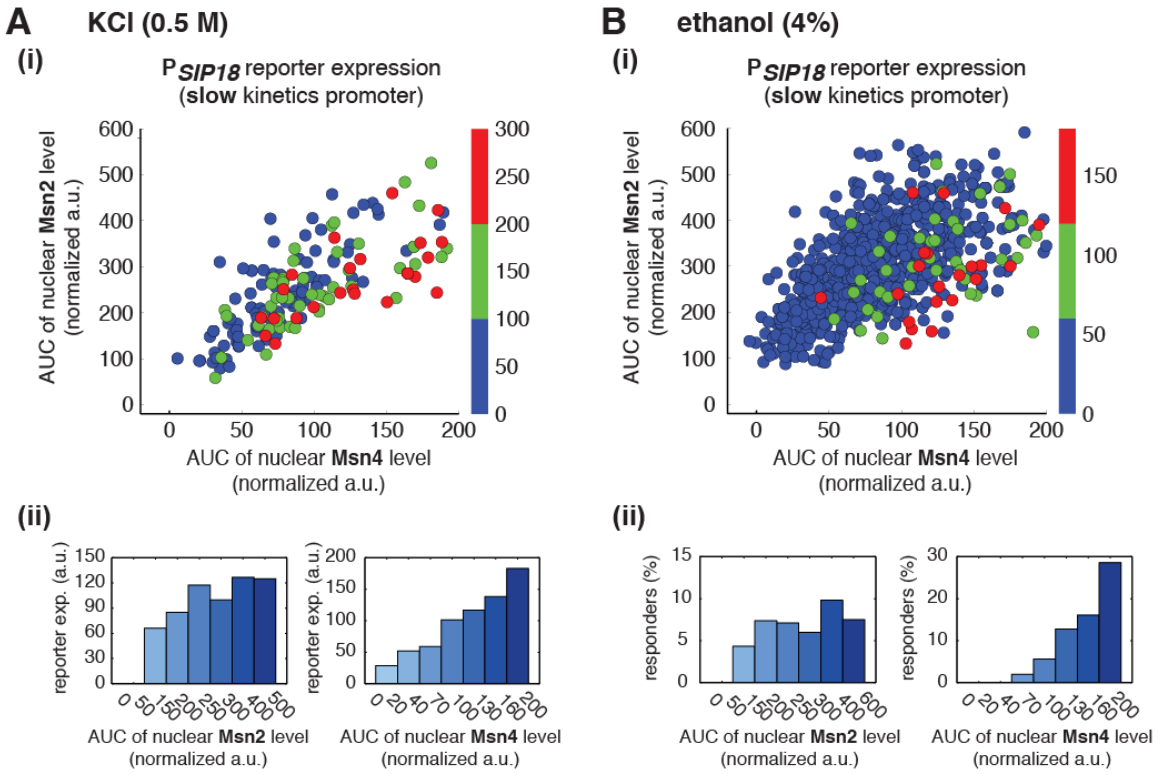

Figure 2.16 Relationship between reporter gene expression and the area-under-the-curve (AUC) of nuclear TF levels in response to natural stresses. Single-cell data in Figure 2.14 were analyzed show the relationship of the slow kinetics promoter P_{SIP18} reporter expression with the AUC of Msn2 and Msn4 nuclear translocation in response to (A) 0.5 M KCl and (B) 4% ethanol. For the ethanol treatment, the AUC is calculated as the sum of TF nuclear levels for the first 30 minutes of stress treatment for each single-cell time trace (data points taken every two minutes). Due to the translational arrest induced by ethanol stress, TF nuclear localization at the later time points would not be able to contribute significantly to gene expression.

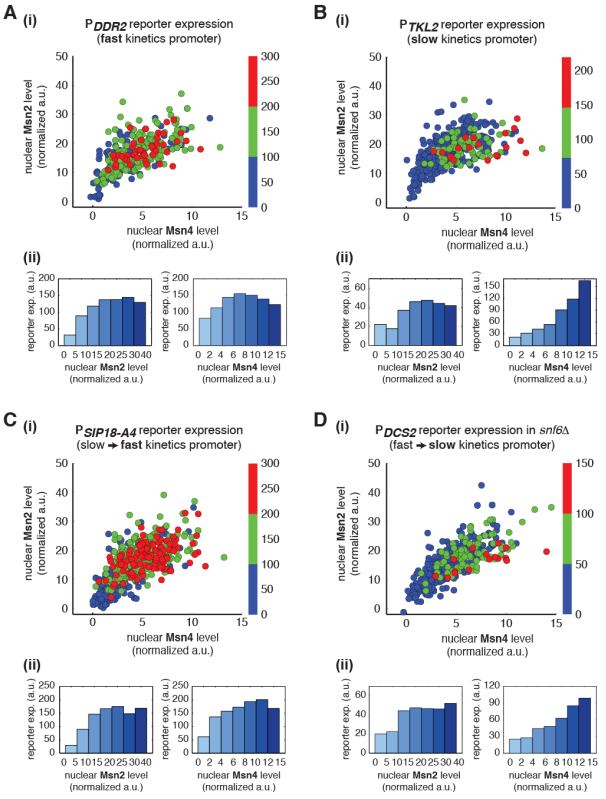

Figure 2.17 Gene regulatory functions of Msn2 and Msn4 on other fast or slow kinetics promoters.

(A) (i) A scatter plot showing the relationship of the fast kinetics promoter P_{DDR2} reporter expression with Msn2 and Msn4 activation at the single cell level. Each dot represents a single cell. Single-cell time traces were tracked over a 3-hour period in which the reporter fluorescence in most cells has already reached the plateau. The x and y axes represent the peak values of Msn4 and Msn2 nuclear translocation (the maximal values in the first 30 min of translocation time traces), respectively; and the dot color represents the maximal level of gene expression as indicated in the color bar. To cover the full dynamic range of TF translocation, the data from the experiments using 30 min inhibitor pulses with 0.1, 0.25, 0.5, 0.75 and 1 μM doses have been combined (n: 407 cells). (ii) Plots show the relationships between P_{DDR2} reporter expression and (left) Msn2 or (right) Msn4, respectively. Single cells are binned based on their Msn2 or Msn4 nuclear level as indicated in the x-axis and the average of reporter expression is calculated for each binned groups of single cells and shown in the bar graphs. Scatter plots and bar graphs showing the relationship between gene expression and Msn2 and Msn4 activation for (**B**) the slow kinetics promoter P_{TKL2} (n: 476 cells), (**C**) the promoter mutant $P_{SIP18\text{-}A4}$ (n: 553 cells), and (**D**) the promoter P_{DCS2} in *snf6Δ* (n: 352 cells). The data analysis and presentation schemes are consistent with those in (A).

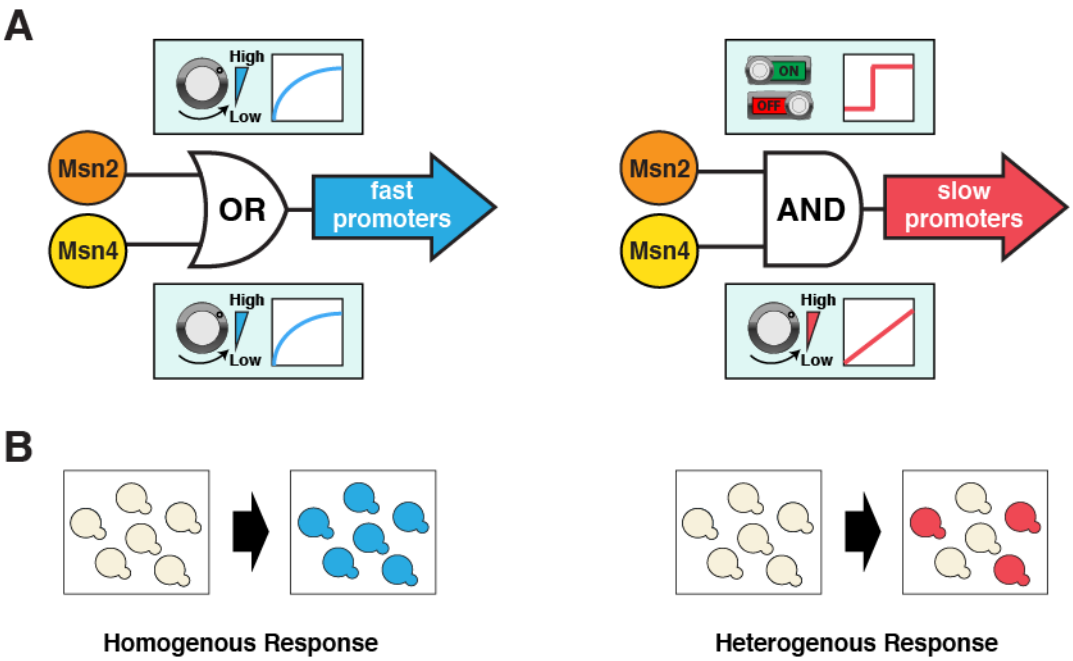

Figure 2.18 Schematics of the gene regulatory logic by Msn2 and Msn4. (**A**) Diagrams illustrating the gene regulatory schemes of Msn2 and Msn4 in controlling (left) fast or (right) slow kinetics promoters. Left: Either Msn2 or Msn4 is sufficient for the induction of fast promoters, constituting an "OR" logic gate. At the single cell level, gene expression shows a similar graded dependence on both Msn2 and Msn4 and reaches saturation upon a low TF activity. Right: Msn2 and Msn4 are both required for the induction of slow promoters, constituting an "AND" logic gate. At the single cell level, Msn2 serves as a low threshold "switch" turning transcription ON or OFF depending on its activity. In contrast, Msn4 functions as a "rheostat", tuning the gene induction level in a linear fashion. (**B**) Diagrams illustrating how the gene regulatory schemes of Msn2 and Msn4 contribute to the heterogeneity in gene expression at the population level. Left: an "OR" logic gate will lead to homogeneous gene expression in a cell population. Right: an "AND" logic gate with the "rheostat" TF Msn4 produces a heterogeneous response in a population of cells.

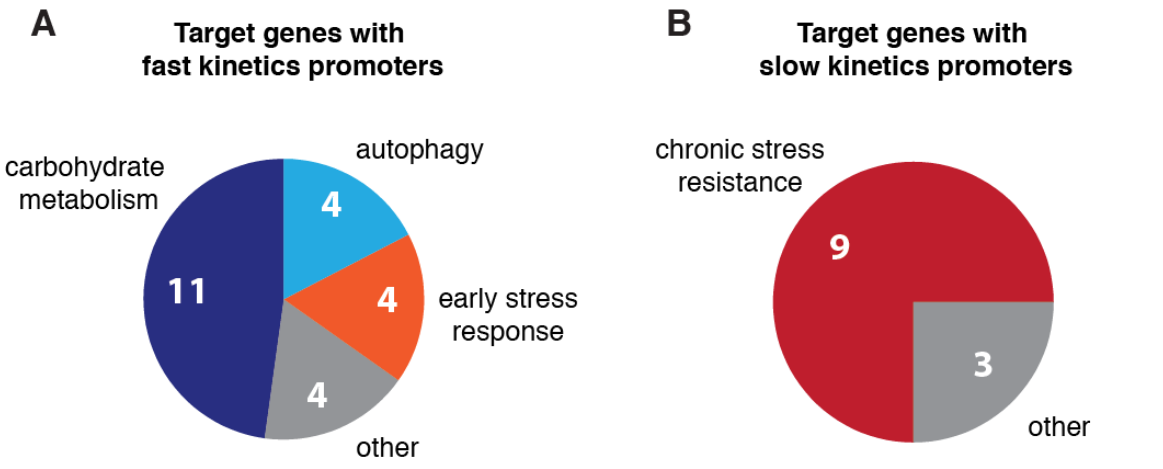

carbohydrate metabolism (11)
PGM2, HXK1, GPH1, GSY2, GSY1, YFR017C, GLC3,TSL1, NTH1, YER067W, CYB2

autophagy (4)
YLR312C, YOL083W, PRC1, CVT19

early transcriptional response during stresses (4)
XBP1, YPL230W, DDR2, EMI2

other (4)
energy metabolism: *CYC7*
mitochondrial protein import: *YBR230C*
mRNA processing: *DCS2*
oxidative stress resistance:*GPX1*

unknown (6)
YNR014W, YPL247C, YHL021C, YNR034W-A, YLR149C, YLR327C

chronic stress resistance (9)
oxidative stress resistance:
GAD1, SIP18, GRX1, GND2, TKL2

ethanol stress resistance: *ALD3*
heat stress resistance *HSP26*
long-term starvation/stationary phase: *YGP1*
long-term starvation/sporulation: *SHC1*

other (3)
carbohydrate metabolism: *ARA1*
energy metabolism: *YKL151C*
Ras/cAMP/PKA signaling: *TFS1*

unknown (2)
YMR196W, YGR043C

Figure 2.19 Biological functions of target genes with fast or slow kinetics promoters.
Pie charts are used to illustrate the functional enrichments for target genes with (**A**) fast and (**B**) slow kinetics promoters. Detailed functional classification for each gene in the two gene groups are shown below the pie charts. Only genes with known functions are included in the pie charts. “Early stress response” includes the genes that are important for early transcriptional response during stresses. The groups of target genes are from Hao and O’Shea, 2012.

Materials and Methods

Yeast strain construction

Standard methods for the growth, maintenance and transformation of yeast and bacteria and for manipulation of DNA were used throughout. All *Saccharomyces cerevisiae* strains used in this study are derived from the W303 background (*ADE+ MATa trp1 leu2 ura3 his3 can1 GAL+ psi+*).

Msn2 was C-terminally tagged with a yeast codon-optimized mCherry by replacing the endogenous stop codon of the *MSN2* locus with *URA3* and then replacing the *URA3* with a linker-mCherry PCR fragment from a pKT vector using 5-FOA. Msn4 was C-terminally tagged with a linker-mCitrineV163A PCR fragment generated from a pKT vector containing yeast codon-optimized mCitrine with the V163A mutation to allow for fast maturation. The endogenous *MSN2* and *MSN4* terminators were left unchanged. *MSN2* and *MSN4* deletion strains (*msn2Δ* and *msn4Δ*, respectively) were made by replacing the endogenous *MSN2* or *MSN4* ORF with *TRP1*. The introduction of gene expression reporters into yeast was performed as described previously (Hansen and O'Shea 2013). The fluorescence reporter gene used is a yeast codon-optimized mTurqouise2. A list of strains is provided in Table 2.1 below.

Table 2.1 Yeast strains used in Chapter 2 study

Strain Name	Description
NH0083	*NHP6a-IRFP:kanMX, TPK1^{M164G}, TPK2^{M147G}, TPK3^{M165G}*
NH0094	*MSN4-mCitrineV163A, MSN2-mCherry, NHP6a-IRFP:kanMX, TPK1^{M164G}, TPK2^{M147G}, TPK3^{M165G}*
NH0095	*msn4Δ::TRP1, MSN2-mCherry, NHP6a-IRFP:kanMX, TPK1^{M164G}, TPK2^{M147G}, TPK3^{M165G}*
NH0108	*MSN4-mCitrineV163A, msn2Δ::natMX, , NHP6a-IRFP:kanMX, TPK1^{M164G}, TPK2^{M147G}, TPK3^{M165G}*
NH0096	*msn4Δ::TRP1, msn2Δ::natMX, NHP6a-IRFP:kanMX, TPK1^{M164G}, TPK2^{M147G}, TPK3^{M165G}*
NH0116	*P_{SIP18}-mTurqouise2-HIS, MSN4-mCitrineV163A, MSN2-mCherry, NHP6a-IRFP:kanMX, TPK1^{M164G}, TPK2^{M147G}, TPK3^{M165G}*
NH0117	*P_{SIP18}- mTurqouise2-HIS, msn4Δ::TRP1, MSN2-mCherry, NHP6a-IRFP:kanMX, TPK1^{M164G}, TPK2^{M147G}, TPK3^{M165G}*
NH0119	*P_{SIP18}- mTurqouise2-HIS, MSN4-mCitrineV163A, msn2Δ::natMX, , NHP6a-IRFP:kanMX, TPK1^{M164G}, TPK2^{M147G}, TPK3^{M165G}*
NH0120	*P_{DCS2}- mTurqouise2-HIS, MSN4-mCitrineV163A, MSN2-mCherry, NHP6a-IRFP:kanMX, TPK1^{M164G}, TPK2^{M147G}, TPK3^{M165G}*
NH0121	*P_{DCS2}- mTurqouise2-HIS, msn4Δ::TRP1, MSN2-mCherry, NHP6a-IRFP:kanMX, TPK1^{M164G}, TPK2^{M147G}, TPK3^{M165G}*
NH0110	*P_{DCS2}- mTurqouise2-HIS, MSN4-mCitrineV163A, msn2Δ::natMX, , NHP6a-IRFP:kanMX, TPK1^{M164G}, TPK2^{M147G}, TPK3^{M165G}*
NH0333	*$P_{SIP18\text{--}A4}$- mTurqouise2-HIS, MSN4-mCitrineV163A, MSN2-mCherry, NHP6a-IRFP:kanMX, TPK1^{M164G}, TPK2^{M147G}, TPK3^{M165G}*
NH0334	*$P_{SIP18\text{--}A4}$- mTurqouise2-HIS, msn4Δ::TRP1, MSN2-mCherry, NHP6a-IRFP:kanMX, TPK1^{M164G}, TPK2^{M147G}, TPK3^{M165G}*
NH0335	*$P_{SIP18\text{-}A4}$- mTurqouise2-HIS, MSN4-mCitrineV163A, msn2Δ::natMX, , NHP6a-IRFP:kanMX, TPK1^{M164G}, TPK2^{M147G}, TPK3^{M165G}*
NH0425	*P_{TKL2}- mTurqouise2-HIS, MSN4-mCitrineV163A, MSN2-mCherry, NHP6a-IRFP:kanMX, TPK1^{M164G}, TPK2^{M147G}, TPK3^{M165G}*
NH0426	*P_{TKL2}- mTurqouise2-HIS, msn4Δ::TRP1, MSN2-mCherry, NHP6a-IRFP:kanMX, TPK1^{M164G}, TPK2^{M147G}, TPK3^{M165G}*
NH0427	*P_{DDR2}- mTurqouise2-HIS, MSN4-mCitrineV163A, MSN2-mCherry, NHP6a-IRFP:kanMX, TPK1^{M164G}, TPK2^{M147G}, TPK3^{M165G}*
NH0428	*P_{DDR2}- mTurqouise2-HIS, msn4Δ::TRP1, , MSN2-mCherry, NHP6a-IRFP:kanMX, TPK1^{M164G}, TPK2^{M147G}, TPK3^{M165G}*
NH0423	*HOG1- mTurqouise2-HIS, MSN4-mCitrineV163A, MSN2-mCherry, NHP6a-IRFP:kanMX, TPK1^{M164G}, TPK2^{M147G}, TPK3^{M165G}*

Table 2.1 Yeast strains used in Chapter 1 study, continued:

Strain Name	Description
NH0424	*HOG1- mTurqouise2-HIS, msn4Δ::TRP1, , MSN2-mCherry, NHP6a-IRFP:kanMX, TPK1^{M164G}, TPK2^{M147G}, TPK3^{M165G}*
NH0237	*MSN2- mCitrineV163A -HIS, NHP6a-IRFP:kanMX*
NH0267	*MSN2- mCherry –TRP1, NHP6a-IRFP:kanMX*

Microfluidics

Making microfluidics wafers and chips

The same microfluidics device was used as that described in chapter 1 and the same fabrication protocols were used.

*Yeast growth conditions for microfluidic*s

Yeast were inoculated in in low fluorescence Synthetic Dextrose (SD) media overnight at 30°C. 2µL, 1µL, or 0.5µL from the overnight culture were then transferred to independent flasks containing 20 mL of SD and grown to an A_{600nm} of 0.4-0.6 (early exponential growth phase) the following day for loading into microfluidics chip.

Setting up microfluidics chip and tubes

For each experiment, two media inlet tubes with 20 mL of media and one waste outlet tube with 10 mL SD were set up next to the microscope. The tubes were set up to allow for a 10 cm height difference between the inlets and the outlet. Soft polyethylene tubing (Intramedic, inner diameter, 0.86 mm; outer diameter, 1.27 mm) was then placed into the media and a 1 mL syringe was used to prime the lines. A binder clip was then used to stop the flow and a 20

gauge connector was inserted into the end of the tubing for later attachment of the line to the microfluidics chip.

The microfluidics chip was placed in a vacuum chamber for 20 minutes before starting the experiment to evacuate any air from the channels. Once removed from the vacuum, water drops were then immediately added to each port to prevent re-introduction of any air. A solution of 2 mg/mL concanavalin A (ConA) was then injected into the channels of the chip using a 1 mL syringe inserted into an ~1.5in segment of polyethylene tubing with a 20 gauge connector. The chip was then left to incubate for roughly 15 minutes. Using a similar method, SD from a fresh syringe was then flowed into our channel used to wash off excess ConA after incubation. Yeast cells were then spun down at 3000 rpm for one minute (Eppendorf 5804/5804R centrifuge) and re-suspended in 3-5 mL of SD depending on OD. The resuspended cells were then loaded into the microfluidics channel and incubated inside the chip for 10 minutes to allow for sufficient adhesion to the glass. A small air bubble followed by a small volume of SD was then intentionally introduced into each channel using our syringe to remove any vertically stacked yeast and obtain a monolayer of yeast cells for imaging. The chip was then mounted onto our microscope using a specially designed holder and taped securely to the stage to prevent unwanted movement. The chip was then connected to the two media inlets first. The flow from the inlet with stress media or 1-NM-PP1 was always immediately cut off using a binder clip allowing flow only from SD to avoid pre-stressing cells. The waste port was

then connected, completing the flow circuit in our device. Tubing was subsequently taped to the stage to minimize any stresses or vibrations on the chip that can cause spurious stage movement during experiments

Time-lapse microscopy

All time-lapse microscopy experiments were performed using a Nikon Ti-E inverted fluorescence microscope with Perfect Focus, coupled to an EMCCD camera (Andor iXon X3 DU897). The light source is a Spectra X LED system. Images were taken using a CFI Plan Apochromat Lambda DM 60X Oil Immersion Objective (NA 1.40 WD 0.13MM). During experiments, the microfluidic device was taped to a customized device holder inserted onto the motorized stage (with encoders) of the microscope. For the experiments only tracking TF dynamics, three positions were chosen for each channel and the microscope was programmed to acquire Phase, YFP, mCherry, and iRFP images every two minutes. For the experiments measuring reporter gene expression, six positions were chosen for each experiment and the microscope was programmed to take iRFP and YFP or mCherry images every two minutes and both Phase and CFP images every 14 minutes for a total of three hours. In all experiments, cells in the device were first exposed to SD media for at least 30 minutes. When the image acquisition started, cells were remained in SD media for the first five minutes to obtain a baseline for each fluorescence channel prior to the introduction of any stressor or 1-NM-PP1. The exposure and intensity settings for each channel

were set as follows: CFP 300ms at 9% lamp intensity, YFP 400ms at 20% lamp intensity, mCherry 300ms at 10% lamp intensity, and iRFP 200ms at 15% lamp intensity. The camera was set to an EM Gain of 300 (within the linear range) for all four flouresence channels.

Image analysis

Fluorescence microscopy image stacks were pre-processed using ImageJ for background subtraction. Images were then processed using a custom MATLAB code for single-cell tracking and fluorescence quantification as described previously (Hao and O'Shea 2012, Hao, Budnik et al. 2013). We determine the sample size of our single-cell data based on similar studies published previously (Hao and O'Shea 2012, Hansen and O'Shea 2013, Hao, Budnik et al. 2013).

Medium and solutions

The low Fluorescence Synthetic Dextrose Media used to culture cells for microfluidics was made up of 1.71g YNB-Folic Acid-Riboflavin Powder, 0.74 g Complete Supplemental Mixture (CSM), 2% glucose, and 5g Ammonium Sulfate per 1L of medium. Concanavalin A (Con A) (Type IV, Sigma-Aldrich) solution containing 5mM $CaCl_2$, 5mM $MnCl_2$, and 2mg/mL concanavalin A was stored at -20°C and thawed at room temperature just before each experiment. 1-NM-PP1 was stored as a 1000x DMSO stock at -20°C and thawed and added to medium

just before an experiment. Stress medium containing KCl was made by diluting SD medium containing 2M KCL or 0.5M KCl to desired concentrations. Stress medium containing ethanol was made fresh just before an experiment by adding an appropriate amount of 100% ethanol to the SD medium.

Acknowledgements

Chapter 2, in full, has been published in *eLife*: Zohreh AkhavanAghdam*, Joydeb Sinha*, Omar. P. Tabbaa* and Nan Hao. "Dynamic control of gene regulatory logic by seemingly redundant transcription factors." eLife (2016). *Denotes co-first authorship. The author of this dissertation was the co-first author of this paper.

Chapter 3: Dynamics of Cellular Memory in Adaptation to Stress

Abstract

Cells must respond appropriately to fluctuating environments in order to survive. Thus, it would be advantageous for a cell to prepare for future severe stresses if its environment demonstrates some initial suboptimal change in conditions. In many organisms, exposure to a mild stress allows the organism to adapt better to a future severe stress, indicating that cellular memory of previous stress is a general feature of many biological systems. The mechanism underlying this cellular memory, however, remains elusive. Using microfluidics and time-lapse microscopy (to monitor a stress response reporter), we modulate the amplitude and duration of mild stress pre-treatment as well as time in between the initial mild stress and the severe stress. Using this system, we have determined that cells acquire an amplitude-dependent short-term memory of previous stress, which is induced and lost rapidly, and a duration-dependent long-term memory which undergoes a plateau phase of stability before finally declining after very long break in between the initial mild stress and severe stress. Finally, we use this information about the different time-scales and dynamical specificity of different types of cellular memory to determine the cellular pathways responsible for the observed memory. Understanding and dissecting memory of previous signaling events could play a huge role in

developing therapies to prevent patient injury or death in response to severe trauma.

Introduction

In nature, organisms are often exposed to fluctuating environments. Therefore, if an organism senses a change in the environment, it would be advantageous for it to prepare for future stresses that might be foreshadowed by the initial change. One can imagine that this is especially pertinent to single cell organisms or individual cells in a fluctuating environment, since their internal environment has very little protection from the outer environment.

In plants, bacteria, flies, and even humans, prior exposure to a previous mild stress allows the system to adapt better to a severe stress in the future, indicating that the concept of a cellular memory of previous stressful events might be a general feature of biological systems (Lou and Yousef 1997, Schenk, Kazan et al. 2000, Durrant and Dong 2004, Scholz, Franz et al. 2005, Matsumoto, Hamada et al. 2007). Determining general mechanisms and motifs involved in this cellular memory could be beneficial in human health, preventing extreme health problems that occur in response to extreme stresses such as stroke, heart attack, radiation exposure, or inflammation.

Previous studies have demonstrated that *Saccharomyces cerevisiae* cells also acquire resistance to severe stress after exposure to a mild stress (Berry and Gasch 2008, Berry, Guan et al. 2011, Guan, Haroon et al. 2012). In Berry

and Gasch 2008, yeast cells exposed to a previous mild stress had increased survival to a more severe dose of that stress and also gained resistance to at least one other type of severe stress (termed cross-protection). It was also determined that nascent protein synthesis was necessary for the acquired stress response, but not basal stress response, which indicates that gene expression triggered by a stress is not required to survive that immediate stress but serves more of a preparative role. Cells lacking *MSN2* and *MSN4* showed a defect in this acquired stress response. In Berry, Guan, et al 2011, the authors identified genes important for acquired resistance to severe oxidative stress after pre-treatment with three different mild stresses (osmotic, heat, or reductive shock) and found that the cells didn't seem to use the same genes for this cross-resistance. Finally, in Guan et al 2012, the authors determined that H_2O_2 tolerance and long-term memory in cells pre-stressed with osmotic stress is due to the production of long-lived Ctt1 protein during the osmotic stress pretreatment, which is then transmitted to daughter cells. They also found that separate from this memory, the pre-stressed cells displayed faster gene expression response to severe H_2O_2.

Thus, we hypothesize that cells use downstream signaling events to encode a "memory" of previous stresses in order to prepare and re-wire cellular processes appropriately in preparation for future severe stresses. We used the yeast stress response pathway as a model system to study and understand the mechanism underlying this memory, which was largely elusive. Since PKA

(Protein Kinase A) inhibition is a common feature of most stresses and the previously mentioned cross-protection studies suggest a common pathway responsible for memory in response to different stresses, we decided to focus our priming studies with PKA inhibition as the priming stimulus. Thus, we utilized a chemical genetics method using the small molecule 1-NM-PP1 which specifically and reversibly inhibits PKA activity combined with microfluidics to modulate the dynamics of priming stimulus that cells are exposed to prior to severe stress treatment. We then compared cellular response to severe osmotic stress with and without priming as a measure of how cells remember the initial priming stimulus. In these experiments, we used quantitative time-lapse microscopy and an observable stress response reporter to determine how processes in the cell are impacted by previous stress signals and key time-scales involved in these processes. From these time-scales, we established a mechanistic understanding of how cellular memory of previous stresses could be occurring.

In these studies, we treated the cells in the microfluidics device with a pulse of PKA inhibitor treatment (using Msn2-mCherry as reporter/output for PKA inhibition) followed by a “break” interval with no treatment before exposing the cells to a severe osmotic stress (0.75M KCl). We also exposed cells to severe osmotic stress without a pre-treatment of PKA inhibition. Thus, PKA inhibition serves as our priming input/stimulus and we can determine the memory of this priming stimulus by comparing the cellular response to severe osmotic stress

with and without PKA inhibition pre-treatment (Figure 3.1A). In our experiments, we could modulate the priming input by changing the duration of prime time, break time, and amplitude to determine how these changes affect the memory of the cells (Figure 3.1B)

We chose severe osmotic stress as our priming output because of the availability of a quantifiable reporter of osmotic stress response, stress-activated protein kinase Hog1, which we endogenously tagged with fluorescent YFP. In response to osmotic stress, Hog1 rapidly translocates to the nucleus to induce an increase in intracellular osmolyte; once the osmolyte balance is restored and the cell recovers from the stress, Hog1 goes out of the nucleus. Thus, the stress response of the cell can be quantified by the duration of Hog1 nuclear localization (Figure 3.1C). We quantified any effect of PKA inhibition on stress response as a variable that we "priming efficiency" (1 subtracted by the duration Hog1 is nuclear localized for that specific PKA inhibition experiment divided by duration Hog1 is nuclear localized in cells that have not been pre-treated with PKA inhibition). This allowed us to compare Hog1 duration and with and without priming to determine how the cell remembers the initial stress (Figure 3.1D).

Results

As previously mentioned, our experimental set up allowed us to modulate the dynamics of the priming stimulus to determine the impact on priming efficiency and cellular memory. We first wanted to determine how long priming

memory lasts. To test this, we kept the priming duration fixed at 45 minutes and amplitude of inhibitor fixed at 3μM and increased break times to see how the long the memory of the 45 minute priming stimulus would be retained (Figure 3.2A). Since we believed that most of the memory would be from priming dependent gene expression that occurred during the 45 minutes of priming stimulus, we expected exponential decay of memory which would follow the dynamics of gene products made during the priming step decaying and being diluted over time (Figure 3.2B). However, we found that cells exhibited the highest amount of priming efficiency with a 10 minute or less break time before severe stress treatment, but rapidly lost a significant amount of priming efficiency after a 15 minute break. We termed this memory that is lost rapidly (half-life of about 15 minutes) short-term memory. After short-term memory is lost, a long-term memory is still retained and is very stable until about 90 minutes of break time (Figure 3.2C). Thus, cells exhibit peak priming efficiency between 0-10 minute break time where cells contain both short-term and long-term memory, after which short-term memory is lost, and only long-term memory is retained and is stable until 90 minutes, when long-term memory finally declines (Figure 3.2D).

Next, we determined how duration of prime time impacts cellular memory of priming stimulus. To do this, we tried three different durations of prime time (45 minutes, 20 minutes, or 15 minutes) with a fixed amplitude of 3μM 1-NM-PP1 while varying the break time before the addition of the severe stress (Figure 3.3A). We found that for all the fixed durations of prime time, cells exhibited the

highest amount of priming efficiency with a 10 minute or less break time before severe stress treatment, but rapidly lost a significant amount of priming efficiency after a 15 minute break. In the 15 minute and 20 minute prime time experiments, cells exhibited no priming effect after a 15 minute break (Figure 3.3B). This demonstrates that short-term memory is not dependent on duration and is lost rapidly, but long-term memory is dependent on the duration of the prime time (since it cannot be induced with a 15 minute prime time) and is retained for longer period of time.

Since the 45 minute prime time curve (Figure 3.2D) exhibits the time-scales of retention and loss of both short-term and long-term memory, we decided to repeat this curve with different amplitudes of PKA inhibition, to determine if short-term or long-term memory dynamics are altered with lower doses of pre-treatment. As shown in Figure 3.4, we found that cells treated with a 45 minute prime time of 1.5μM (green) and 0.75μM (blue) 1-NM-PP1 with varying break times no longer exhibit short-term memory at 0-10 minute break time or a stable region of long-term memory retention between 30-90 minutes. Instead, priming efficiency appeared to decline linearly over time, indicating that short-term memory and some stability of long-term memory (between 30-90 minutes) is dependent on amplitude of the pre-treatment signal.

Therefore, we have found that that short-term memory and some level of long-term memory stability (between 30-90 minutes) is dependent on the amplitude of priming stimulus while long-term memory is dependent on the

duration priming stimulus. Next, we used this information about the different time-scales involved in cellular memory to guide us in determining the mechanisms underlying short-term and long-term memory. Since short-term memory is induced rapidly (within 15 minutes of inhibitor addition) and disappears rapidly, we hypothesized that the mechanism underlying this memory must not be occur through gene expression but rather post-translational regulation of PKA targets. Since long-term memory is duration dependent and long lasting, we hypothesized that it is gene expression dependent.

To test this hypothesis, we picked a condition in which cells only exhibit long-term memory, 45 minutes of 0.75μM 1-NM-PP1 with a 30 minute break (Figure 3.5A), and combined this priming stimulus with cyclohexamide, a translational inhibitor. We hypothesized that long-term memory would be diminished with cyclohexamide if it is gene expression dependent. As expected, long-term memory was diminished in cells exposed to priming stimulus and cyclohexamide compared to priming stimulus alone (Figure 3.5B). To test if this is specific to long-term memory, we picked a priming condition in which the cells only exhibit short-term memory, 15 minutes of 3μM 1-NM-PP1 with a 10 minute break (Figure 3.5C), and determined priming efficiency with and without cyclohexamide treatment. Short-term memory was not affected by cyclohexamide, indicating that gene expression is required for long-term, but not short-term memory (Figure 3.5D).

We hypothesized that short-term memory, which is not dependent on gene expression, occurs through PKA dependent post translational modification, specifically of metabolic pathway components since cells often have to tune these pathways rapidly in response to fluctuating changes in nutrient and growth conditions in the environment. To test this hypothesis, we mutated putative and known PKA targets involved in metabolic and protectant stress-response pathways and compared their priming efficiency to that of WT cells when treated with 15 minutes of 3μM 1-NM-PP1 with a 10 minute break, a condition in which cells exhibit short-term memory but no long-term memory (Figure 3.6A). We found that a strain defective in trehalose metabolism (*hxk2Δtps1Δ*) displayed no short-term memory in this condition when compared to the WT strain (Figure 3.6B). It is important to note that a *hxk2Δtps1Δ* strain was used because *tps1Δ* strains are unable to grow on glucose due to hyperaccumulation of sugar phosphates, but this growth is restored in a *hxk2Δtps1Δ* double mutant in which the *HXK2* mutation reduces sugar phosphate accumulation (Hohmann, Neves et al. 1993). *TPS1* (trehalose-6-phosphate synthase gene) is a component of the trehalose synthase enzyme complex which is involved in the trehalose production (De Virgilio, Burckert et al. 1993, Reinders, Burckert et al. 1997). Trehalose is a dissacharide produced by many organisms under stressful conditions and stationary growth phase and was originally thought to serve as a reserve carbohydrate but now has been implicated in yeast survival in response to many different stresses by acting as membrane protectant and protein

stabilizer (reviewed in (Hounsa, Brandt et al. 1998). Additionally, mutant strains unable to produce trehalose have been found to be sensitive to osmotic stress (Hounsa, Brandt et al. 1998).

To further determine how trehalose production affects short-term and long-term memory dynamics, we treated the *hxk2Δtps1Δ* strain with 45 minutes of 3μM 1-NM-PP1 with varying break times and compared the resulting priming efficiency curves with that of the WT 3μM 1-NM-PP1 45 minute prime curve, which exhibits the time-scales of retention and loss of both short-term and memory as previously described (Figure 3.3). *hxk2Δtps1Δ* cells no longer exhibit short-term memory at 0-10 minute break time compared to wild type cells (Figure 3.6B- blue (*hxk2Δtps1Δ)* versus red (WT) line). The plateau of long-term memory between 30-90 minutes, however, was retained, indicating that TPS1 is required for short-term but not long-term memory. Thus, we hypothesize that priming may induce post-translational modifications of trehalose production enzymes causing them to rapidly increase trehalose levels in the cell, resulting in a short-term memory which is then rapidly lost when PKA inhibition is removed. Interestingly, NTH1 (a trehalose degradation enzyme) is post-translationally activated by PKA (Souza, De Mesquita et al. 2002, Schepers, Van Zeebroeck et al. 2012). Thus, in response to high doses of PKA inhibition, TPS1 is activated, making more trehalose, in the meanwhile, NTH1 is inhibited so it cannot degrade trehalose. Thus, NTH1 inhibition combined with TPS1 activation causes rapid trehalose accumulation with PKA inhibition. However, when the PKA inhibition is gone,

TPS1 is inhibited and NTH1 is activated to remove trehalose quickly. This network can accelerate response rate and removal rate, which explains why short-term memory is induced quickly (within 15 minutes) and lost rapidly (after a 15 minute break time)- see Figure 3.2D. We will further validate the role of trehalose in short-term memory by determining if short-term memory is prolonged with NTH1 deletion or trehalose addition.

To determine the mechanisms underlying long-term memory retention, we mutated Pat1, a P-body scaffolding protein which is phosphorylated by PKA (Ramachandran, Shah et al. 2011)- Figure 3.7A. We focused on P-bodies as putative long-term memory regulators because eukaryotic cells accumulate mRNAs and proteins at these sites (reviewed in (Ramachandran, Shah et al. 2011). Thus, we hypothesized that some of the mRNAs and proteins produced during priming could be stored in P-bodies following the priming event, explaining why the cells don't exhibit linear memory loss after short-term memory loss but a plateau during 30-90 minutes break in which memory is stable (see Figure 3.2). Indeed, the *pat1*Δ strain treated with 45 minutes of inhibitor followed by various break times observes a more linear decrease of memory when compared to the WT strain and memory is no longer kept stable between 30-90 minutes (Figure 3.7B). Thus, P-bodies may play an important role in long-term memory retention, stabilizing mRNA and proteins made during the initial PKA inhibition.

Since long-term memory is gene expression dependent, we considered Msn2/4, transcription factors whose nuclear localization is dependent on PKA as

previously mentioned in chapters 1 and 2, as candidates involved in transcribing gene products responsible for long-term memory (Gorner, Durchschlag et al. 1998). The *msn2/4Δ* strain, did indeed have decreased priming efficiency in response to a 45 minute prime of 3μM 1-NM-PP1 with a 60 minute break compared to WT (Figure 3.8). In this priming condition, WT cells only exhibit long-term memory (see Figure 3.2). However, some long-term memory is still retained in the *msn2/4Δ* strain, indicating that other transcription factors may be involved. We will test other PKA regulated transcription factors such as Hot1, Sko1, Yap1, Gcn4, Gis1, Skn7 and also test priming efficiency with combinations of transcription factor deletion mutants.

Discussion

In summary, cells exposed to PKA inhibition (primed with 1-NM-PP1) retain memory of the priming stimulus and have higher stress resistance to severe osmotic stress compared to unprimed cells. The extent of this memory is dependent on the dynamics of the PKA inhibition (the amplitude and duration of the PKA inhibition) and the time in between the initial PKA inhibition and severe stress response (which we refer to as break time). Cells exposed to 3μM 1-NM-PP1 exhibit a short-term memory of PKA inhibition which is induced rapidly and lost rapidly likely due to the fact that PKA inhibition causes NTH1 inhibition combined with TPS1 activation which results in rapid trehalose accumulation. However, when the PKA inhibition is gone, TPS1 is inhibited and NTH1 is

activated to remove trehalose quickly. This short-term memory is amplitude dependent as it is not seen with lower amplitudes of PKA inhibition.

Long-term memory, on the other hand, is duration dependent: it is not induced in cells exposed to 15 minutes of 3μM 1-NM-PP1, but is induced in cells exposed to 45 minutes of 3μM 1-NM-PP1. As demonstrated in Figure 3.5, long-term memory occurs through gene expression. Interestingly, many of the mRNAs produced during PKA inhibition are retained and stored in P-bodies to allow for long-term memory retention in case severe stress returns, hence why we observed a plateau phase of long-term memory (Figure 3.2C+D). The plateau phase of long-term memory is dependent on amplitude of inhibitor. In future experiments, we will perform FISH experiments to determine if mRNA stability does indeed show a plateau phase during long-term memory in cells treated with 3μM 1-NM-PP1, but not in cells treated with lower doses of inhibitor. A summary of the short-term and long-term memory pathways can be found in Figure 3.9.

Since long-term memory is duration dependent and short-term is amplitude dependent, in response to a transient high amplitude priming stimulus, cells will only exhibit short-term memory of the priming stimulus since the stimulus was transient and most likely required a quick, reversible response.
In response to a low amplitude, longer duration priming stimulus, however, only long-term memory but not short-term memory will be exhibited, perhaps preparing cells in case a more severe stress comes is on the way, but not urgently changing metabolic pathways to deal with the stress. In response to a

longer, higher amplitude priming stimulus, however, both short-term and long-term memory will be exhibited. Short-term memory in yeast stress response is analogous to the innate immune response in humans, respond to something quickly but not lasting for very long. While long-term memory is similar to the adaptive immune response, retaining memory of previous stresses for a long period of time. This type of system could apply to many other organisms and systems in which priming effects are seen.

PKA is involved in many different cellular events and signaling pathways, but how these processes respond to different dynamics of PKA inhibition and the short-term and long-term effects of PKA-induced changes on these cellular processes remains elusive. Our system allowed us to determine that different PKA inhibition dynamics has an observable effect on cellular memory. Mutant strains then allowed us to determine which PKA-targeted cellular pathways are responsible for the memory dynamics. Theoretically, it follows that with this information, we can selectively induce a specific PKA-targeted pathway depending on the amplitude and duration of PKA inhibition. Since we also determined the time-scales that different memory occurs in, we can also understand how long the PKA-targeted pathway effect will last. Teasing out cellular signaling dynamics in a systematic way like this is important for understanding side effects and efficacy of drugs as many clinicians have observed that giving patients higher dose of a drug for a shorter amount of time produces different side effects and drug interactions compared to a lower dose of

a drug for a longer period of time. Additionally, if a drug or treatment is produced to induce “priming” or cellular memory for the prevention of death or injury in response to severe heart attacks, strokes, or inflammation, it will be important to study dynamics of the drug required to induce the memory and how long the drug or pre-treatment would be effective for.

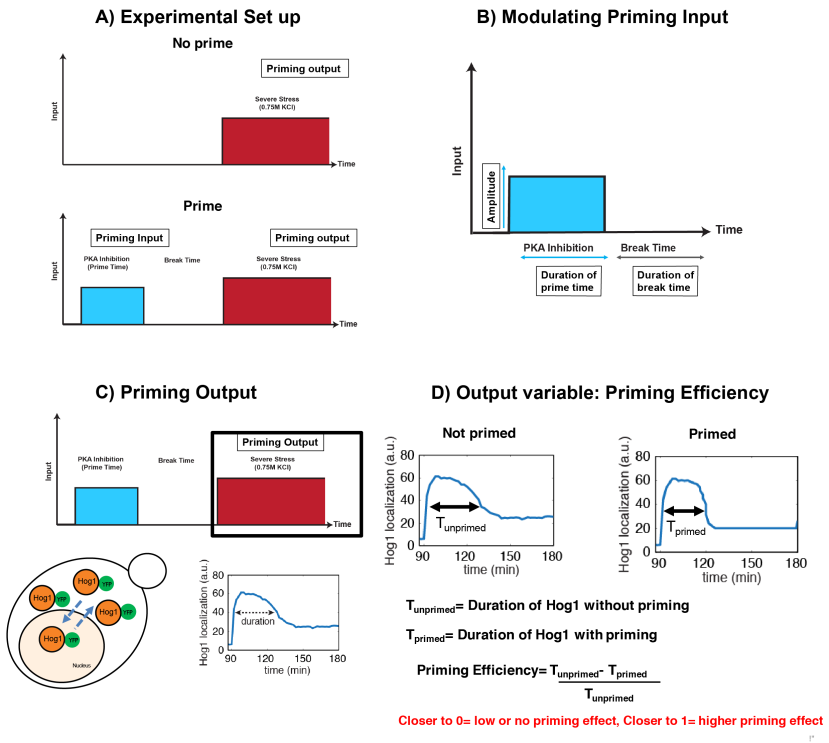

Figure 3.1 Experimental set up for priming experiments

(A) Cells were exposed to severe osmotic stress (0.75M KCl) without a pre-treatment of PKA inhibition (no prime) and compared to cells primed with a pulse of PKA inhibitor treatment) followed by a "break" interval before exposing the cells to a severe osmotic stress (0.75M KCl). Thus, PKA inhibition serves as our priming input/stimulus and we can determine the memory of this priming stimulus by comparing the cellular response to severe stress with and without PKA inhibition pre-treatment. (B) We could modulate the priming input by changing the duration of prime time, break time, and amplitude to determine how these changes affect the memory of the cells. (C) We chose severe osmotic stress as our priming output because of the availability of a quantifiable reporter of osmotic stress response, Hog1, which we endogenously tagged with fluorescent YFP. In response to osmotic stress, Hog1 rapidly translocates to the nucleus and once the cell recovers from the stress, Hog1 goes out of the nucleus. Thus, the stress response of the cell can be quantified by the duration of Hog1 nuclear localization (D) We quantified any effect of PKA inhibition on stress response as a variable that we "priming efficiency" (1 subtracted by the duration Hog1 is nuclear localized for that specific PKA inhibition experiment divided by duration Hog1 is nuclear localized in cells that have not been pre-treated with PKA inhibition). This allowed us to compare Hog1 duration and with and without priming to determine how the cell remembers the initial stress.

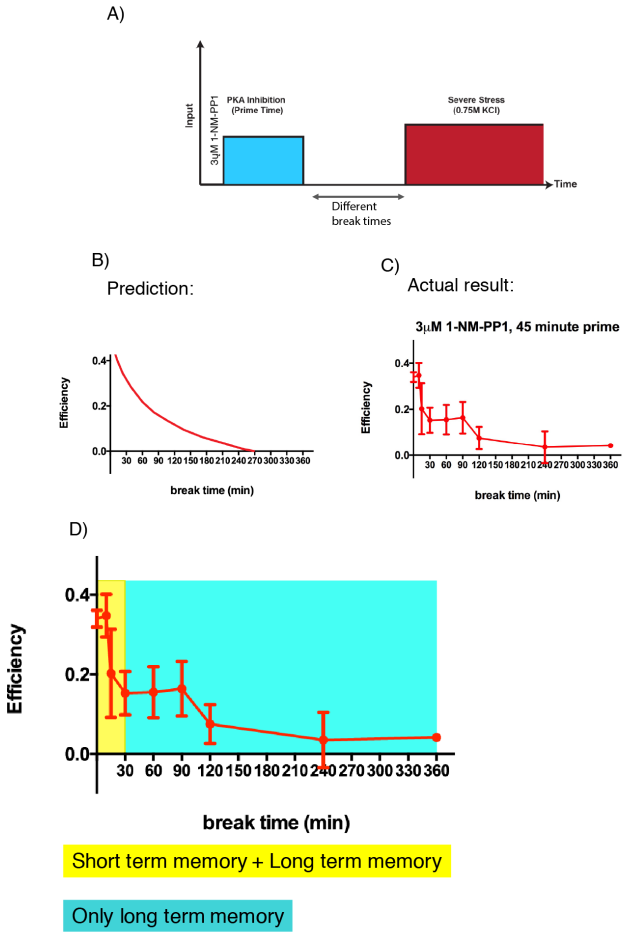

Figure 3.2 Cells exhibit short-term and long-term memory of priming stimulus

(A) We kept the priming duration fixed at 45 minutes and amplitude of inhibitor fixed at 3μM and increased break times to see how the long the memory of the 45 minute priming stimulus would last. (B) Since we believed that most of the memory would be from gene expression that occurred during the 45 minutes of priming stimulus, we expected exponential decay of memory which would follow the dynamics of gene products step decaying and being diluted over time (C) Dynamics of retention and loss of cellular memory: cells exhibited the highest amount of priming efficiency with a 10 minute or less break time before severe stress treatment, but rapidly lost a significant amount of priming efficiency after a 15 minute break. We termed this memory that is lost rapidly (half-life of about 15 minutes) short-term memory. After short-term memory is lost, a long-term memory is still retained and is very stable until about 90 minutes of break time (D). Cells exhibit two phases: peak priming efficiency between 0-10 minutes break time where cells contain both short-term and long-term memory, after which short-term memory is lost, and only long-term memory is retained and is stable until 90 minutes, when long-term memory finally declines.

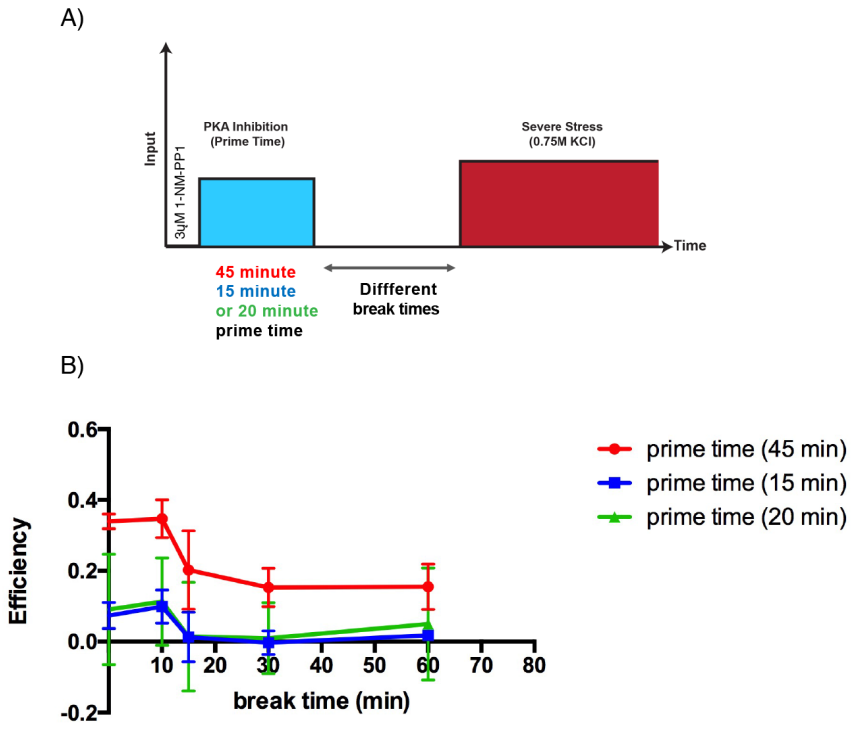

Figure 3.3 Long-term memory, but not short-term memory, of priming stimulus is duration dependent

(A) To test the effect of priming duration on memory, we treated the cells with three different durations of prime time (45 minutes, 20 minutes, or 15 minutes) with a fixed amplitude of 3μM 1-NM-PP1 while varying the break time before the addition of the severe stress (B) We found that for all the fixed durations of prime time, cells exhibited the highest amount of priming efficiency with a 10 minute or less break time before severe stress treatment, but rapidly lost a significant amount of priming efficiency after a 15 minute break. In the 15 minute and 20 minute prime time experiments, cells exhibited no priming effect after a 15 minute break. Thus, short-term memory is not dependent on duration, but long-term memory is dependent on the duration of the prime time (since it cannot be induced with a 15 minute prime time).

A)

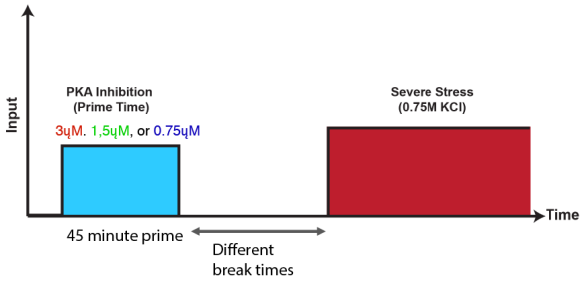

B)

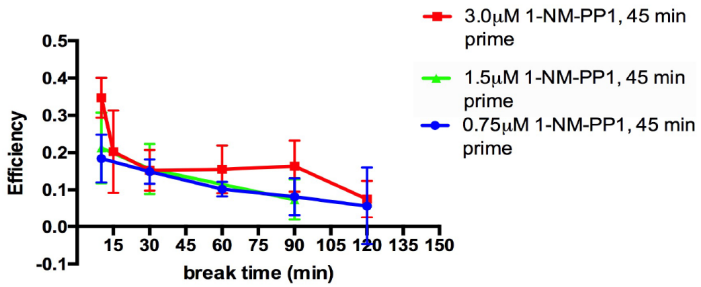

Figure 3.4 Short-term memory and some stability of long-term memory is amplitude dependent

(A) Since the 45 minute prime time curve (Figure 3.2D) exhibits the time-scales of retention and loss of both short-term and long-term memory, we decided to repeat this curve with different amplitudes of PKA inhibition, to determine how amplitude of priming stimulus impacts memory. (B) We found that cells treated with a 45 minute prime time of 1.5μM (green) and 0.75μM (blue) 1-NM-PP1 with varying break times no longer exhibit short-term memory at 0-10 minute break time or a stable region of long-term memory retention between 30-90 minutes. Instead, priming efficiency appeared to decline linearly over time, indicating that short-term memory and some stability of long-term memory (between 30-90 minutes break) is dependent on amplitude of the pre-treatment signal.

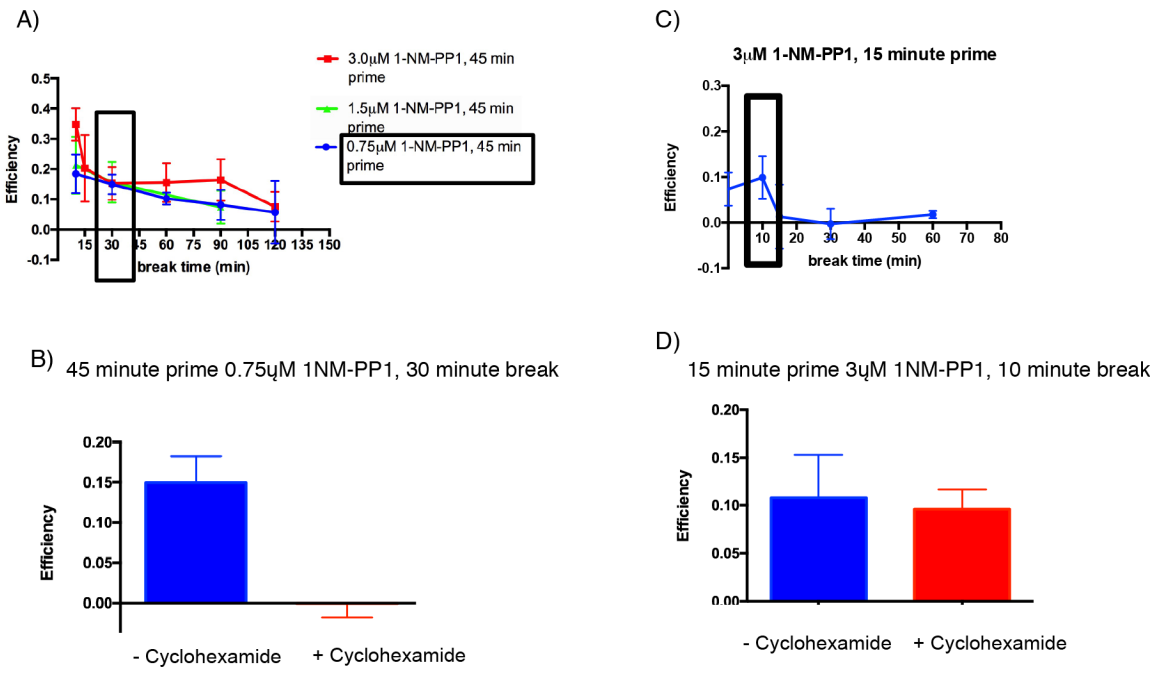

Figure 3.5 Gene expression is required for long-term memory but not short-term memory

(A) To determine the role of gene expression on long-term memory, we picked a condition in which cells only exhibit long-term memory, 45 minutes of 0.75μM 1-NM-PP1 with a 30 minute break (black rectangle), and combined this priming stimulus with cyclohexamide, a translational inhibitor. (B) Long-term memory was diminished in cells exposed to priming stimulus and cyclohexamide compared to priming stimulus alone (C). To test if this is specific to long-term memory, we picked a priming condition in which the cells only exhibit short-term memory, 15 minutes of 3μM 1-NM-PP1 with a 10 minute break (black rectangle), and determined priming efficiency with and without cyclohexamide treatment. (D) Short-term memory was not affected by cyclohexamide, indicating that gene expression is required for long-term, but not short-term memory.

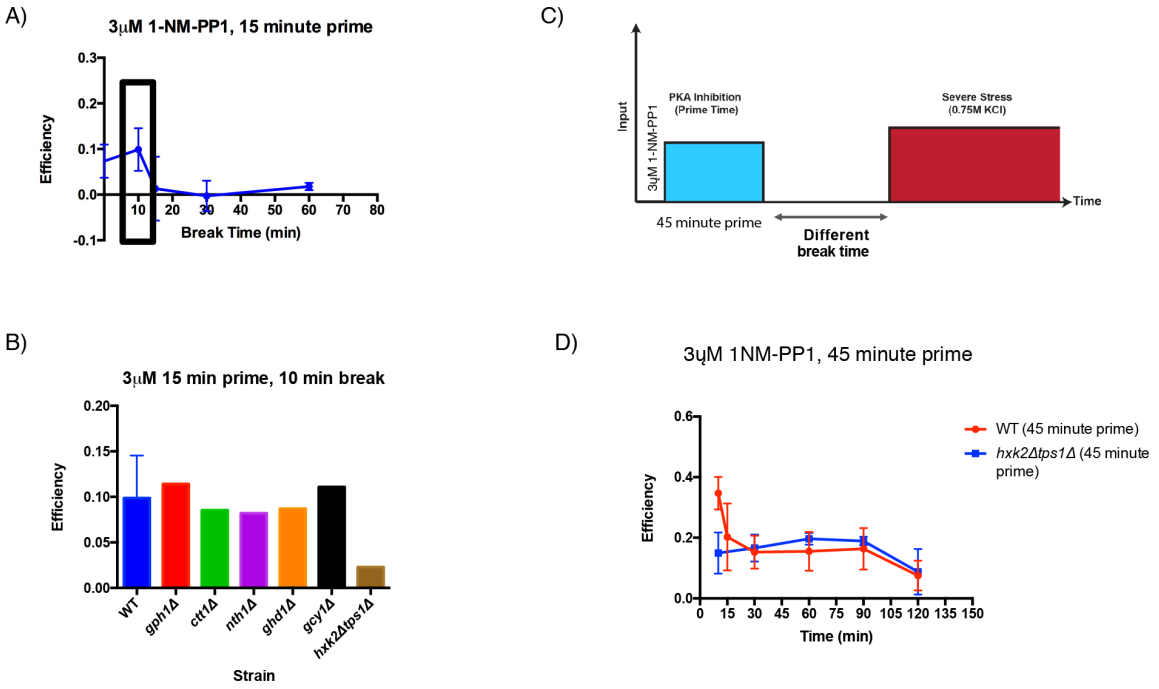

Figure 3.6 *hxk2Δ/tps1Δ*, a strain defective in trehalose production, no longer exhibits short-term memory

(A) To determine mechanism underlying short term memory, we mutated putative and known PKA targets involved in metabolic and protectant stress-response pathways and compared their priming efficiency to that of WT cells when treated with 15 minutes of 3μM 1-NM-PP1 with a 10 minute break, a condition in which cells exhibit short-term memory but no long-term memory (B) We found that a strain defective in trehalose metabolism (*hxk2Δtps1Δ*) displayed no short-memory in this condition when compared to the WT strain (C) To further determine how trehalose production affects short-term and long-term memory dynamics, we treated the *hxk2Δtps1Δ* strain with 45 minutes of 3μM 1-NM-PP1 with varying break times and compared the resulting priming efficiency curves with that of the WT 3μM 1-NM-PP1 45 minute prime curve, which exhibits the time-scales of retention and loss of both short-term and memory as previously described (Figure 3.3). (D) *hxk2Δtps1Δ* cells no longer exhibit short-term memory at 0-10 minute break time compared to wild type cells (blue (*hxk2Δtps1Δ)* versus red (WT) line). The plateau of long-term memory between 30-90 minutes, however, was retained, indicating that TPS1 is required for short-term but not long-term memory.

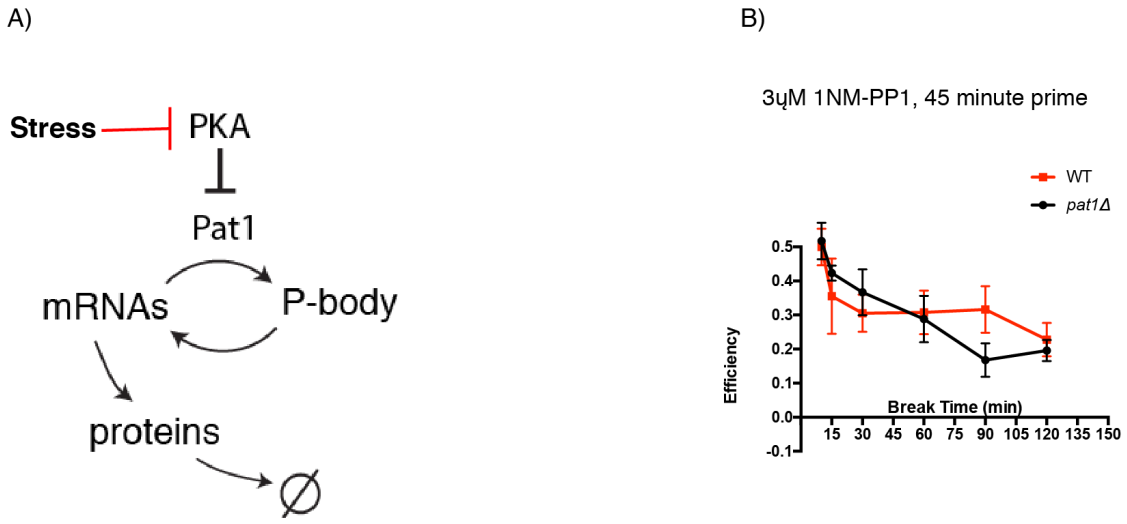

Figure 3.7 *PAT1* is required for long-term memory retention

(A) To determine the mechanisms underlying long-term memory stability seen in Figure 3.2D, we mutated Pat1, a P-body scaffolding protein which is phosphorylated by PKA, We hypothesized that since eukaryotic cells accumulate mRNAs and proteins at these sites, some of the mRNAs and proteins produced during priming could be stored in P-bodies following the priming event, explaining why the cells don't exhibit linear memory loss after short-term memory loss but a plateau during 30-90 minutes break in which memory is stable. (B) Cells lacking the *PAT1* gene were treated with 45 minutes of 3μM 1-NM-PP1 with varying break times (black). These *pat1Δ* cells exhibit a linear decrease in priming efficiency and no longer retain a plateau phase in which long-term memory is stable between 30-90 minutes as seen in WT cells (red). Thus, RNA and protein storage after PKA inhibition may be important for some long-term memory stability.

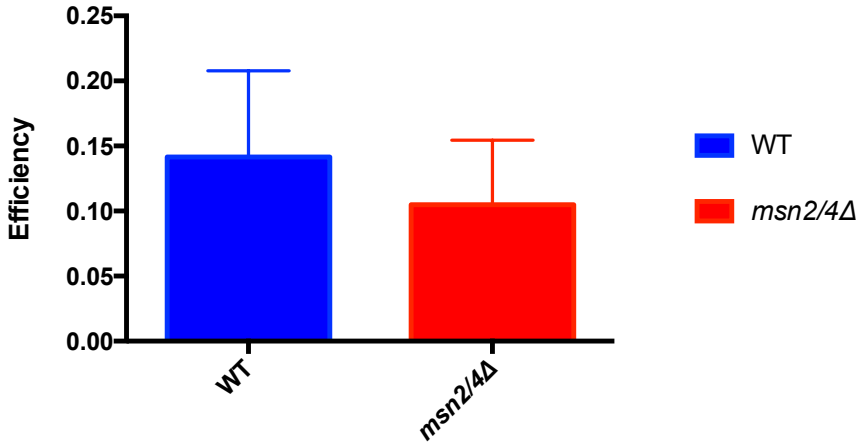

Figure 3.8 Msn2/4 play a role in some PKA-dependent long-term memory

Strains lacking *MSN2* and *MSN4* genes had lower priming efficiency compared to WT cells in response to 3μM 1-NM-PP1 for 45 minutes and 60 minutes break (a condition in which WT cells contain long-term memory). Therefore, Msn2/4-mediated transcription could partly be responsible for some of the long-term memory.

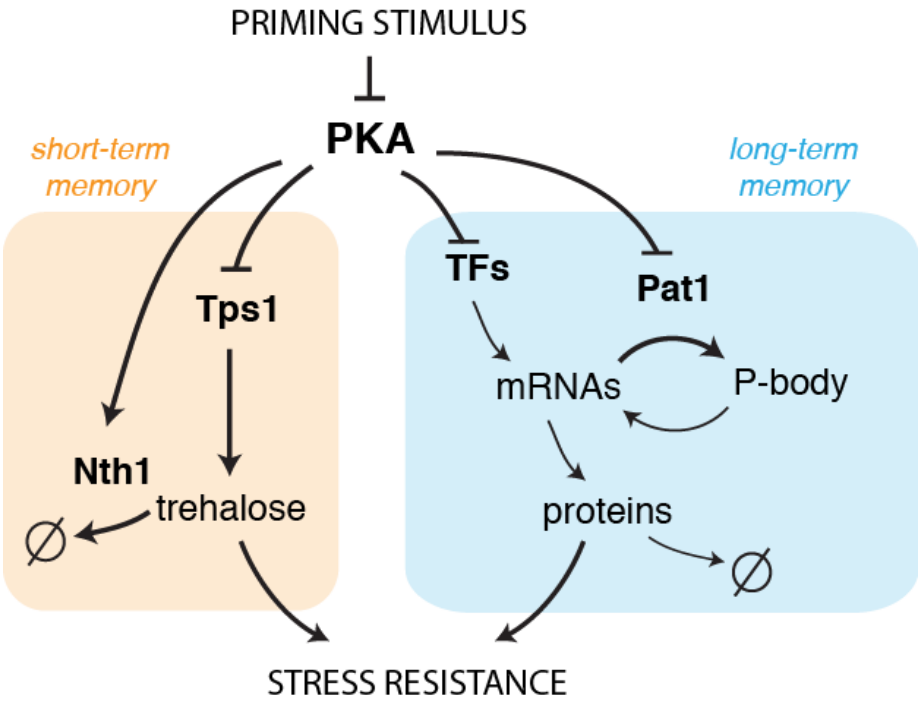

Figure 3.9 Diagram of short term memory and long term memory pathways
(A) Cells exposed to a high amplitude priming stimulus exhibit a short-term memory of priming which is induced rapidly and lost rapidly likely due to the fact that PKA inhibition causes NTH1 inhibition combined with TPS1 activation which results in rapid trehalose accumulation. However, when the PKA inhibition is gone, TPS1 is inhibited and NTH1 is activated to remove trehalose quickly.
(B) Long-term memory of priming stimulus is duration dependent and occurs through priming dependent gene expression. Additionally, some of the mRNAs produced during PKA inhibition are retained and stored in P-bodies to allow for long-term memory retention in case severe stress returns, hence why a plateau phase of long-term memory is observed. This plateau phase of long-term memory is amplitude dependent.

Materials and Methods

Yeast strain construction

Standard methods for the growth, maintenance and transformation of yeast and bacteria and for manipulation of DNA were used throughout. All *Saccharomyces cerevisiae* strains used in this study are derived from the W303 background (*ADE+ MATa trp1 leu2 ura3 his3 can1 GAL+ psi+*). A list of strains is provided in Table 3.1.

Msn2 was C-terminally tagged with a linker-mCherry-TRP PCR fragment generated from a pKT vector containing *TRP1*. Hog1 was C-terminally tagged with a linker-mCitrineV163A PCR fragment generated from a pKT vector containing yeast codon-optimized mCitrine with the V163A mutation to allow for fast maturation and *HIS1*. The endogenous *MSN2* and *HOG1* terminators were left unchanged. *pat1Δ, ctt1Δ, gph1Δ, nth1Δ*, and gcy1*Δ* strains used in were made by replacing the endogenous gene's ORF with *URA3*. The *hxk2Δtps1Δ* strain was made by replacing the endogenous *HXK2* ORF with *LEU2* followed by replacing the endogenous TPS1 ORF with *URA3*. The *msn2/4Δ* strain with the C-terminally tagged was made by C-terminally tagging Hog1 as described above from the pKT vector in strain NH096 listed in Table 3.1 (*msn4Δ::TRP1, msn2Δ::natMX, NHP6a-IRFP:kanMX, TPK1^{M164G}, TPK2^{M147G}, TPK3^{M165G}).* A list of strains is listed in Table 3.1.

Table 3.1 Yeast Strains used in Chapter 3 Study.

Strain	Description
NH441	*HOG1-mCitrineV163A-HIS, MSN2-mCherry-TRP, NHP6a-IRFP:kanMX, TPK1^{M164G}, TPK2^{M147G}, TPK3^{M165G}*
NH442	*HOG1-mCitrineV163A-HIS, msn4Δ::TRP1, msn2Δ::natMX, NHP6a-IRFP:kanMX, TPK1^{M164G}, TPK2^{M147G}, TPK3^{M165G}*
NH517	*HOG1-mCitrineV163A-HIS, pat1Δ::URA3, MSN2-mCherry-TRP, NHP6a-IRFP:kanMX, TPK1^{M164G}, TPK2^{M147G}, TPK3^{M165G}*
NH562	*HOG1-mCitrineV163A-HIS, gph1Δ::URA3, MSN2-mCherry-TRP, NHP6a-IRFP:kanMX, TPK1^{M164G}, TPK2^{M147G}, TPK3^{M165G}*
NH563	*HOG1-mCitrineV163A-HIS, fbp1Δ::URA3, MSN2-mCherry-TRP, NHP6a-IRFP:kanMX, TPK1^{M164G}, TPK2^{M147G}, TPK3^{M165G}*
NH565	*HOG1-mCitrineV163A-HIS, nth1Δ::URA3, MSN2-mCherry-TRP, NHP6a-IRFP:kanMX, TPK1^{M164G}, TPK2^{M147G}, TPK3^{M165G}*
NH566	*HOG1-mCitrineV163A-HIS, ctt1Δ::URA3, MSN2-mCherry-TRP, NHP6a-IRFP:kanMX, TPK1^{M164G}, TPK2^{M147G}, TPK3^{M165G}*
NH567	*HOG1-mCitrineV163A-HIS, gdh1Δ::URA3, MSN2-mCherry-TRP, NHP6a-IRFP:kanMX, TPK1^{M164G}, TPK2^{M147G}, TPK3^{M165G}*
NH568	*HOG1-mCitrineV163A-HIS, gcy1Δ::URA3, MSN2-mCherry-TRP, NHP6a-IRFP:kanMX, TPK1^{M164G}, TPK2^{M147G}, TPK3^{M165G}*
NH569	*HOG1-mCitrineV163A-HIS, tps1Δ::URA3, , hxk2Δ::LEU2, MSN2-mCherry-TRP, NHP6a-IRFP:kanMX, TPK1^{M164G}, TPK2^{M147G}, TPK3^{M165G}*

Microfluidics

Yeast growth conditions for microfluidics

Yeast were inoculated in in low fluorescence Synthetic Dextrose (SD) media overnight at 30°C. 2µL, 1µL, or 0.5µL from the overnight culture were then transferred to independent flasks containing 20 mL of SD and grown to an A_{600nm} of 0.4-0.6 (early exponential growth phase) the following day for loading into microfluidics chip.

Making microfluidics wafers and chips

The microfluidics device used in this study is modified from a previously reported device (Hersen, McClean et al. 2008), so that four independent experiments can be run in parallel on a single chip. The mask was designed to allow for bonding of four antiparallel Y-shaped devices on one microfluidics chip. The SU8 wafer was fabricated using standard photolithography with channel width 400μm and channel height 111μm.

Microfluidic chips were made by pouring PDMS (polydimethylsiloxane) onto the wafer, degassing, and curing in 80°C oven for one hour. The PDMS was then removed from the wafer and individual chips were cut and hole punched using a Harris Uni-Core 1.00 puncher. The Y shaped devices were hole punched to allow for 3 inlets (one for SD media, one for SD + inhibitor media, and one for SD+ 0.75M KCl) and one outlet for waste. The chips and coverslips were cleaned and bonded as described in chapter 1.

Setting up microfluidics chip and tubes

For each experiment, three media inlet tubes (SD, SD+ 1-NM-PP1, and SD + 0.75M KCl) with 20 mL of media and one waste outlet tube with 10 mL SD were set up next to the microscope. The tubes were set up to allow for a 10 cm height difference between the inlets and the outlet. Soft polyethylene tubing (Intramedic, inner diameter, 0.86 mm; outer diameter, 1.27 mm) was then placed into the media and a 1 mL syringe was used to prime the lines. A binder clip was

then used to stop the flow and a 20 gauge connector was inserted into the end of the tubing for later attachment of the line to the microfluidics chip.

Loading of the microfluidics chip was done as described in chapter 1 and chapter 2 of this thesis- the microfluidics chip was placed in a vacuum chamber for 20 minutes before starting the experiment to evacuate any air from the channels. Once removed from the vacuum, water drops were then immediately added to each port to prevent re-introduction of any air. A solution of 2 mg/mL concanavalin A (ConA) was then injected into the channels of the chip using a 1 mL syringe inserted into an ~1.5in segment of polyethylene tubing with a 20 gauge connector. The chip was then left to incubate for roughly 15 minutes. Using a similar method, SD from a fresh syringe was then flowed into our channel used to wash off excess ConA after incubation. Yeast cells were then spun down at 3000 rpm for one minute (Eppendorf 5804/5804R centrifuge) and re-suspended in 3-5 mL of SD depending on OD. The resuspended cells were then loaded into the microfluidics channel and incubated inside the chip for 10 minutes to allow for sufficient adhesion to the glass. A small air bubble followed by a small volume of SD was then intentionally introduced into each channel using our syringe to remove any vertically stacked yeast and obtain a monolayer of yeast cells for imaging. The chip was then mounted onto our microscope using a specially designed holder and taped securely to the stage to prevent unwanted movement.

The chip was then connected to the three media inlets first. The flow from the inlet with SD + 1-NM-PP1 and SD + 0.75M KCl was always immediately cut off using a binder clip allowing flow only from SD to avoid pre-stressing cells. The waste port was then connected, completing the flow circuit in our device. Tubing was subsequently taped to the stage to minimize any stresses or vibrations on the chip that can cause spurious stage movement during experiments

Time-lapse microscopy

All time-lapse microscopy experiments were performed using a Nikon Ti-E inverted fluorescence microscope with Perfect Focus, coupled to an EMCCD camera (Andor iXon X3 DU897). The light source is a Spectra X LED system. Images were taken using a CFI Plan Apochromat Lambda DM 60X Oil Immersion Objective (NA 1.40 WD 0.13MM). During experiments, the microfluidic device was taped to a customized device holder inserted onto the motorized stage (with encoders) of the microscope. For the experiments, three positions were chosen for each channel and the microscope was programmed to acquire Phase, YFP, mCherry, and iRFP images every two minutes. In all experiments, cells in the device were first exposed to SD media for at least 30 minutes. When the image acquisition started, cells were remained in SD media for the first five minutes to obtain a baseline for each fluorescence channel prior to the introduction of 1-NM-PP1 (for the priming). The exposure and intensity settings for each channel were set as follows: YFP 400ms at 20% lamp intensity,

mCherry 300ms at 10% lamp intensity, and iRFP 300ms at 15% lamp intensity. The camera was set to an EM Gain of 300 (within the linear range) for all four flouresence channels.

Image analysis

Fluorescence microscopy image stacks were pre-processed using ImageJ for background subtraction. Images were then processed using a custom MATLAB code for single-cell tracking and fluorescence quantification as described previously (Hao and O'Shea 2012, Hao, Budnik et al. 2013). We determine the sample size of our single-cell data based on similar studies published previously (Hao and O'Shea 2012, Hansen and O'Shea 2013, Hao, Budnik et al. 2013).

Medium and solutions

The low fluorescence Synthetic Dextrose (SD) Media used to culture cells for microfluidics was made up of 1.71g YNB-Folic Acid-Riboflavin Powder, 0.74 g Complete Supplemental Mixture (CSM), 2% glucose, and 5g Ammonium Sulfate per 1L of medium. Concanavalin A (Con A) (Type IV, Sigma-Aldrich) solution containing 5mM $CaCl_2$, 5mM $MnCl_2$, and 2mg/mL concanavalin A was stored at -20°C and thawed at room temperature just before each experiment. 1-NM-PP1 was stored as a 1000x DMSO stock at -20°C and thawed and added to medium just before an experiment. SD + 0.75M KCl medium was made up of 55.913g

KCl, 1.71g YNB-Folic Acid-Riboflavin Powder, 0.74 g Complete Supplemental Mixture (CSM), 2% glucose, and 5g Ammonium Sulfate per 1L of medium.

Acknowledgements

Chapter 3 will be prepared for submission for the publication of the material by December 2017: Zohreh AkhavanAghdam, Yanfei Jiang, Nan Hao. “Dynamics of Cellular Memory in Adaptation to Stress”. The dissertation author is the co-first author and investigator of the paper.

Future Directions/Prospects

In Chapter 1, we used modeling and experiments to demonstrate that different upstream network structures in glucose limitation versus osmotic stress could be responsible for the differences we see in Msn2 translocation dynamics. However, we would have a much stronger case for this model if we mutated sites in the PKA or SNF1 pathway that are regulated by each other and showed that this resulted in altered Msn2 translocation dynamics in response to glucose limitation. This would, of course, require a lot of biochemical experiments and there may be many locations in each upstream pathway where they interact. Lastly, it remains unknown how upstream pathway interactions cause sustained Msn2 dynamics and perhaps that sustained dynamics could be disrupted with mutants altering network structures in upstream pathways.

On a similar subject, I began a project during my PhD in which I tried to investigate how importin and exportin localization and Ran-GTP gradient changes in response to nutrient availability could alter Msn2 dynamics, but never completed this project. This project was inspired by a paper which demonstrated that glucose availability regulates the subcellular localization of importin-β family members due to alterations of the Ran-GTP gradient in response to glucose deprivation (Huang and Hopper 2014). It is possible that some of the differences in Msn2 localization in different conditions could be a result of changes to nuclear pore complex members or important/exportin localization.

In Chapter 2, we studied combinatorial gene regulation by homologous TFs and demonstrated that homolog TFs Msn2 and Msn4 have distinct gene regulatory roles. For slow kinetic promoters, Msn2 functions as a “switch” governing the ON and OFF state of genes, while Msn4 functions as a “rheostat” to tune the level of gene expression. In response to a prolonged input, however, the slow kinetic promoter no longer requires both Msn2 and Msn4 to be fully induced and both factors contribute similarly. We hypothesize that Msn2 might serve as switch by recruiting factors that open up tightly packed nucleosomes around the slow kinetic promoters, which is then followed by Msn4 binding and recruiting a Msn4 specific binding partner that is responsible for remodeling or modifying the chromatin to promote and stabilize chromatin disassembly, hence tuning the level of gene expression. This is supported by the fact that Msn4 nuclear localization is usually delayed about 2-3 min under inhibitor or natural stress conditions when compared to Msn2 nuclear localization. To support this, we have some preliminary data to suggest that Msn4 nuclear localization is sped up in Msn2 deleted cells. However, to explore this hypothesis, it would be beneficial to determine if Msn2 and Msn4 have different binding partners and then perform these single cell combinatorial gene regulation experiments in strains with these binding partners deleted in order to determine if Msn2 and Msn4 gene regulatory functions are altered. Additionally, it would be interesting to systemically delete domains (most likely some regions on Msn2/4

transactivation domains) responsible for their distinct gene regulatory roles in response to transient inputs.

From our data in Chapter 2, we hypothesize that cells contain Msn4 in addition to Msn2 in order to diversify their gene expression (slow kinetic gene expression) in response to stress, without having leaky gene expression when it is not certain that the cells are under chronic stressful conditions. Thus, Msn2 serves as a low threshold switch to keep slow kinetic genes tightly controlled without leaky expression in response to transient fluctuations in the environment. This would be especially pertinent if slow kinetic gene products are harmful for the cells or require more energy than fast kinetic gene products to be produced. If cells only contained this Msn2 “switch” to determine slow kinetic gene expression, cells could not induce heterogenic gene expression or bet hedge in the case that a transient stress or fluctuations really are predicting stressful times ahead. Thus, Msn4 allows cells to have some level of controlled heterogeneity in which some cells (those with a specific ratio of Msn2 and Msn4) diversify their gene expression and induce slow kinetic promoter genes in case chronic stress conditions are looming. In response to a prolonged stress, however, this bet hedging strategy is no longer necessary and slow kinetic gene expression is fully induced.

Target genes with fast kinetics promoters are primarily involved in metabolic pathways whereas the majority of target genes with slow kinetics promoters are involved in cellular protection against chronic stresses. Thus, cells

could use fast kinetic promoter genes to quickly be able to modulate their metabolism in response to changes in nutrient availability in the environment. However, slow kinetic promoter genes are required for chronic stress conditions, which might occur less frequently in nature. Additionally, cellular processes involved in these chronic stress response pathways might require more energy, and thus the cell would only want to activate these slow kinetic promoter genes in response to prolonged stress. Therefore, cells would have slow kinetic promoters under tighter control to avoid initiating their gene expression in response to minor fluctuations and prioritize fast kinetic gene expression in response to changes in metabolism or fluctuating environments. It would also be interesting to determine if fast kinetic promoter genes are highly post-translationally regulated whereas slow kinetic promoter genes are not. If this were the case, it would be less risky for the cell to have leaky or rapid induction of fast kinetic promoter genes, since many of them of them would not be activated unless they were post-translationally modified in response to the right environmental conditions. Thus, perhaps these fast kinetic promoter genes are turned on and ready to be modified in preparing the cell for future changes in nutrient availability, which happens much more frequently than chronic stress. It would be informative to do some functional assays with fast versus slow kinetic promoter genes, such as overexpressing or speeding up expression of individual or groups of slow kinetic promoter gene products and determining if leaky expression of these genes really does decrease fitness when there is no stress, but increases fitness when

there is chronic stress. We hypothesize that speeding up fast kinetic promoter gene expression, in contrast, would not result in decreased fitness when there is no stress. Additionally, we could also slow down or decrease expression of fast kinetic promoter genes and measure fitness in response to metabolic changes.

Since the ratio of Msn2 and Msn4 determines slow kinetic promoter gene levels, slow kinetic promoter gene expression in response to a transient input would be dramatically different if the ratio of Msn2 to Msn4 was altered in certain conditions. For example, in a natural condition in which Msn2 protein level stays constant, but Msn4 protein level is increased, slow kinetic promoter gene induction would be greatly increased. Interestingly, there is some evidence that in response to stressful environments, the expression of *MSN4* is induced as part of the ESR and that this is reflected in Msn4 protein level (DeRisi, Iyer et al. 1997, Garreau, Hasan et al. 2000, Gasch, Spellman et al. 2000). Levels of *MSN2* nor its gene product, however, have not been shown to be regulated in response to stress or environmental changes. Thus, cells might also contain two TFs that control the same set of genes in order to have one TF (Msn2) that remains at constant levels, and another TF (Msn4) whose levels is responsive to the environment and metabolic conditions and can therefore alter gene expression programs depending on the metabolic state the cells are in prior to stress addition. Interestingly, we have some preliminary data that suggests that Msn4 levels, but not Msn2 levels, are higher in rapamycin treated cells. Thus, Msn4 might be responsive to amino acid and nitrogen levels in the environment and

may alter slow kinetic gene expression levels as a response. One project that I began pursuing (but never finished) involved determining if Msn2 or Msn4 levels change in response to different environmental conditions and how this affects their combinatorial gene expression. This involved making a NLS whose expression is controlled by the Msn4 promoter (pMsn4-NLS) and determining if this pMsn4-NLS increased in response to various environmental conditions (rapamycin, low glucose, low amino acid). I also made pMsn2-NLS as a control. Additionally, I started to make inducible Msn4 and Msn2 strains in order to tune levels of Msn2 and Msn4 and determine how changes in their ratio would alter fast and slow kinetic promoter gene expression. This gene expression in response to the artificially tuning of Msn2/Msn4 ratios could then be compared to gene expression in response to natural conditions in which Msn2/Msn4 ratios are altered.

In Chapter 2, we were only able to look at a few Msn2/Msn4 target genes because we used single cell techniques. In the future, we would like to track Msn2/Msn4 single-cell gene regulation at the whole genome level. Additionally, in our system, we replaced the ORF of the Msn2/4 target genes with CFP, thus we only measured how promoter activation is regulated by Msn2/4 dynamics. Since many of these genes are involved in downstream networks, it would be interesting to perform these Msn2/Msn4 single-cell gene regulation experiments at the whole genome level with tagged proteins rather than with promoters serving as the reporters. How the downstream target genes interact to form a

complex network and how these transcriptional networks process TF dynamics to control cellular functions is a question that has yet to be answered.

Additionally, despite some previous studies on the subject, it is still not fully understand why fast kinetic promoters and slow kinetic promoters have different activation times. Although it would be difficult to acquire dynamic data from Hi-C or additional ChIP-seq experiments, these techniques would allow us to have a better idea about the chromatin structure around Msn2/4 target gene promoters or Msn2/4 binding sites before and after stress addition. Systematically altering STRE numbers and locations in other Msn2/4 target promoters and then performing single cell gene regulation experiments with these mutants (as performed in Hansen and O'Shea, 2015), would also help determine why different target genes have different activation times. Moving Msn2/4 target gene promoters to different parts of the genome would determine if there are some other structures in those locations that help determine promoter activation times in addition to STRE sites and nucleosome positioning on promoters. It could also be informative to observe the dynamics of these fast and slow kinetic promoters over a longer period of time in response to longer periods of stress. We would like to determine how the dynamics of fast or slow kinetic promoters is inherited in daughter cells and reveal if deletion of chromatin modifiers or remodelers alters these dynamics.

In Chapter 3 we treated cells with a pulse of PKA inhibition, followed by a break in between, and finally severe osmotic stress. Using this system, we

determined that cells acquire an amplitude-dependent short-term memory of previous stress, which is induced and lost rapidly, and a duration-dependent long-term memory which undergoes a plateau phase of stability before finally declining after very long break in between the initial mild stress and severe stress. We hope to use this system with different adaptation markers for different stresses such as oxidative and ethanol stress. We would like to determine if these different stresses also have different types of cellular memory and what mechanisms underlie this memory.

Throughout this project, we found some interesting results that could become another story or project to pursue. We saw that a *fbp1Δ* strain has highly increased short-term memory in response to a 15 minute treatment of 3μM PKA 1-NM-PP1 followed by a 10 minute break compared to WT. These results could tell us more about upstream interactions between the PKA pathway and gluconeogenesis since FBP1 is involved in gluconeogenesis. Thus, performing these experiments with various mutants from other pathways could help us identify cross-talk or interactions between the PKA pathway and other pathways and also give us information about the time-scales of these interactions.

Lastly, we would like to perform these “priming” experiments with natural stress signals and other pathway inhibitors (EG- rapamycin). This system can help us learn more about cellular memory in response to different dynamics of other upstream signals other than PKA inhibition.

References

AkhavanAghdam, Z., J. Sinha, O. P. Tabbaa and N. Hao (2016). "Dynamic control of gene regulatory logic by seemingly redundant transcription factors." Elife **5**.

Alon, U. (2007). "Network motifs: theory and experimental approaches." Nat Rev Genet **8**(6): 450-461.

Bardwell, L., X. Zou, Q. Nie and N. L. Komarova (2007). "Mathematical models of specificity in cell signaling." Biophys J **92**(10): 3425-3441.

Barrett, L., M. Orlova, M. Maziarz and S. Kuchin (2012). "Protein kinase A contributes to the negative control of Snf1 protein kinase in Saccharomyces cerevisiae." Eukaryot Cell **11**(2): 119-128.

Batchelor, E., A. Loewer, C. Mock and G. Lahav (2011). "Stimulus-dependent dynamics of p53 in single cells." Mol Syst Biol **7**: 488.

Behar, M. and A. Hoffmann (2010). "Understanding the temporal codes of intra-cellular signals." Curr Opin Genet Dev **20**(6): 684-693.

Berry, D. B. and A. P. Gasch (2008). "Stress-activated genomic expression changes serve a preparative role for impending stress in yeast." Mol Biol Cell **19**(11): 4580-4587.

Berry, D. B., Q. Guan, J. Hose, S. Haroon, M. Gebbia, L. E. Heisler, C. Nislow, G. Giaever and A. P. Gasch (2011). "Multiple means to the same end: the genetic basis of acquired stress resistance in yeast." PLoS Genet **7**(11): e1002353.

Besozzi, D., P. Cazzaniga, D. Pescini, G. Mauri, S. Colombo and E. Martegani (2012). "The role of feedback control mechanisms on the establishment of oscillatory regimes in the Ras/cAMP/PKA pathway in S. cerevisiae." EURASIP J Bioinform Syst Biol **2012**(1): 10.

Breker, M., M. Gymrek and M. Schuldiner (2013). "A novel single-cell screening platform reveals proteome plasticity during yeast stress responses." J Cell Biol **200**(6): 839-850.

Cai, L., C. K. Dalal and M. B. Elowitz (2008). "Frequency-modulated nuclear localization bursts coordinate gene regulation." Nature **455**(7212): 485-490.

Cao, Y., D. T. Gillespie and L. R. Petzold (2007). "Adaptive explicit-implicit tau-leaping method with automatic tau selection." J Chem Phys **126**(22): 224101.

Chou, S., S. Zhao, Y. Song, H. Liu and Q. Nie (2008). "Fus3-triggered Tec1 degradation modulates mating transcriptional output during the pheromone response." Mol Syst Biol **4**: 212.

Conrad, M., J. Schothorst, H. N. Kankipati, G. Van Zeebroeck, M. Rubio-Texeira and J. M. Thevelein (2014). "Nutrient sensing and signaling in the yeast Saccharomyces cerevisiae." FEMS Microbiol Rev **38**(2): 254-299.

Dalal, C. K., L. Cai, Y. Lin, K. Rahbar and M. B. Elowitz (2014). "Pulsatile dynamics in the yeast proteome." Curr Biol **24**(18): 2189-2194.

De Virgilio, C., N. Burckert, W. Bell, P. Jeno, T. Boller and A. Wiemken (1993). "Disruption of TPS2, the gene encoding the 100-kDa subunit of the trehalose-6-phosphate synthase/phosphatase complex in Saccharomyces cerevisiae, causes accumulation of trehalose-6-phosphate and loss of trehalose-6-phosphate phosphatase activity." Eur J Biochem **212**(2): 315-323.

De Wever, V., W. Reiter, A. Ballarini, G. Ammerer and C. Brocard (2005). "A dual role for PP1 in shaping the Msn2-dependent transcriptional response to glucose starvation." EMBO J **24**(23): 4115-4123.

DeRisi, J. L., V. R. Iyer and P. O. Brown (1997). "Exploring the metabolic and genetic control of gene expression on a genomic scale." Science **278**(5338): 680-686.

Ding, J., X. Huang, L. Zhang, N. Zhao, D. Yang and K. Zhang (2009). "Tolerance and stress response to ethanol in the yeast Saccharomyces cerevisiae." Appl Microbiol Biotechnol **85**(2): 253-263.

Durrant, W. E. and X. Dong (2004). "Systemic acquired resistance." Annu Rev Phytopathol **42**: 185-209.

Garmendia-Torres, C., A. Goldbeter and M. Jacquet (2007). "Nucleocytoplasmic oscillations of the yeast transcription factor Msn2: evidence for periodic PKA activation." Curr Biol **17**(12): 1044-1049.

Garreau, H., R. N. Hasan, G. Renault, F. Estruch, E. Boy-Marcotte and M. Jacquet (2000). "Hyperphosphorylation of Msn2p and Msn4p in response to heat shock and the diauxic shift is inhibited by cAMP in Saccharomyces cerevisiae." Microbiology **146 (Pt 9)**: 2113-2120.

Gasch, A. P., P. T. Spellman, C. M. Kao, O. Carmel-Harel, M. B. Eisen, G. Storz, D. Botstein and P. O. Brown (2000). "Genomic expression programs in the response of yeast cells to environmental changes." Mol Biol Cell **11**(12): 4241-4257.

Ghaemmaghami, S., W. K. Huh, K. Bower, R. W. Howson, A. Belle, N. Dephoure, E. K. O'Shea and J. S. Weissman (2003). "Global analysis of protein expression in yeast." Nature **425**(6959): 737-741.

Gonze, D., M. Jacquet and A. Goldbeter (2008). "Stochastic modelling of nucleocytoplasmic oscillations of the transcription factor Msn2 in yeast." J R Soc Interface **5 Suppl 1**: S95-109.

Gorner, W., E. Durchschlag, M. T. Martinez-Pastor, F. Estruch, G. Ammerer, B. Hamilton, H. Ruis and C. Schuller (1998). "Nuclear localization of the C2H2 zinc finger protein Msn2p is regulated by stress and protein kinase A activity." Genes Dev **12**(4): 586-597.

Gorner, W., E. Durchschlag, J. Wolf, E. L. Brown, G. Ammerer, H. Ruis and C. Schuller (2002). "Acute glucose starvation activates the nuclear localization signal of a stress-specific yeast transcription factor." EMBO J **21**(1-2): 135-144.

Guan, Q., S. Haroon, D. G. Bravo, J. L. Will and A. P. Gasch (2012). "Cellular memory of acquired stress resistance in Saccharomyces cerevisiae." Genetics **192**(2): 495-505.

Hansen, A. S., N. Hao and E. K. O'Shea (2015). "High-throughput microfluidics to control and measure signaling dynamics in single yeast cells." Nat Protoc **10**(8): 1181-1197.

Hansen, A. S. and E. K. O'Shea (2013). "Promoter decoding of transcription factor dynamics involves a trade-off between noise and control of gene expression." Mol Syst Biol **9**: 704.

Hansen, A. S. and E. K. O'Shea (2015). "cis Determinants of Promoter Threshold and Activation Timescale." Cell Rep **12**(8): 1226-1233.

Hansen, A. S. and E. K. O'Shea (2015). "Limits on information transduction through amplitude and frequency regulation of transcription factor activity." Elife **4**.

Hansen, A. S. and E. K. O'Shea (2016). "Encoding four gene expression programs in the activation dynamics of a single transcription factor." Curr Biol **26**(7): R269-271.

Hao, N., B. A. Budnik, J. Gunawardena and E. K. O'Shea (2013). "Tunable signal processing through modular control of transcription factor translocation." Science **339**(6118): 460-464.

Hao, N. and E. K. O'Shea (2012). "Signal-dependent dynamics of transcription factor translocation controls gene expression." Nat Struct Mol Biol **19**(1): 31-39.

Hardie, D. G. (2007). "AMP-activated/SNF1 protein kinases: conserved guardians of cellular energy." Nat Rev Mol Cell Biol **8**(10): 774-785.

Hersen, P., M. N. McClean, L. Mahadevan and S. Ramanathan (2008). "Signal processing by the HOG MAP kinase pathway." Proc Natl Acad Sci U S A **105**(20): 7165-7170.

Hohmann, S., M. J. Neves, W. de Koning, R. Alijo, J. Ramos and J. M. Thevelein (1993). "The growth and signalling defects of the ggs1 (fdp1/byp1) deletion mutant on glucose are suppressed by a deletion of the gene encoding hexokinase PII." Curr Genet **23**(4): 281-289.

Hong, S. P. and M. Carlson (2007). "Regulation of snf1 protein kinase in response to environmental stress." J Biol Chem **282**(23): 16838-16845.

Hoops, S., S. Sahle, R. Gauges, C. Lee, J. Pahle, N. Simus, M. Singhal, L. Xu, P. Mendes and U. Kummer (2006). "COPASI--a COmplex PAthway SImulator." Bioinformatics **22**(24): 3067-3074.

Hounsa, C. G., E. V. Brandt, J. Thevelein, S. Hohmann and B. A. Prior (1998). "Role of trehalose in survival of Saccharomyces cerevisiae under osmotic stress." Microbiology **144 (Pt 3)**: 671-680.

Houser, J. R., E. Ford, M. J. Nagiec, B. Errede and T. C. Elston (2012). "Positive roles for negative regulators in the mating response of yeast." Mol Syst Biol **8**: 586.

Huang, H. Y. and A. K. Hopper (2014). "Separate responses of karyopherins to glucose and amino acid availability regulate nucleocytoplasmic transport." Mol Biol Cell **25**(18): 2840-2852.

Jiang, R. and M. Carlson (1996). "Glucose regulates protein interactions within the yeast SNF1 protein kinase complex." Genes Dev **10**(24): 3105-3115.

Lahav, G., N. Rosenfeld, A. Sigal, N. Geva-Zatorsky, A. J. Levine, M. B. Elowitz and U. Alon (2004). "Dynamics of the p53-Mdm2 feedback loop in individual cells." Nat Genet **36**(2): 147-150.

Lev Bar-Or, R., R. Maya, L. A. Segel, U. Alon, A. J. Levine and M. Oren (2000). "Generation of oscillations by the p53-Mdm2 feedback loop: a theoretical and experimental study." Proc Natl Acad Sci U S A **97**(21): 11250-11255.

Lin, Y., C. H. Sohn, C. K. Dalal, L. Cai and M. B. Elowitz (2015). "Combinatorial gene regulation by modulation of relative pulse timing." Nature **527**(7576): 54-58.

Lou, Y. and A. E. Yousef (1997). "Adaptation to sublethal environmental stresses protects Listeria monocytogenes against lethal preservation factors." Appl Environ Microbiol **63**(4): 1252-1255.

Ma, W., A. Trusina, H. El-Samad, W. A. Lim and C. Tang (2009). "Defining network topologies that can achieve biochemical adaptation." Cell **138**(4): 760-773.

Marshall, C. J. (1995). "Specificity of receptor tyrosine kinase signaling: transient versus sustained extracellular signal-regulated kinase activation." Cell **80**(2): 179-185.

Martinez-Pastor, M. T., G. Marchler, C. Schuller, A. Marchler-Bauer, H. Ruis and F. Estruch (1996). "The Saccharomyces cerevisiae zinc finger proteins Msn2p and Msn4p are required for transcriptional induction through the stress response element (STRE)." EMBO J **15**(9): 2227-2235.

Matsumoto, H., N. Hamada, A. Takahashi, Y. Kobayashi and T. Ohnishi (2007). "Vanguards of paradigm shift in radiation biology: radiation-induced adaptive and bystander responses." J Radiat Res **48**(2): 97-106.

Milo, R., S. Itzkovitz, N. Kashtan, R. Levitt, S. Shen-Orr, I. Ayzenshtat, M. Sheffer and U. Alon (2004). "Superfamilies of evolved and designed networks." Science **303**(5663): 1538-1542.

Milo, R., S. Shen-Orr, S. Itzkovitz, N. Kashtan, D. Chklovskii and U. Alon (2002). "Network motifs: simple building blocks of complex networks." Science **298**(5594): 824-827.

Nelson, D. E., A. E. Ihekwaba, M. Elliott, J. R. Johnson, C. A. Gibney, B. E. Foreman, G. Nelson, V. See, C. A. Horton, D. G. Spiller, S. W. Edwards, H. P. McDowell, J. F. Unitt, E. Sullivan, R. Grimley, N. Benson, D. Broomhead, D. B. Kell and M. R. White (2004). "Oscillations in NF-kappaB signaling control the dynamics of gene expression." Science **306**(5696): 704-708.

Nicastro, R., F. Tripodi, M. Gaggini, A. Castoldi, V. Reghellin, S. Nonnis, G. Tedeschi and P. Coccetti (2015). "Snf1 Phosphorylates Adenylate Cyclase and Negatively Regulates Protein Kinase A-dependent Transcription in Saccharomyces cerevisiae." J Biol Chem **290**(41): 24715-24726.

Nikawa, J., S. Cameron, T. Toda, K. M. Ferguson and M. Wigler (1987). "Rigorous feedback control of cAMP levels in Saccharomyces cerevisiae." Genes Dev **1**(9): 931-937.

Novak, B. and J. J. Tyson (2008). "Design principles of biochemical oscillators." Nat Rev Mol Cell Biol **9**(12): 981-991.

Pescini, D., P. Cazzaniga, D. Besozzi, G. Mauri, L. Amigoni, S. Colombo and E. Martegani (2012). "Simulation of the Ras/cAMP/PKA pathway in budding yeast highlights the establishment of stable oscillatory states." Biotechnol Adv **30**(1): 99-107.

Petrenko, N., R. V. Chereji, M. N. McClean, A. V. Morozov and J. R. Broach (2013). "Noise and interlocking signaling pathways promote distinct transcription factor dynamics in response to different stresses." Mol Biol Cell **24**(12): 2045-2057.

Purvis, J. E., K. W. Karhohs, C. Mock, E. Batchelor, A. Loewer and G. Lahav (2012). "p53 dynamics control cell fate." Science **336**(6087): 1440-1444.

Purvis, J. E. and G. Lahav (2013). "Encoding and decoding cellular information through signaling dynamics." Cell **152**(5): 945-956.

Raffaghello, L., C. Lee, F. M. Safdie, M. Wei, F. Madia, G. Bianchi and V. D. Longo (2008). "Starvation-dependent differential stress resistance protects normal but not cancer cells against high-dose chemotherapy." Proc Natl Acad Sci U S A **105**(24): 8215-8220.

Ramachandran, V., K. H. Shah and P. K. Herman (2011). "The cAMP-dependent protein kinase signaling pathway is a key regulator of P body foci formation." Mol Cell **43**(6): 973-981.

Reinders, A., N. Burckert, S. Hohmann, J. M. Thevelein, T. Boller, A. Wiemken and C. De Virgilio (1997). "Structural analysis of the subunits of the trehalose-6-phosphate synthase/phosphatase complex in Saccharomyces cerevisiae and their function during heat shock." Mol Microbiol **24**(4): 687-695.

Savvides, A., S. Ali, M. Tester and V. Fotopoulos (2016). "Chemical Priming of Plants Against Multiple Abiotic Stresses: Mission Possible?" Trends Plant Sci **21**(4): 329-340.

Schenk, P. M., K. Kazan, I. Wilson, J. P. Anderson, T. Richmond, S. C. Somerville and J. M. Manners (2000). "Coordinated plant defense responses in Arabidopsis revealed by microarray analysis." Proc Natl Acad Sci U S A **97**(21): 11655-11660.

Schepers, W., G. Van Zeebroeck, M. Pinkse, P. Verhaert and J. M. Thevelein (2012). "In vivo phosphorylation of Ser21 and Ser83 during nutrient-induced activation of the yeast protein kinase A (PKA) target trehalase." J Biol Chem **287**(53): 44130-44142.

Schmitt, A. P. and K. McEntee (1996). "Msn2p, a zinc finger DNA-binding protein, is the transcriptional activator of the multistress response in Saccharomyces cerevisiae." Proc Natl Acad Sci U S A **93**(12): 5777-5782.

Scholz, H., M. Franz and U. Heberlein (2005). "The hangover gene defines a stress pathway required for ethanol tolerance development." Nature **436**(7052): 845-847.

Shashkova, S., N. Welkenhuysen and S. Hohmann (2015). "Molecular communication: crosstalk between the Snf1 and other signaling pathways." FEMS Yeast Res **15**(4): fov026.

Souza, A. C., J. F. De Mesquita, A. D. Panek, J. T. Silva and V. M. Paschoalin (2002). "Evidence for a modulation of neutral trehalase activity by Ca2+ and cAMP signaling pathways in Saccharomyces cerevisiae." Braz J Med Biol Res **35**(1): 11-16.

Stanley, D., A. Bandara, S. Fraser, P. J. Chambers and G. A. Stanley (2010). "The ethanol stress response and ethanol tolerance of Saccharomyces cerevisiae." J Appl Microbiol **109**(1): 13-24.

Stewart-Ornstein, J., C. Nelson, J. DeRisi, J. S. Weissman and H. El-Samad (2013). "Msn2 coordinates a stoichiometric gene expression program." Curr Biol **23**(23): 2336-2345.

Stricker, J., S. Cookson, M. R. Bennett, W. H. Mather, L. S. Tsimring and J. Hasty (2008). "A fast, robust and tunable synthetic gene oscillator." Nature **456**(7221): 516-519.

Tay, S., J. J. Hughey, T. K. Lee, T. Lipniacki, S. R. Quake and M. W. Covert (2010). "Single-cell NF-kappaB dynamics reveal digital activation and analogue information processing." Nature.

Tyas, L., V. A. Brophy, A. Pope, A. J. Rivett and J. M. Tavare (2000). "Rapid caspase-3 activation during apoptosis revealed using fluorescence-resonance energy transfer." EMBO Rep **1**(3): 266-270.

Villarino, A., A. Laurence, G. W. Robinson, M. Bonelli, B. Dema, B. Afzali, H. Y. Shih, H. W. Sun, S. R. Brooks, L. Hennighausen, Y. Kanno and J. J. O'Shea (2016). "Signal transducer and activator of transcription 5 (STAT5) paralog dose governs T cell effector and regulatory functions." Elife **5**.

Werner, S. L., D. Barken and A. Hoffmann (2005). "Stimulus specificity of gene expression programs determined by temporal control of IKK activity." Science **309**(5742): 1857-1861.

Yissachar, N., T. Sharar Fischler, A. A. Cohen, S. Reich-Zeliger, D. Russ, E. Shifrut, Z. Porat and N. Friedman (2013). "Dynamic response diversity of NFAT isoforms in individual living cells." Mol Cell **49**(2): 322-330.

Zaman, S., S. I. Lippman, X. Zhao and J. R. Broach (2008). "How Saccharomyces Responds to Nutrients." Annu Rev Genet.